NASA CONTRACTOR REPORT

NASA CR-2039

ANALYTICAL AND EXPERIMENTAL INVESTIGATION OF AIRCRAFT METAL STRUCTURES REINFORCED WITH FILAMENTARY COMPOSITES

Phase II - Structural Fatigue, Thermal Cycling, Creep, and Residual Strength

by B. Blichfeldt and J. E. McCarty

Prepared by
THE BOEING COMPANY
Seattle, Wash. 98124
for Langley Research Center

NATIONAL AERONAUTICS AND SPACE ADMINISTRATION • WASHINGTON, D. C. • JUNE 1972

1. Report No.	2. Government Accession No.	3. Recipient's Catalog No.
NASA CR-2039		

4. Title and Subtitle: ANALYTICAL AND EXPERIMENTAL INVESTIGATION OF AIRCRAFT METAL STRUCTURES REINFORCED WITH FILAMENTARY COMPOSITES. PHASE II – STRUCTURAL FATIGUE, THERMAL CYCLING, CREEP, AND RESIDUAL STRENGTH

5. Report Date: June 1972

6. Performing Organization Code:

7. Author(s): B. Blichfeldt and J. E. McCarty

8. Performing Organization Report No.: D6-60136-2

9. Performing Organization Name and Address:
The Boeing Company
Seattle, Washington

10. Work Unit No.:

11. Contract or Grant No.: NAS1-8858

12. Sponsoring Agency Name and Address:
National Aeronautics and Space Administration
Washington, D.C. 20546

13. Type of Report and Period Covered: CONTRACTOR REPORT

14. Sponsoring Agency Code:

15. Supplementary Notes:
This report supplements material presented in NASA CR-1859

16. Abstract

Specimens representative of metal aircraft structural components reinforced with boron filamentary composites were manufactured and tested under cyclic loading, cyclic temperature, or continuously applied loading to evaluate some of the factors that affect structural integrity under cyclic conditions. Bonded, stepped joints were used throughout to provide composite-to-metal transition regions at load introduction points.

Honeycomb panels with titanium or aluminum faces reinforced with unidirectional boron composite were fatigue tested at constant amplitude under completely reversed loading. Results indicated that the matrix material was the most fatigue-sensitive part of the design, with debonding initiating in the stepped joints. However, comparisons with equal weight all-metal specimens show a 10 to 50 times improved fatigue life. Fatigue crack propagation and residual strength were studied for several different stiffened panel concepts, and were found to vary considerably depending on the configuration. Weight savings up to 30 percent may be realized with the better concepts when compared to all-metal structure. Composite-reinforced metal specimens were also subjected to creep and thermal cycling tests. The creep tests at 50 percent of tensile ultimate load were inconclusive due to large scatter in the limited tests. Thermal cycling of stepped joint tensile specimens resulted in a ten percent decrease in residual strength after 4000 cycles.

17. Key Words (Suggested by Author(s))	18. Distribution Statement
Filamentary composites Composite reinforced metals Boron-epoxy Boron-polyimide Fatigue Thermal cycling Residual strength	Unclassified - Unlimited

19. Security Classif. (of this report)	20. Security Classif. (of this page)	21. No. of Pages	22. Price*
Unclassified	Unclassified	111	$3.00

*For sale by the National Technical Information Service, Springfield, Virginia 22151

FOREWORD

This report was prepared by The Boeing Company under NASA contract NAS1-8858 and covers the work performed during the period of September 1969 through October 1970 on phase II of a three-phase contract. The contract is being administered under the direction of Richard E. Pride, head of the Composites Section, and the phase II work was monitored by Walter Illg, head of the Fatigue Section, both of the Materials Division, NASA Langley Research Center.

The authors wish to acknowledge the contributions of the following Boeing personnel: A. H. McClure, materials; T. G. Couvion, testing; K. P. Hernley, manufacturing; and C. B. Watts, manufacturing.

CONTENTS

TABLES

FIGURES

FIGURES–Continued

FIGURES—Concluded

ANALYTICAL AND EXPERIMENTAL INVESTIGATION OF AIRCRAFT METAL STRUCTURES REINFORCED WITH FILAMENTARY COMPOSITES

Phase II Report

Structural Fatigue, Thermal Cycling,

Creep, and Residual Strength

By B. Blichfeldt and J. E. McCarty

The Boeing Company

SUMMARY

Phase I of this contract (NAS1-8858, see ref. 1), investigated the design and manufacturing feasibility of aircraft metal structures reinforced with boron filament composites. Static strengths of both reinforced honeycomb and skin-stringer concepts were obtained in phase I testing. In phase II, structures representative of aircraft panels were fabricated and tested to evaluate some factors that affect the integrity of the structure under static and fluctuating thermal exposure, fatigue life, crack retardation capabilities, and residual strength.

The material used in both phases included 7075-T6 aluminum, 6Al-4V titanium (conditions I and III), and boron-epoxy and boron-polyimide composites. Some of the structural arrangements developed in phase I for reinforced honeycomb and skin-stringer panels were used in the phase II investigation. Throughout this phase, as well as in phase I, stepped joints were used to join the composite to the metal in order to provide all-metal splice regions.

Honeycomb panels with metal faces reinforced with boron composite were fatigue tested at constant amplitude under completely reversed loading ($R = -1$). Titanium face skins were reinforced with both boron-epoxy and boron-polyimide composites; the aluminum face skins were reinforced only with the boron-epoxy composite. The boron-epoxy specimens were tested at room temperature. The boron-polyimide-reinforced specimens were tested at both room temperature and 450° F (505° K).

Test results indicated that the matrix material at the stepped composite-to-metal joint was the critical fatigue-sensitive part of the design concept. Metal structures reinforced with boron-filament composites show 10 to 50 times improved fatigue life for the same weight or, for equal fatigue life, a 20% to 40% weight saving over more-conventional structural concepts.

The effects of stiffener configuration on fatigue crack propagation and residual strength were studied for several honeycomb and skin-stringer reinforcement concepts. The panels were tested by introducing an initial crack and cycling the panel to obtain crack growth rates. After significant crack growth was obtained, each specimen was loaded to failure to determine residual strength. The results of this testing showed that crack retardation varies with distribution of reinforcement and that various aspects, such as visible damage growth rate and residual static strength, depend on the configuration. Weight savings of up to 30% may be realized when comparing the fatigue and fracture performance of reinforcement concepts with that of all-metal structure.

Composite-reinforced metal specimens were subjected to thermal cycling and creep tests. The metal-to-composite interface (adhesive) was investigated using interlaminar-shear specimens. The specimens made with epoxy adhesive were cycled between 160° F (344° K) and -65° F (219° K); the specimens made with polyimide adhesive were cycled between 450° F (505° K) and -65° F (219° K). Subsequent short-beam bending tests showed 50% to 90% reductions in strength and stiffness of the epoxy system. The polyimide adhesive system showed 20% to 35% degradation due to temperature cycling. Further study is necessary.

The metal-to-composite interface (matrix), typical of the conditions in the joint region, was investigated under creep loading. The specimens contained a composite-to-metal stepped joint. The results of the creep tests were inconsistent, and no significant conclusions can be drawn. Further study is necessary.

INTRODUCTION

The application of advanced high-modulus and high-strength filamentary composites to aircraft structures has been shown to offer significant weight-saving potential. The development of application concepts for advanced composites has generally been approached by considering the fibers and matrix as a single material and then treating that material as a metal with respect to structural configurations, analysis, and manufacture. This substitution approach requires the use of a substantial amount of high-cost fibers in areas of low payoff, such as skins, as well as in areas of high payoff. Selective reinforcement with filamentary composites in areas of high payoff, such as stringers and flanges, provides low-risk, low-cost configurations and retains a high percentage of the weight-saving potential. The approach taken in this investigation was to consider the cofunctioning of composite and metal in selectively reinforced concepts.

During phase I of this contract (ref. 1), the weight savings available by use of the reinforcing concept were demonstrated by designing, fabricating, and testing compression panels. Weight savings of up to 30% were obtained. These weight savings may be reduced, however, when the additional aircraft structural requirements of environmental stability, fatigue life, damage containment, and residual strength are considered. The objective of phase II was to test and evaluate the reinforcement concepts and draw conclusions about material combinations and structural configurations with respect to fatigue and thermal requirements. The properties of the matrix are the least known of the materials in these structural concepts and have the greatest potential for sensitivity to thermal and fatigue degradation. Therefore, design concepts may be controlled by the performance of the matrix material.

The investigation was divided into four parts: fatigue, thermal cycling, creep, and crack propagation and residual strength.

The results of the fatigue tests are given in terms of life curves at different alternating strain levels. Examination of the failure modes shows that fatigue performance is matrix limited, in contrast to static performance, which is fiber limited.

Simple three-point-bend specimens were used to investigate adhesive behavior. Stuctural laminates, including the stepped load-transfer region, were tested in tension to evaluate matrix behavior. Composite response to temperature cycling and static-temperature creep was investigated. The temperature cycling produced a 50% to 70% decrease in the epoxy properties and a 30% decrease in the polyimide properties. Creep rupture was a significant problem with the epoxy adhesive (matrix) at the step length selected.

In the damage investigations of the basic sections of the various concepts, metal-to-metal debonding was a problem in all concepts with polyimide and in hat-stringer panels with simple skin. Damage containment properties of the tested concepts are compared with conventional structure in terms of crack propagation rates and in terms of residual strength per unit mass. The results show weight-saving potential of up to 30%.

To fully understand the interaction between design requirements and adhesive capability, more work should be devoted to the basic adhesive and basic matrix properties as they influence the design of advanced composite concepts.

SYMBOLS

The units used for physical quantities defined in this paper are given in both the U.S. customary units and in the international system of units (SI).

A	area, square inches, (square meters)
a	amplitude
co	composite
E	modulus of elasticity, pounds per square inch (Newtons per square meter)
f	fiber
HC	honeycomb
HRP	Polyimide fiberglass honeycomb
K_t	stress concentration factor (theoretical)
ℓ	step length, inches (meters)
NF	normal force per unit length, pounds force per inch (Newtons per meter)
P	load, pounds force (Newtons)
Pi	polyimide
Q	shear force per unit length, pounds force per inch (Newtons per meter)
R	stress ratio in fatigue, minimum stress/maximum stress
T	temperature, degrees Fahrenheit (degrees Kelvin)
W	mass per surface area, pounds mass per square inch (kilograms per square meter)
α	ratio of damaged to undamaged strength
$\Delta\lambda$	change in gage length, inches (meters)
δ	inelastic deformation, inches (meters)
ϵ	strain
κ	coefficient of thermal expansion, strain per degree temperature
λ	gage length, inches (meters)
ρ	density, pounds mass per cubic inch (kilograms per cubic decimeter)
σ	normal stress, pounds force per square inch (Newtons per square meter)
τ	shear stress, pounds force per square inch (Newtons per square meter)

FATIGUE

Objective

The objective of this fatigue investigation was to evaluate the ability of boron-filament-composite-reinforced metal structures, which included stepped joints, to function in a fatigue environment of complete stress reversal (R = -1) at room and elevated temperature.

Background and Approach

The fatigue life of a composite-reinforced metal structural concept may be governed by the performance of the fibers, the metal, the adhesive, or the matrix. The strain amplitude of the metal and fibers during fatigue loading is a measure of how much structural weight is necessary to perform in a given fatigue environment. The matrix is strained in shear in the load-transfer region (stepped joint) where the fiber strain changes from 0 to a value constant along the fiber. The magnitude of the shear stress increases with fiber stress and decreases with step length. In reference 1, it was shown that full fiber strength σ_f = 340 ksi was obtained with three step lengths: 0.30 in., (7.6 mm), 0.40 in., (10.1 mm), and 0.50 in. (12.7 mm). A normal procedure in developing fatigue-resistant structure is to begin with a structure that satisfies the static requirements, then proceed by reducing stress concentrations or gross stresses until the objective is met. In the fatigue investigation of composite-reinforced metal structures, the severe stress concentration seems to be determined by shear stress in the matrix and, for this configuration, by the step length. A step length of 0.40 in. (10.1 mm) was selected for the fatigue test.

A stress ratio of R = -1 was chosen because it is the most severe test, involving both tension and compression.

The nature of the fatigue response of a cured resin (viscoelastic material) is not well understood, but a strong frequency dependency was expected. Frequencies of 0.12 and 16.7 Hz were used in this investigation, providing an indication of frequency effects.

Specimens and Testing

The specimens shown in figure 1 were fabricated for fatigue testing. The boron composite skins and the stepped titanium load-transfer regions (structural laminate), were fabricated in one piece during a primary curing operation. The metal skins, structural laminate, honeycomb core, and spacer blocks were assembled in a secondary curing operation.

A 140-kip (623 kN) capacity Riehle-Los hydraulic fatigue machine (shown in figure 2) was used for the tests. The specimens were gripped by friction fixtures that were loaded hydraulically.

Radiant heat lamps used for the 450° F (505° K) tests are shown in figure 3. The thermocouple arrangements to control and record temperature are also shown in figure 3.

Although stresses in individual materials of a laminate are most significant for fatigue, the present tests are conveniently presented in terms of strain. Stresses are easily determined by multiplying by the appropriate modulus of elasticity.

Load-strain curves were calculated for two points on the specimens, as shown in figure 4. The curves were developed from the following equation:

$$P = \epsilon_0 (\Sigma AE)_0 = \epsilon_2 (\Sigma AE)_2 \quad (1)$$

where the subscripts 0 and 2 refer to points 0 and 2, respectively, in figure 4.

Values of ϵ_0 were selected to give test lives between 0.01 and 1000 kc. The corresponding test machine loads were determined from the curve.

Strain gages were installed on one boron-epoxy-aluminum specimen, and readings were taken at several loads as shown in figure 4. The gage readings were in good agreement with theory for ϵ_0. The strain ϵ_2 is a peak value at the edge of the load-transfer step (see fig. 13). Therefore, the gage recorded less than the theoretical maximum value.

Test results for all specimens are shown in tables 1, 2, and 3. In these tables, the number of cycles to final failure is recorded, along with the selected values for ϵ_0. The specimen identification shows the face sheet material, the matrix material, the fiber stress, and a specimen sequence number.

Temperature measurements taken during the elevated-temperature tests are shown in table 4. Temperature variations during the tests were negligible.

Typical specimen failures are shown in figures 5 through 8.

Analysis and Discussion

All of the specimen test data points were plotted with strain as a function of the number of cycles to failure. Curves were then drawn through the data points for each group of specimens. Figures 9, 10, and 11 show the curves for aluminum-boron-epoxy, titanium-boron-epoxy, and titanium-boron-polyimide composites.

The boron-epoxy specimens were not frequency sensitive as indicated by a good match of the curves for two frequencies (figs. 9 and 10). The mismatch of the curves for boron-polyimide (fig. 11) at 450° F (505° K) indicated that lower frequencies were detrimental to life for this material at elevated temperatures. Limited test data at 70° F (293° K) indicated improved life compared to 450° F (505° K) results. The boron-polyimide composite is intended for service up to 450° F (505° K), therefore, most of the specimens were tested at this temperature.

Fatigue performance of current riveted aluminum is characterized by S-N curves for specimens incorporating unloaded or lightly loaded rivets or other representative fasteners. These specimens with loaded holes represent the minimum stress risers possible in riveted

structure. NACA has used K_t for stress risers in early publications (refs. 2 and 3). The best current riveted structure corresponds to K_t = 2.5 to 4.0, and the best bonded structure to K_t = 1.5.

To assess the fatigue performance of the composite-reinforced metals shown in figures 9, 10, and 11, a comparison was made with the performance of metal specimens representative of the performance of the best current aluminum and titanium structure with a K_t of 1.5 to 2.0 and having cross sections of the same weight as the composite-reinforced specimens.

In figure 12, the lives of the reinforced titanium and aluminum specimens are compared to titanium and aluminum specimens of the same weight (0.0434 lbm/in.) (7.72×10^{-4} kg/mm). NACA data for aluminum (K_t = 1.5 to 4.0) and AFML data for titanium (K_t = 1.0 and 2.82) at room and elevated temperatures were available for comparison. It is seen that for equal weight the reinforced titanium and aluminum have longer lives than aluminum with K_t of 1.5 and titanium with K_t of 1.0. From this it can be seen that reinforced titanium and aluminum honeycomb structures can be built with fatigue performance superior to conventional metal structure with typical K_t values of 2.5 to 3.5.

Except for a few specimens that failed in fewer than 100 cycles, fatigue failures started in the area of the load-transfer region. Figure 5 shows one typical low-cycle failure.

A failure typical of the reinforced-aluminum specimen is shown in figure 6. The failed surface shows a fatigue failure in the matrix that bonds the fibers to the steps of the load-transfer region and in the aluminum face sheet (straight part). The rest of the failure surface comprises two curved lines in the aluminum sheet and a darker cohesive failure in the matrix, indicating a residual static failure. An early failure indication is shown in the far end of the specimen, where a crack has opened in the aluminum face sheet. A life prediction for the aluminum face sheet shows that the fatigue failure is unlikely to have started in the aluminum, which indicates that the matrix is the first part to fail.

The failure shown in figure 7 is typical for the reinforced-titanium specimen. The failure surface comprises fatigue failure in the matrix, fatigue failure in the stepped fitting of the load-transfer region, and residual static failure in the titanium face sheet. Again, a life prediction for the titanium indicates that something other than the titanium is the first part to fail.

The failure in figure 8 is typical of the low-cycle failures in the boron-polyimide-reinforced titanium specimens tested at 450° F. The specimen shows debonding between the stepped load-transfer fitting and the fibers and unbroken titanium face sheets. Other boron-polyimide-reinforced specimens had broken face sheets but were otherwise similar in appearance.

To follow up on these findings, and to explore the difference in failures in the reinforced-aluminum specimens (fatigue failure in face sheet) and in the reinforced-titanium specimen (fatigue failure in the stepped fitting), an elastic analysis was made to find the strain along the load-transfer region for different degrees of failure in the adhesive (see fig. 13). The analysis assumes an average strain of 1000 μin./in. in the cut B-B and examines the

strains in the face sheet at point 2 plus the strains in the corners of the load-transfer region. The strain values in the steps are derived from:

$$\epsilon_{max} = \frac{\Sigma(EA)_o}{\Sigma EA}\epsilon_o K_t \qquad (2)$$

where ϵ_o = 1000 μ in./in., and values of K_t are derived from reference 5.

When the matrix is broken on two steps, the load will be carried along cut A-A in figure 13. In this way, the strains in the corners of the load-transfer fitting will vary as the debonding progresses from point 1 until the accumulated damage in one corner is sufficient to initiate a crack. The strain values at the edges of the steps are shown in figure 14 for the unbroken specimens.

The strain values in the reinforced-aluminum specimen are shown in figure 15 for a developing adhesive failure. It is seen that the value in the sheet at point 2 (fig. 13) never exceeds the highest value at a step, but the two strains occur in different materials so skin cracks may occur before cracks from the steps. Figures 16 and 17 similarly show strain values in the two types of reinforced-titanium specimens for different degrees of debonding.

Based on the evidence from the failed specimens, and on the analysis shown above, it is suggested that a typical failure was initiated in the matrix in the load-transfer region at point 1 (fig. 13), and that it developed along the interface between fibers and metal until one of three events occurred:

- The face sheet broke in fatigue at point 2, leading to static failure along the rest of the interface. This was typical for the aluminum-boron-epoxy system (fig. 6).

- The titanium broke at a step (point 3, fig. 13) from fatigue. This was typical for titanium-boron-epoxy systems (fig. 7).

- The matrix failure was completed and led to buckling of the face sheet. This was typical for the titanium-boron-polyimide systems (fig. 8).

The observation was made that, for the same strain amplitude and therefore shear stress amplitude in the load-transfer region, the reinforced-aluminum specimens always failed at shorter lives than the reinforced-titanium specimens.

Conclusions and Recommendations

A number of conclusions can be drawn from the results concerning reinforced metal structure with stepped load-transfer region having equal step length and one ply per step:

- The life of reinforced aluminum and reinforced titanium at room temperature is longer than lives of all-aluminum (K_t = 1.5) and all-titanium (K_t = 1.0) structure of the same weight.

- The life of reinforced titanium at 450°F (505°K) is as good or better than titanium with $K_t = 2.82$ at 400°F (477°K).

- The fatigue life of the reinforced specimens was determined by the load transfer region design and the matrix performance.

- Further improvements in fatigue performance may be possible by changing the load-transfer region design to lower the adhesive stresses.

TABLE 1.–LIFE OF ALUMINUM-BORON-EPOXY

Specimen[a]	Strain, ϵ_{1a}, μ	Frequency, Hz	Life, kc	
			Individual	Log mean
7075 BP-090-1	1600	16.7	189.200	
-2	1600	16.7	171.180	182.000
-3	1600	16.7	184.140	
7075 BP-130-1	2300	16.7	64.760	
-2	2300	16.7	56.640	61.500
-3	2300	16.7	64.060	
7075 BP-150-1	2650	16.7	36.260	
-2	2650	16.7	34.520	34.700
-3	2650	16.7	33.740	
7075 BP-180-1	3200	16.7	16.250	
-2	3200	16.7	17.560	18.400
-3	3200	16.7	21.860	
7075 BP-200-1	3550	16.7	12.320	
-2	3550	16.7	14.090	13.700
-3	3550	16.7	14.790	
7075 BP-240-1LC	4250	0.12	5.085	
-2LC	4250	0.12	4.574	4.510
-3LC	4250	0.12	3.937	
7075 BP-290-1LC	5150	0.12	0.017	
-2LC	5150	0.12	0.262	0.049
-3LC	5150	0.12	0.026	

[a]Specimen code: Metal symbol, matrix symbol–fiber stress amplitude in ksi–sequence number.

TABLE 2.–LIFE OF TITANIUM-BORON-EPOXY

Specimen[a]	Strain, ϵ_{1a}, μ	Frequency, Hz	Life, kc	
			Individual	Log mean
64 BP-090-1	1600	16.7	921.97	
-2	1600	16.7	827.23	645.00
-3	1600	16.7	347.02	
64 PB-110-1	1900	16.7	106.45	
-2	1900	16.7	168.93	184.00
-3	1900	16.7	182.22	
64 PB-120-1	2100	16.7	85.73	
-2	2100	16.7	351.88	181.00
-3	2100	16.7	195.75	
64 PB-130-1	2250	16.7	95.46	
-2	2250	16.7	117.88	94.50
-3	2250	16.7	74.75	
64 BP-150-1	2600	16.7	45.90	
-2	2600	16.7	48.78	44.70
-3	2600	16.7	39.31	
64 BP-180-1	3100	16.7	24.440	
-2	3100	16.7	36.120	32.300
-3	3100	16.7	38.530	
64 BP-200-1	3500	16.7	17.040	
-2	3500	16.7	16.050	14.100
-3	3500	16.7	9.850	
64 BP-230-1	4000	16.7	19.720	
-2	4000	16.7	17.920	16.820
-3	4000	16.7	13.460	
64 BP-260-1	4500	16.7	6.270	
-2	4500	16.7	4.150	5.250
-3	4500	16.7	5.590	
64 PB-260-1LC	4500	0.12	3.228	
-2LC	4500	0.12	5.321	4.400
-3LC	6500[b]	0.12[b]	0.001[b]	
-3RLC	4500	0.12	4.818	
64 BP-290-1LC	5050	0.12	0.901	
-2LC	5050	0.12	0.377	0.565
-3LC	5050	0.12	0.525	
64 BP-320-1LC	5550	0.12	0.035	
-2LC	5550	0.12	0.029	0.036
-3LC	5550	0.12	0.049	

[a]Specimen code: Metal symbol, matrix symbol–fiber stress amplitude in ksi–sequence number.

[b]Overloaded by mistake; not included in average.

TABLE 3.–LIFE OF TITANIUM-BORON-POLYIMIDE

Specimen[a]	Strain, ϵ_{1a}, μ	Temperature, °F	Frequency, Hz	Life, kc	
				Individual	Log mean
64 Pi-090-1	1600	450 ± 20	16.7	254.0	
-2	1600	450 ± 20	16.7	434.3	465.0
-3	1600	450 ± 20	16.7	NF[b]	
64 Pi-110-1LC	1900	450 ± 20	0.12	1.178	
-2LC	1900	450 ± 20	0.12	1.688	2.42
-3LC	1900	450 ± 20	0.12	7.063	
64 Pi-110-1	1900	450 ± 20	16.7	105.1	
-2	1900	450 ± 20	16.7	5.9	32.2
-3	1900	450 ± 20	16.7	51.3	
64 Pi-130-1	2250	450 ± 20	16.7	14.69	
-2	2250	450 ± 20	16.7	2.53	6.85
-3	2250	450 ± 20	16.7	8.68	
64 Pi-150-1	2600	450 ± 20	16.7	2.500	
-2	2600	450 ± 20	16.7	1.300	1.290
-3	2600	450 ± 20	16.7	0.640	
64 Pi-150-1LC	2600	450 ± 20	0.12	0.206	
-2LC	2600	450 ± 20	0.12	0.171	0.154
-3LC	2600	450 ± 20	0.12	0.103	
64 Pi-180-1	3100	450 ± 20	16.7	0.970	–
64 Pi-200-1LC	3500	450 ± 20	0.12	0.107	
-2LC	3500	450 ± 20	0.12	0.079	0.062
-3LC	3500	450 ± 20	0.12	0.027	
64 Pi-230-1LC[b]	4000	450 ± 20	0.12	0.032	
-2LC	4000	450 ± 20	0.12	0.006	0.019
-3LC	4000	450 ± 20	0.12	0.035	
64 Pi-260-1LC	4500	70 ± 5	0.12	0.105	
-2LC	4500	70 ± 5	0.12	0.089	0.013
-3LC	4500	70 ± 5	0.12	0.122	
64 Pi-260-4LC[b]	4550	450 ± 20	0.12	0.017	
-5LC	4550	450 ± 20	0.12	0.017	0.048
-6LC	4550	450 ± 20	0.12	0.008	
64 Pi-290-1LC	5050	70 ± 5	0.12	0.112	
-2LC	5050	70 ± 5	0.12	0.023	0.048
-3LC	5050	70 ± 5	0.12	0.041	

[a]Specimen code: Metal symbol, matrix symbol–fiber stress amplitude in ksi–sequence number.

[b]No failure during cycling, but failed at 36 600 lb at 450°F following cycling test.

TABLE 4.—TEMPERATURES FOR TITANIUM-BORON-POLYIMIDE SPECIMENS

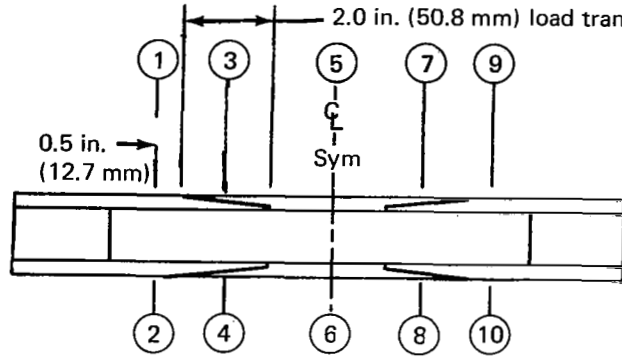

Specimen[a]	Temperature measurements at beginning of test, °F									
	1	2	3	4	5	6	7	8	9	10
64 Pi-260-4	434	445	466	455	455	470	423	430	375	380
-5	440	450	473	455	456	460	420	419	359	362
-6	443	450	473	439	460	470	426	427	386	385
64 Pi-230-1	443	451	474	428	464	469	445	436	398	390
-2	442	455	478	447	466	466	437	436	387	395
-3	435	435	470	422	466	455	441	426	395	382
64 Pi-200-1	420	426	469	460	470	456	445	426	397	382
-2	435	443	469	467	468	464	435	430	389	386
-3	430	442	465	465	465	468	430	435	390	390
64 Pi-180-1	410	425	422	445	485	475	465	465	445	445
64 Pi-150-1	430	490	470	465	455	455	425	425	365	375
-2	430	440	470	470	460	455	425	415	380	370
-3	430	–	445	470	470	440	440	420	360	320
-1LC	416	436	465	465	467	466	443	425	400	370
-2LC	442	467	440	460	464	464	440	432	384	374
-3LC	436	471	443	462	464	456	432	420	395	378
64 Pi-130-1	415	440	460	465	460	465	445	445	380	380
-2	400	420	440	450	455	468	466	459	390	380
-3	405	435	470	475	455	460	440	420	350	320
64 Pi-110-1	440	440	475	440	450	455	420	420	380	380
-2	445	445	480	450	450	460	425	420	375	360
-3	445	445	465	465	455	455	425	405	375	365
-1LC	435	460	446	465	473	462	435	425	380	370
-2LC	450	470	456	468	468	467	435	430	390	380
-3LC	425	460	450	470	470	455	450	430	405	370
64 Pi-090-1	430	433	462	471	448	455	427	411	379	367
-2	422	427	456	457	450	461	430	425	369	360
-3	410	432	467	473	455	460	430	424	370	365

[a]Specimen code: Material symbol, matrix symbol—fiber stress amplitude in ksi—sequence number.

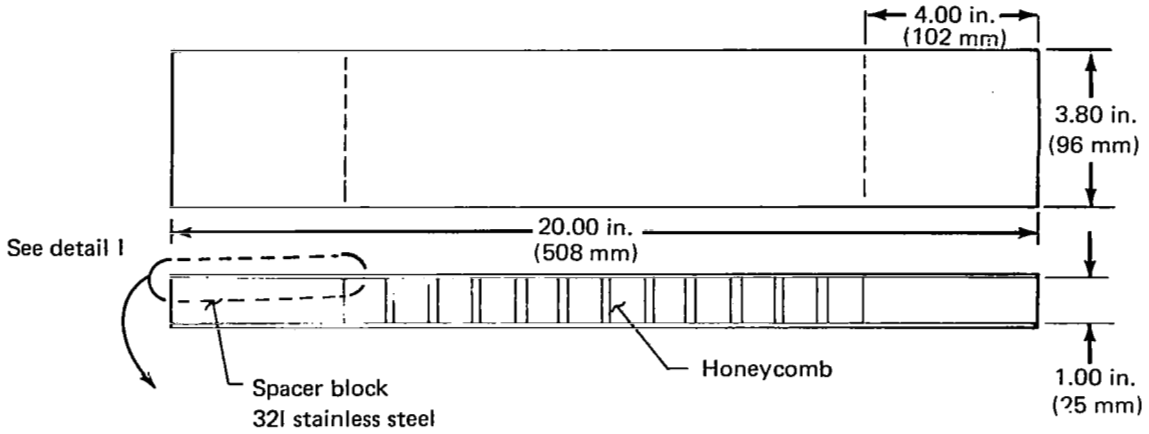

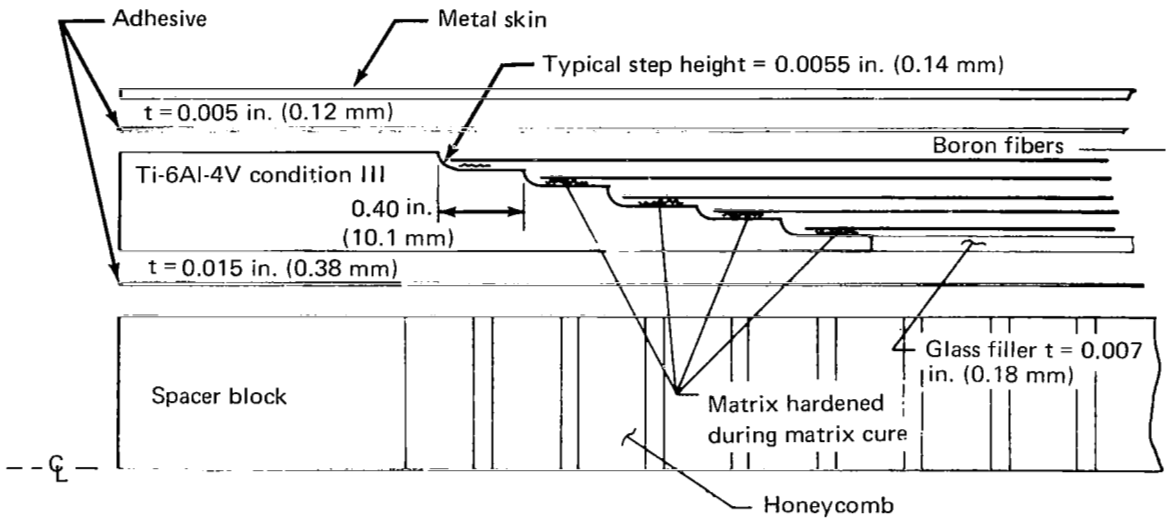

DETAIL I

Specimen type	Matrix	Adhesive	Face skin			Honeycomb[a] core
			Metal	Gage		
				in.	mm	
Al-B-epoxy	BP 907	AF 126	Al-7075-T6	0.025	0.64	8.1-1/8-20 (Al)
Ti-B-epoxy	BP 907	AF 126	Ti-6Al-4V	0.007	0.18	8.1-1/8-20 (Al)
Ti-B-Pi	35-520	FM 34B	Ti-6Al-4V	0.007	0.18	5.0-3/16 (HRP)

[a]Numbers indicate weight (lb/cu ft), cell size (in.), and foil thickness (tenths of mil).

FIGURE 1.–STEPPED-JOINT FATIGUE SPECIMENS

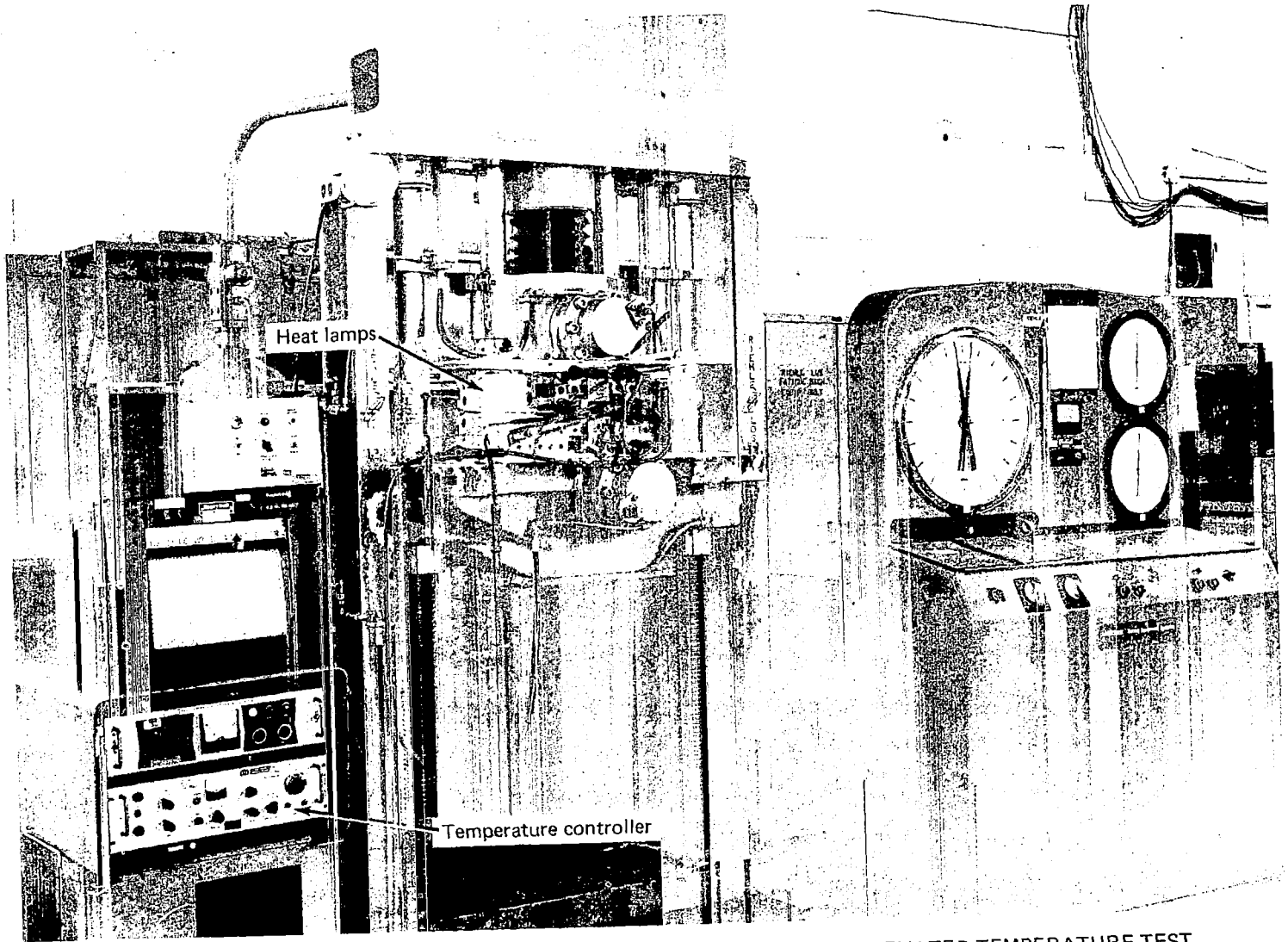

FIGURE 2.—140-KIP CAPACITY RIEHLE-LOS FATIGUE MACHINE DURING ELEVATED-TEMPERATURE TEST

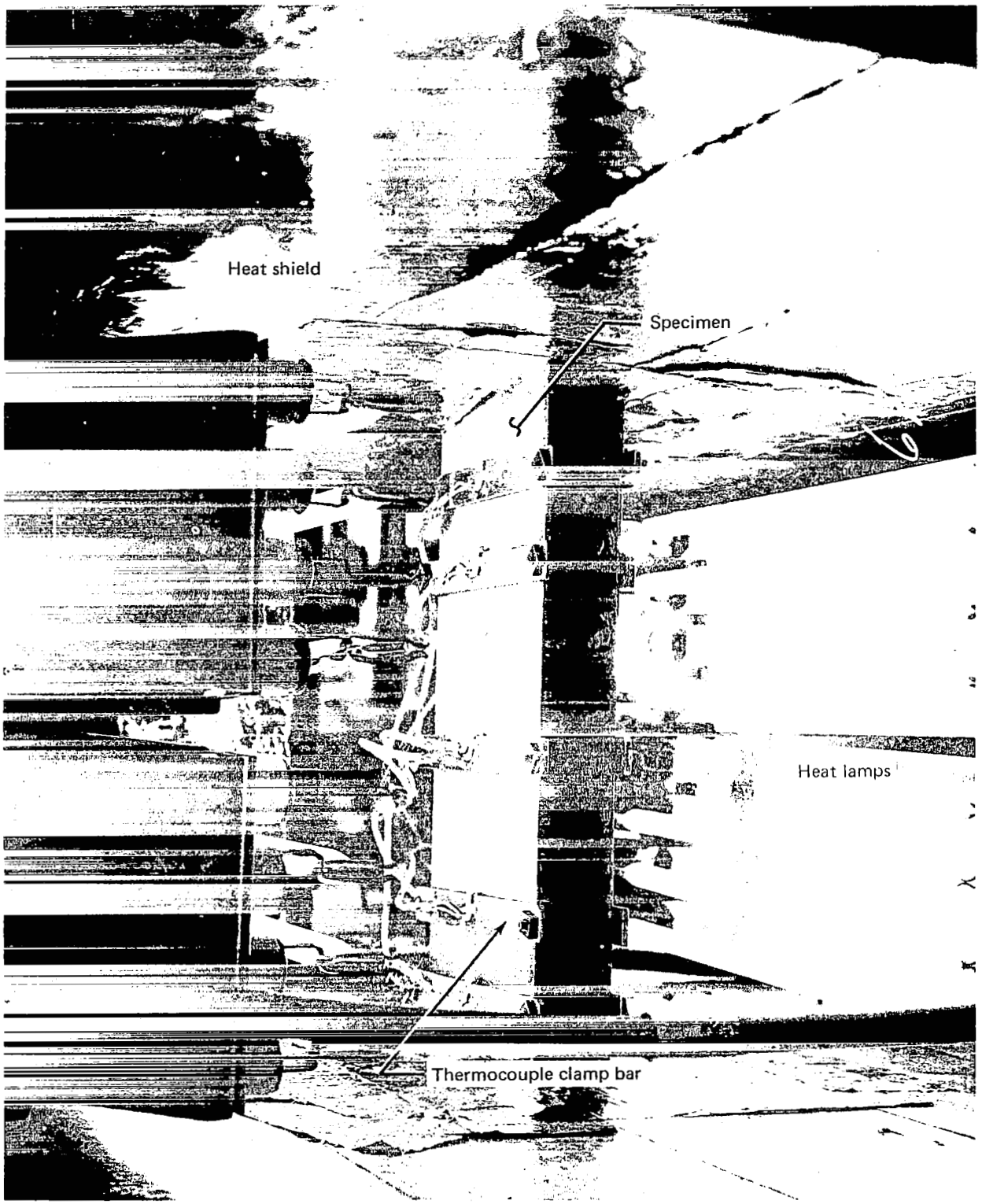

FIGURE 3.–FATIGUE TESTING AT 450° F (505° K)

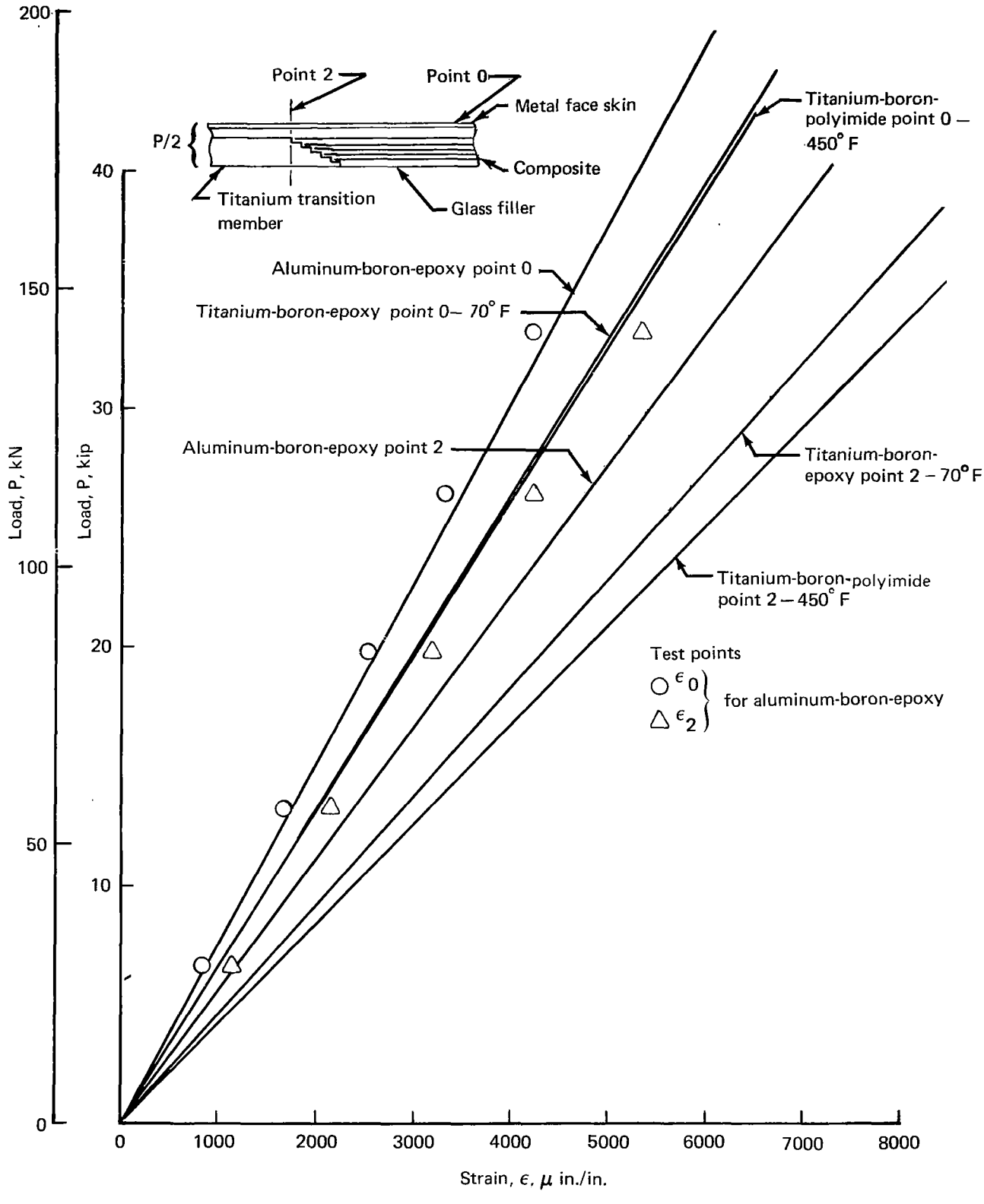

FIGURE 4.—STRAIN AS A FUNCTION OF LOAD FOR STEPPED-JOINT FATIGUE SPECIMEN

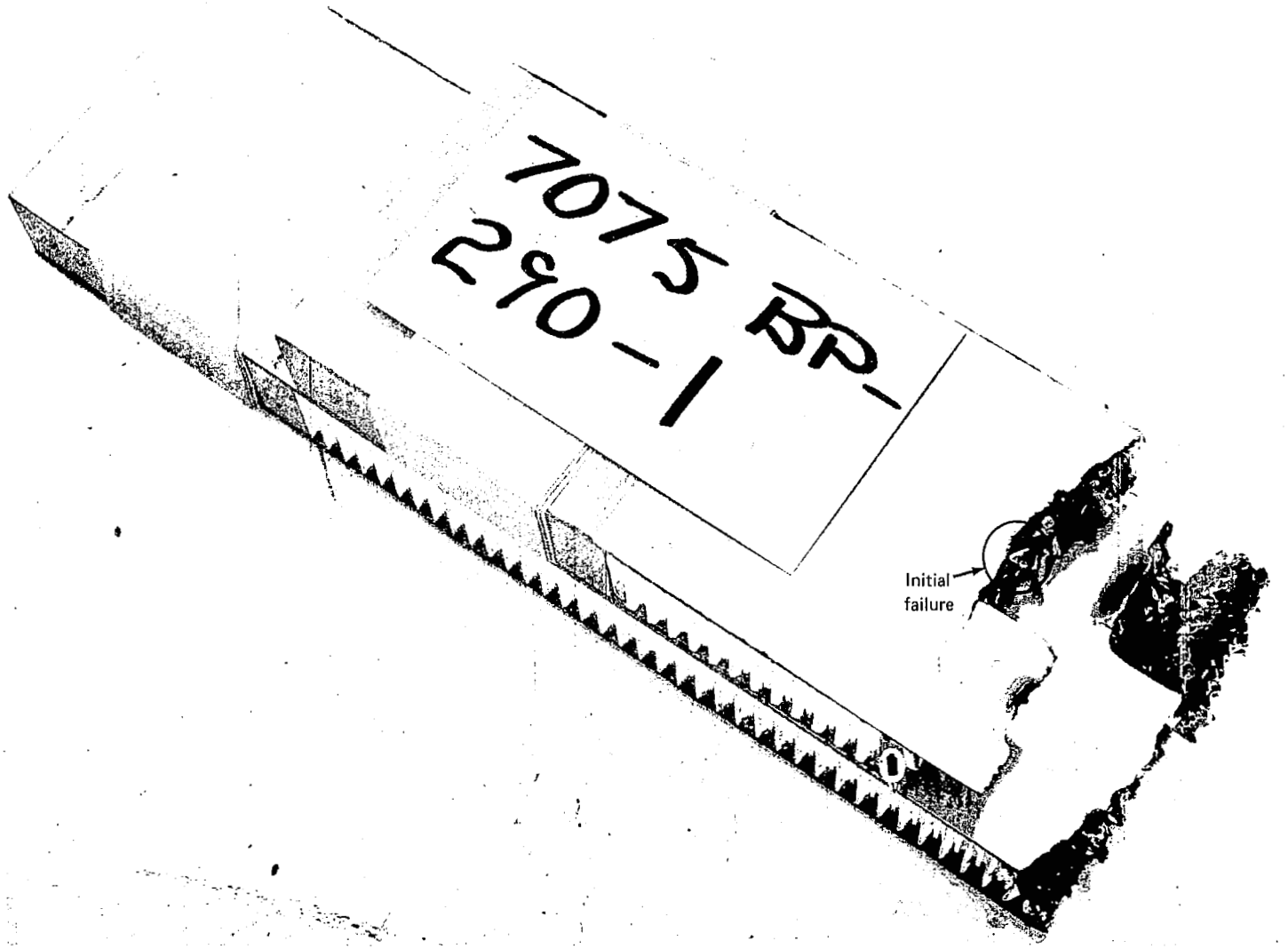

FIGURE 5.– ALUMINUM-BORON-EPOXY FATIGUE SPECIMEN CYCLED AT 0.12 HZ FOR 17 CYCLES

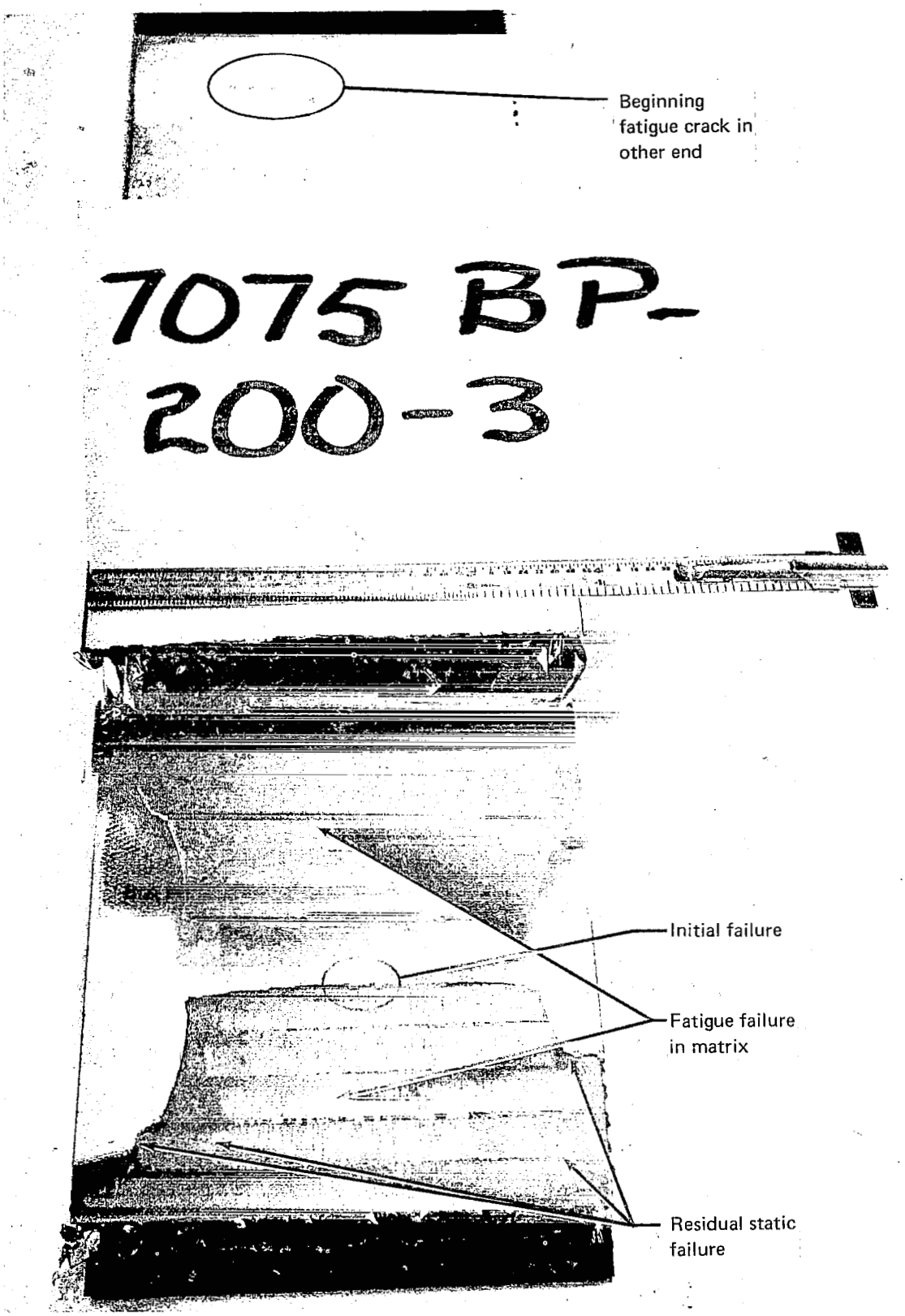

FIGURE 6.—ALUMINUM-BORON-EPOXY SPECIMEN CYCLED AT 16.7 HZ FOR 14 790 CYCLES

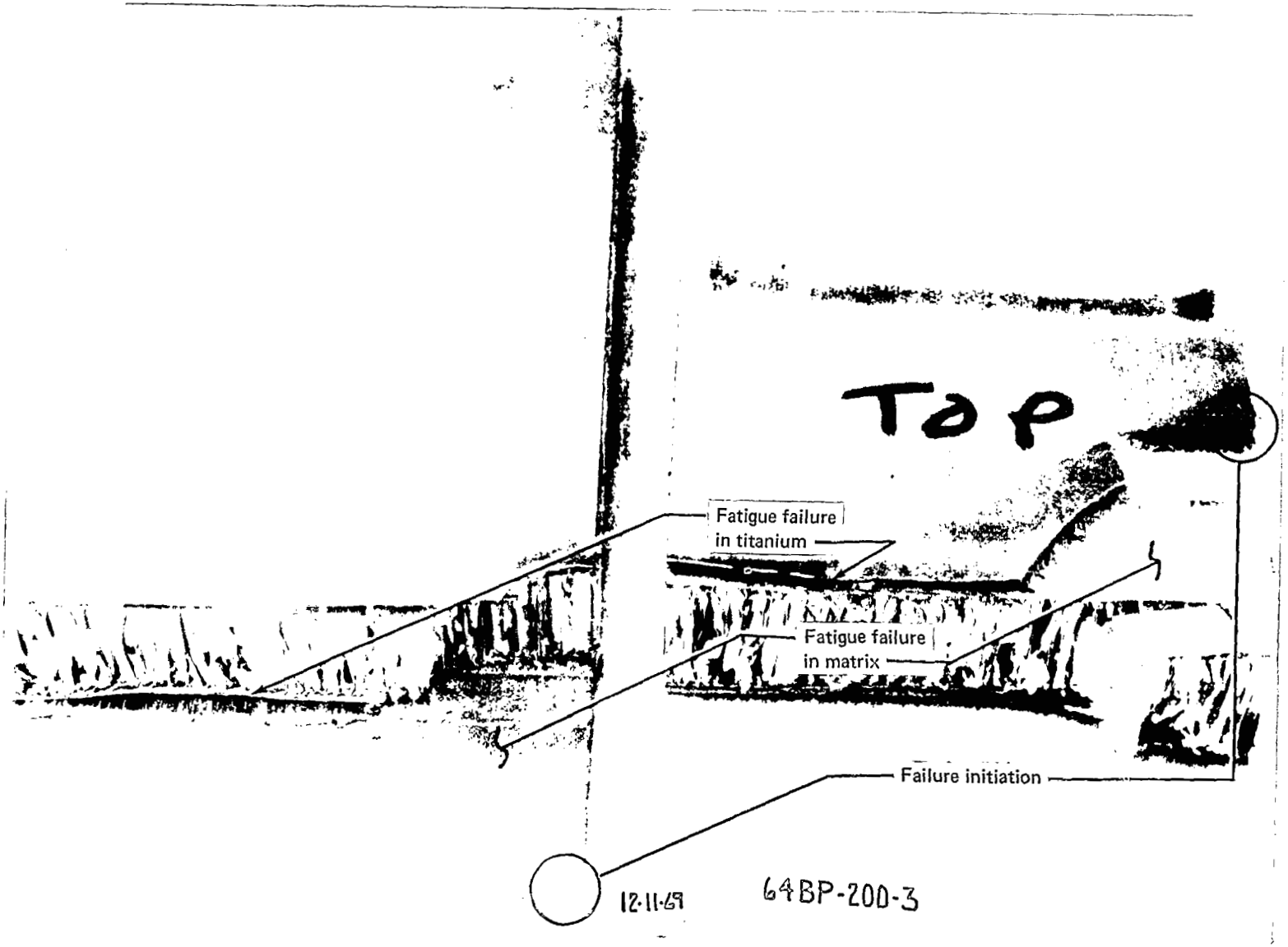

FIGURE 7.—TITANIUM-BORON-EPOXY SPECIMEN CYCLED AT 16.7 HZ FOR 9850 CYCLES

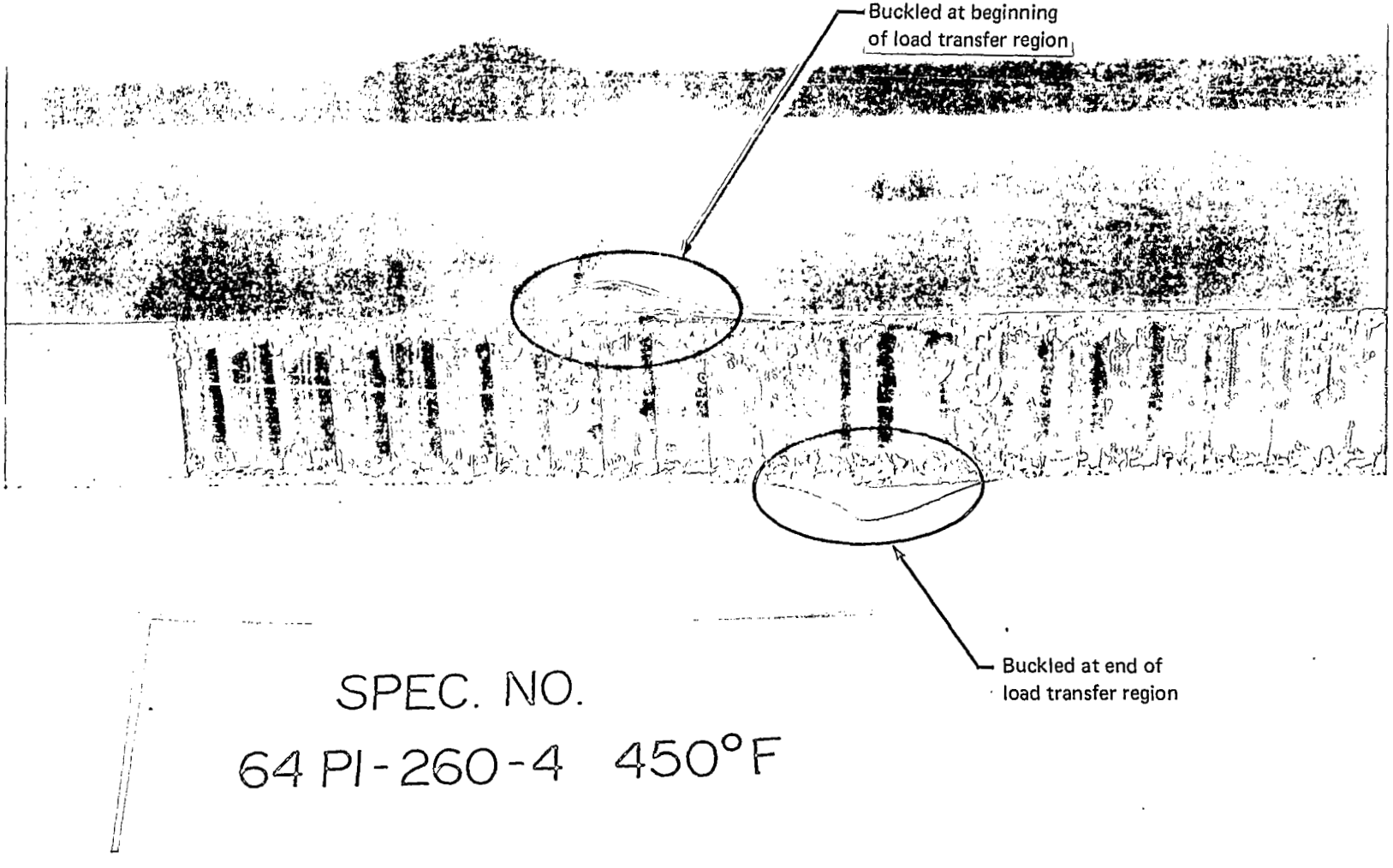

FIGURE 8.—TITANIUM-BORON-POLYIMIDE SPECIMENS CYCLED AT 0.12 HZ FOR 17 CYCLES

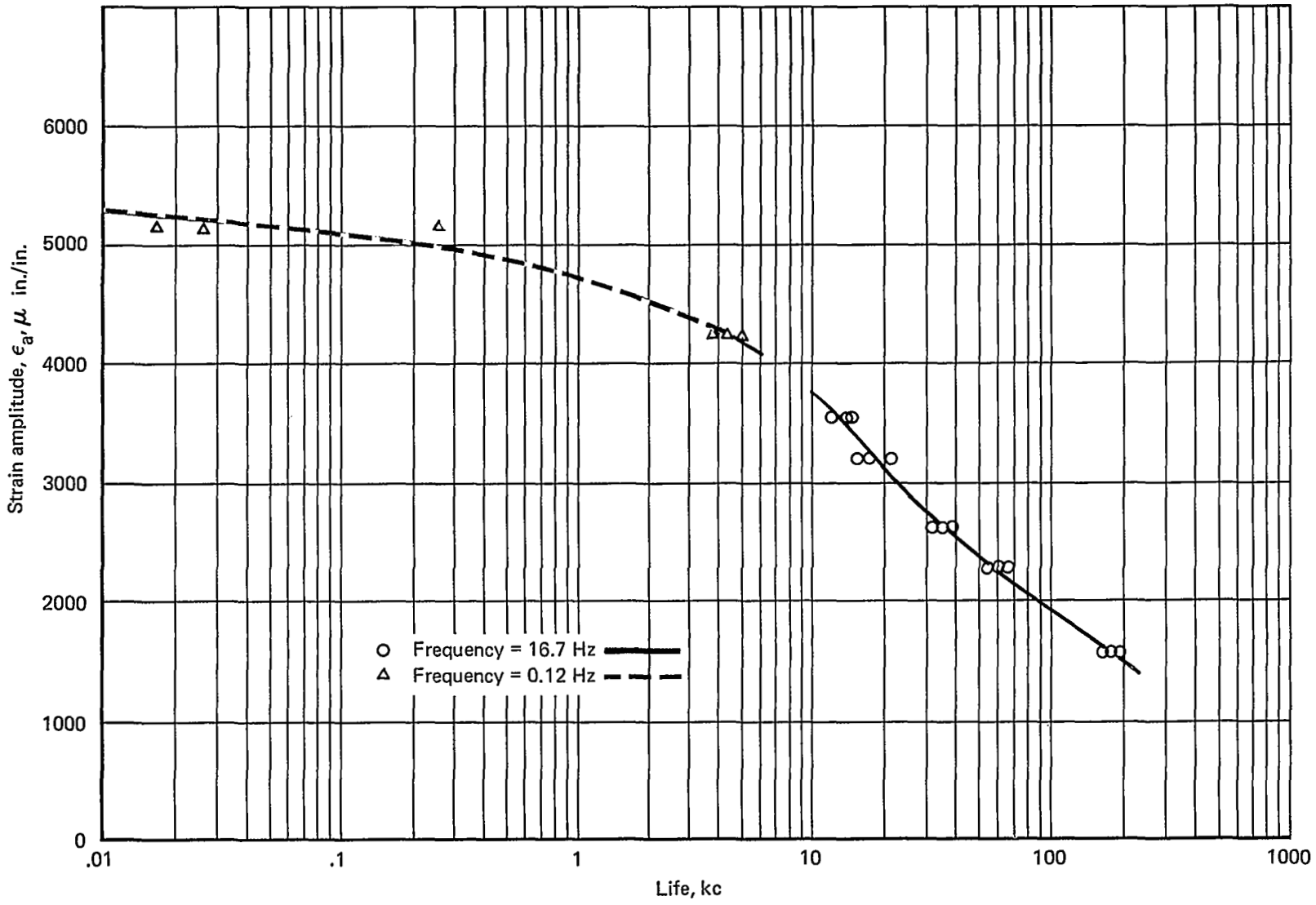

FIGURE 9.—FATIGUE LIFE CURVES FOR ALUMINUM-BORON-EPOXY AT TWO FREQUENCIES, 70° F (293° K), AND R = -1

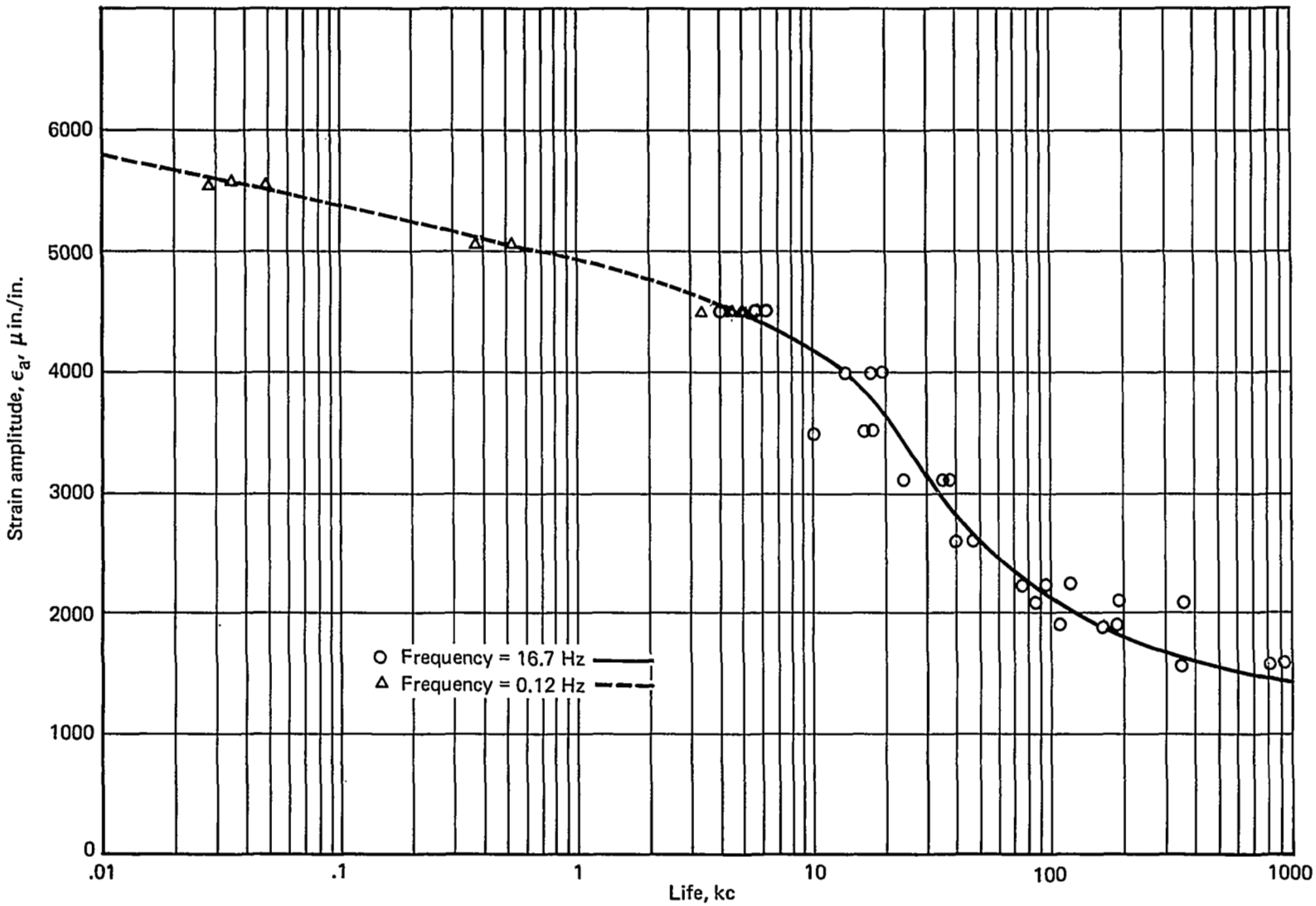

FIGURE 10.—FATIGUE LIFE CURVES FOR TITANIUM-BORON-EPOXY AT TWO FREQUENCIES, 70° F (293° K), AND R = -1

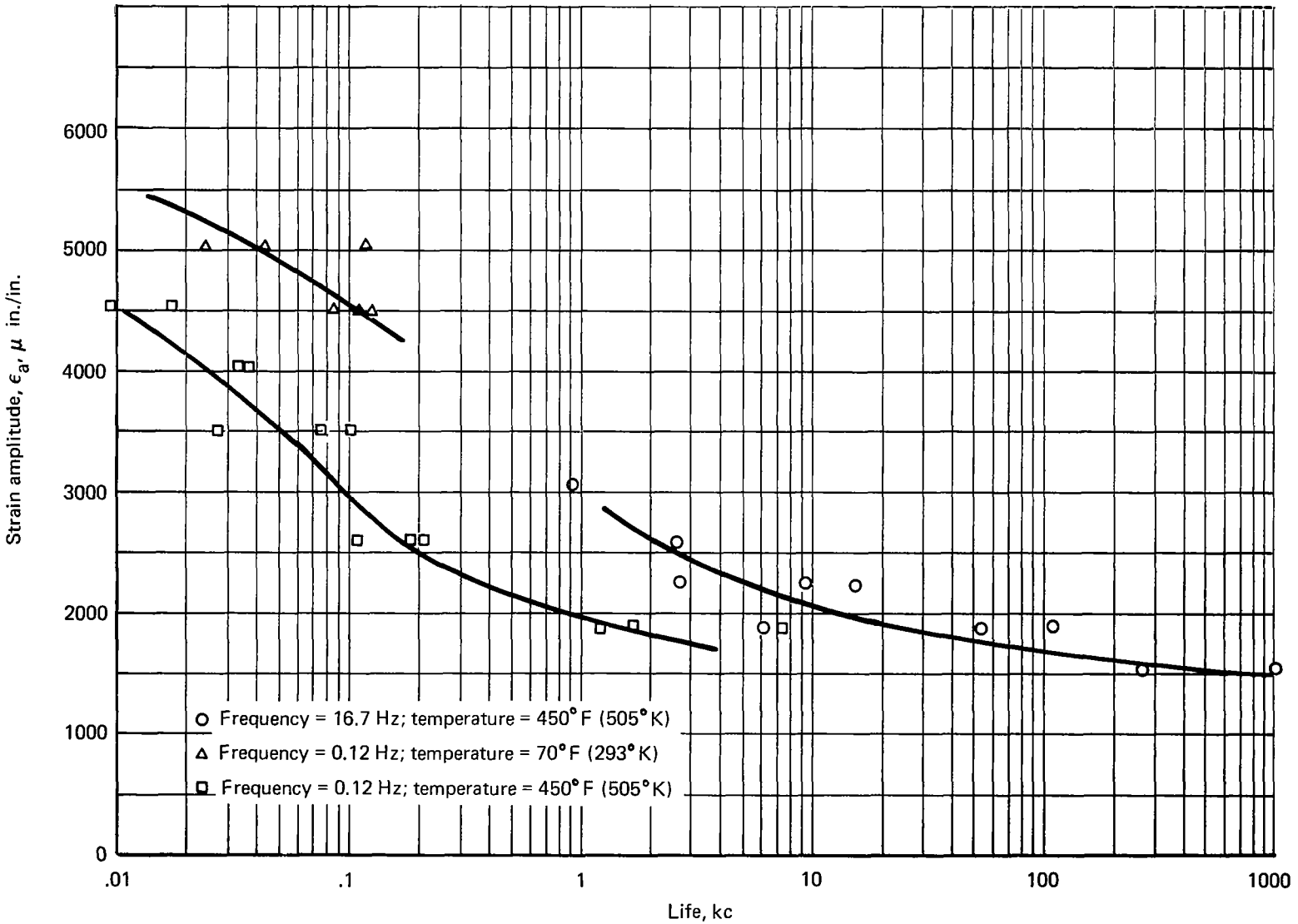

FIGURE 11.—FATIGUE LIFE CURVES FOR TITANIUM-BORON-POLYIMIDE AT TWO FREQUENCIES, TWO TEMPERATURES, AND R = -1

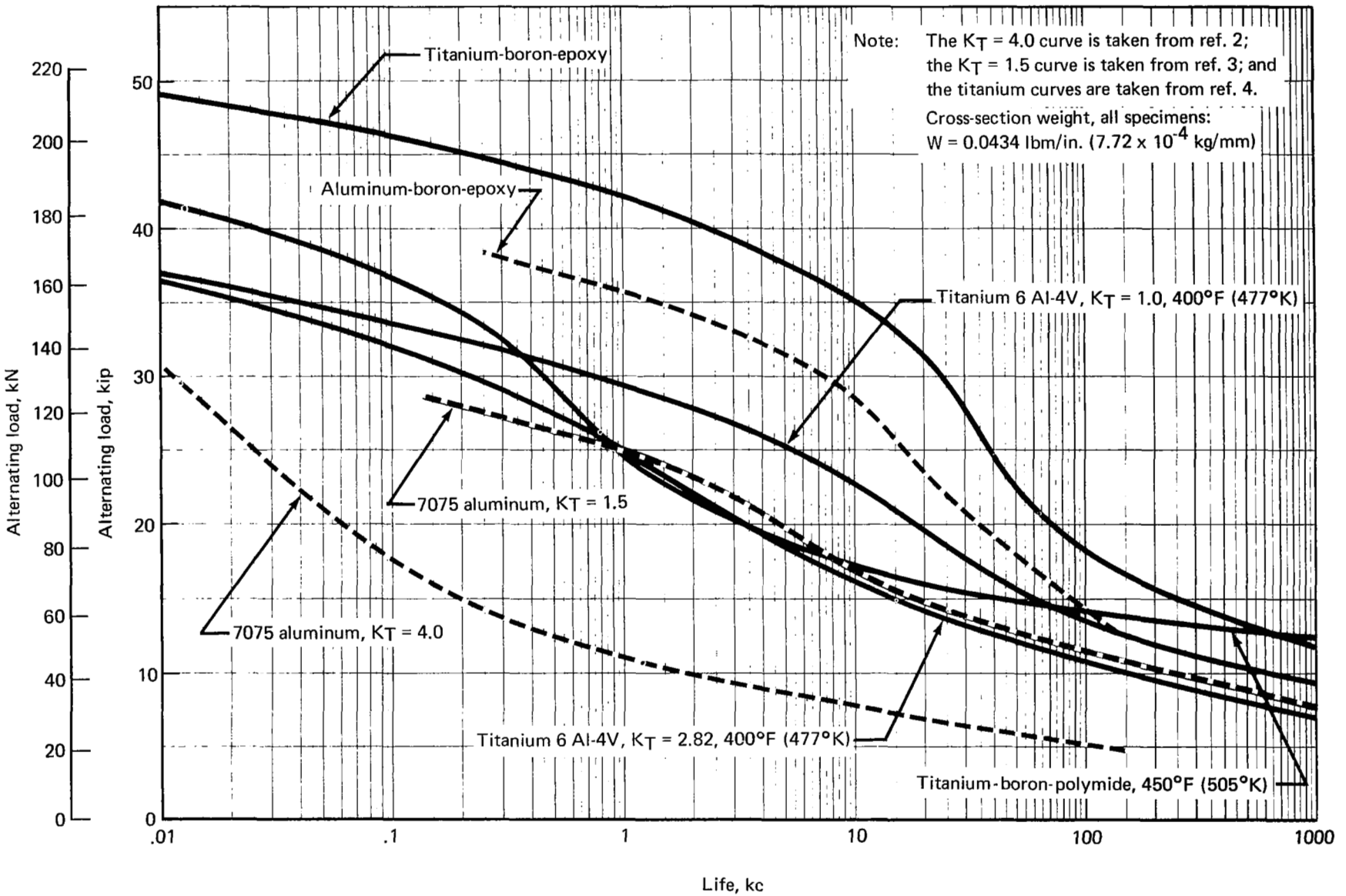

FIGURE 12.– COMPARISON OF REINFORCED AND UNREINFORCED SPECIMENS OF EQUAL WEIGHT

① In matrix at end of longest fiber
② In metal at end of longest fiber (point where debond starts)
③ In stepped fitting (Point where debond ends)
④ In stepped fitting where crack develops

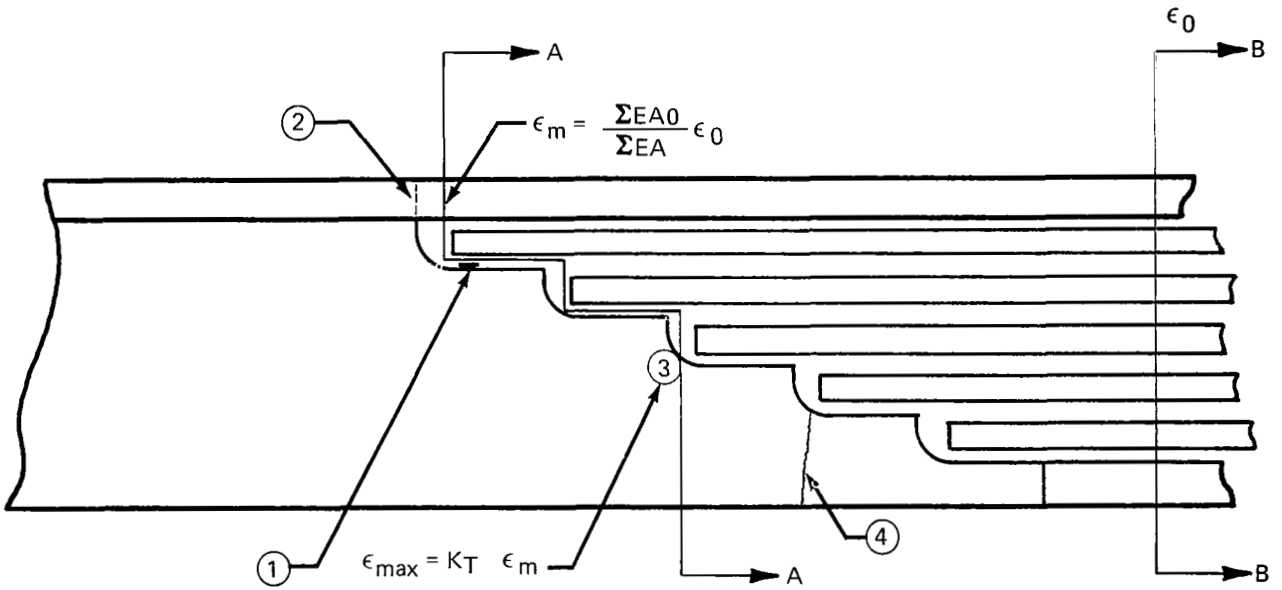

FIGURE 13.–FATIGUE FAILURE PROGRESSION IN STEPPED LOAD TRANSFER REGION

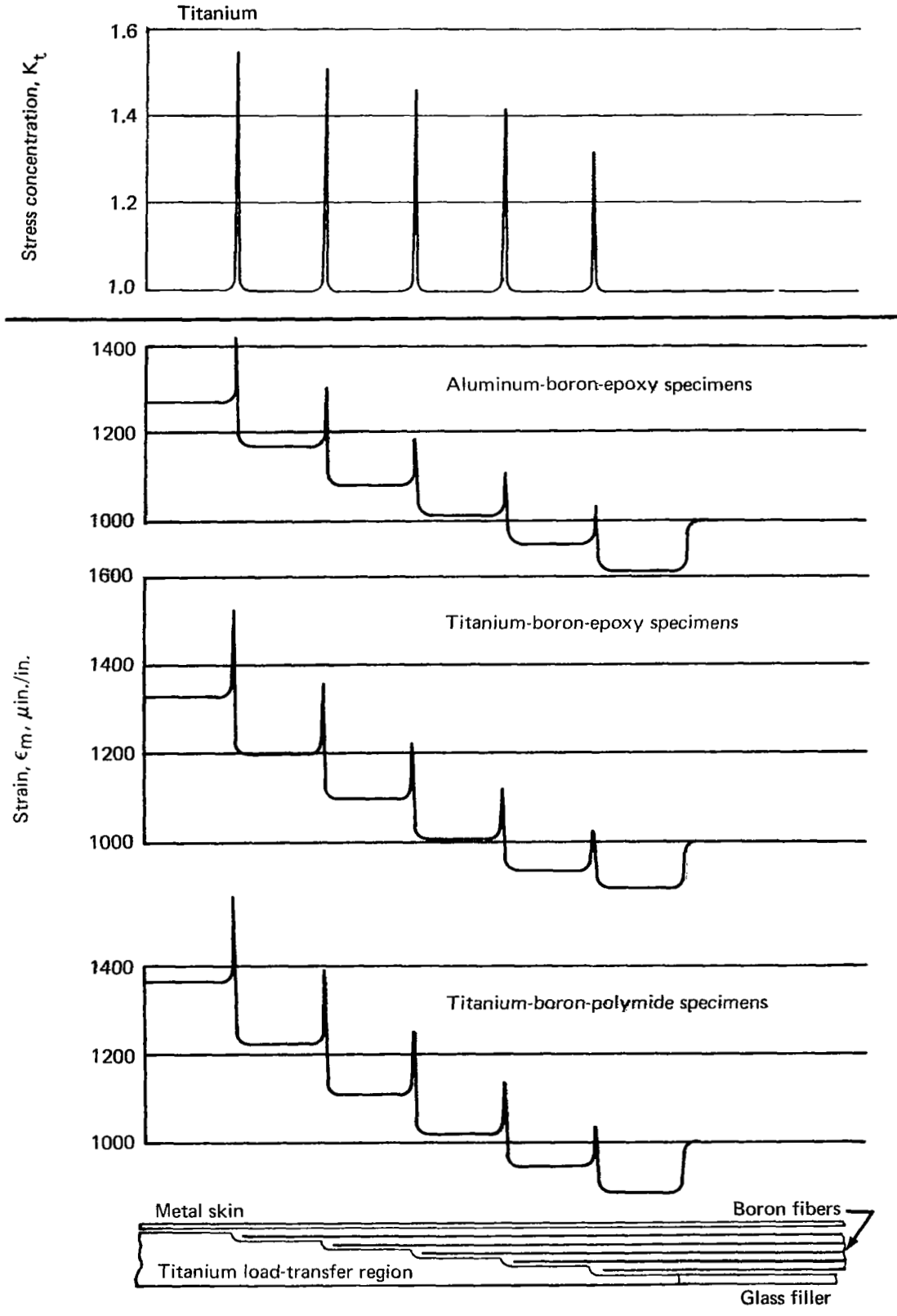

FIGURE 14.–STRAIN IN TITANIUM LOAD TRANSFER REGION FOR FATIGUE SPECIMENS

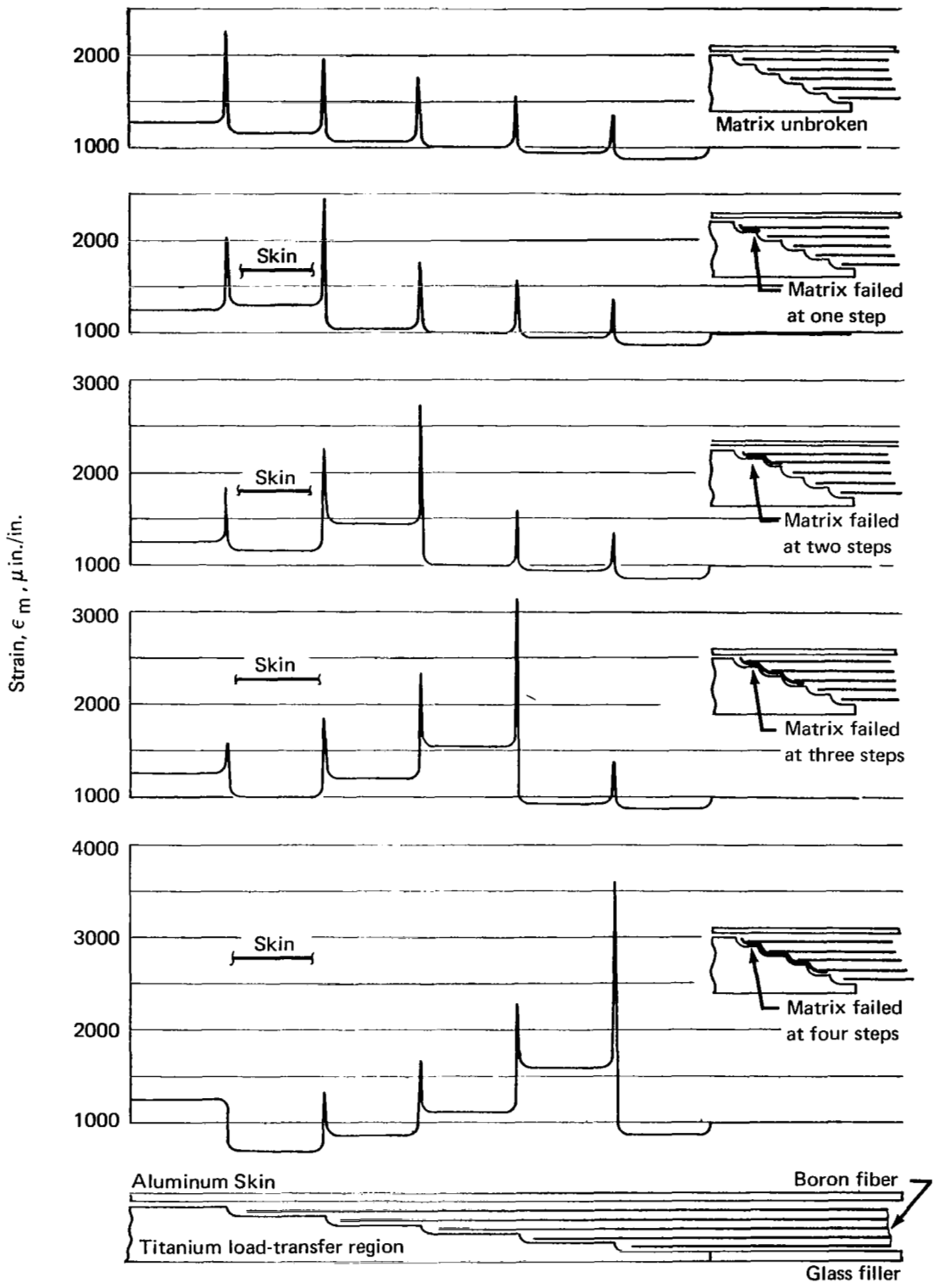

FIGURE 15.—STRAIN IN TITANIUM LOAD TRANSFER REGION FOR ALUMINUM-BORON-EPOXY FATIGUE SPECIMENS

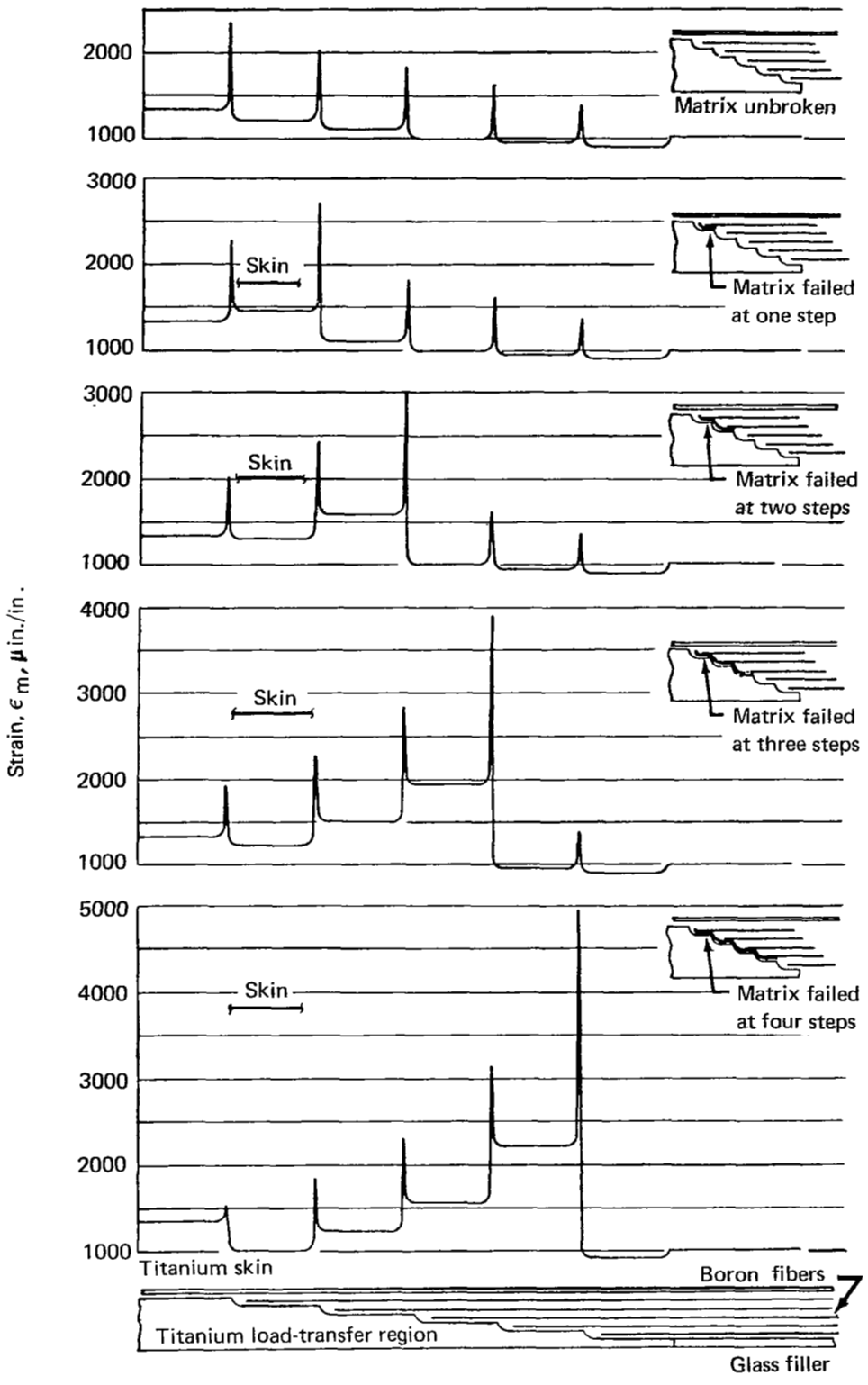

FIGURE 16.—STRAIN IN TITANIUM LOAD TRANSFER REGION FOR TITANIUM-BORON-EPOXY FATIGUE SPECIMENS

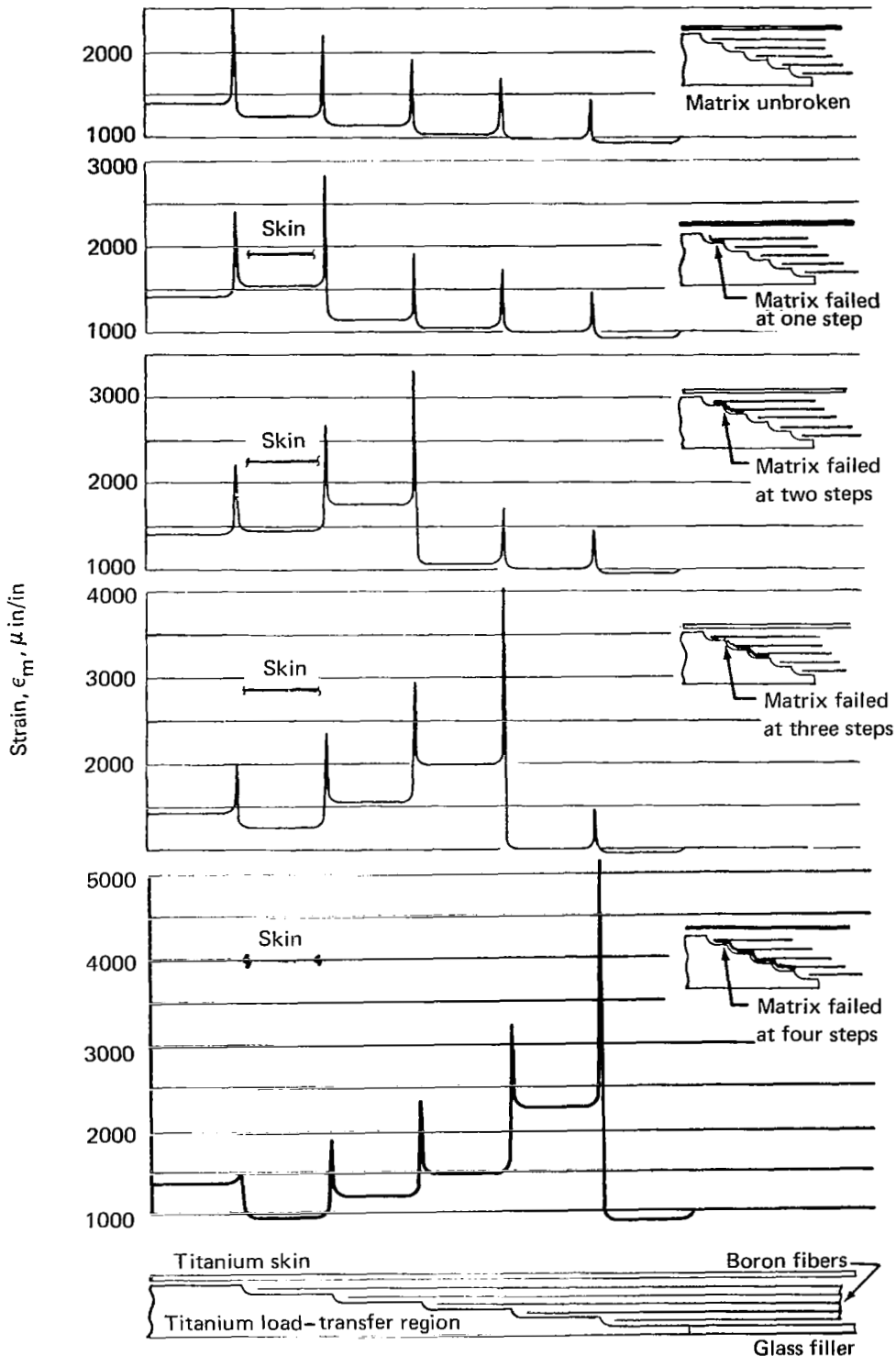

FIGURE 17.–STRAIN IN TITANIUM LOAD TRANSFER REGION FOR TITANIUM-BORON-POLYIMIDE FATIGUE SPECIMENS

THERMAL CYCLING

Objective

The objective of this portion of the investigation was to determine the effects of thermal cycling on the strength and stiffness of a metal-composite laminate between the maximum and minimum temperatures expected in subsonic and supersonic flight.

Background and Approach

One of the functions of the matrix in a metal-composite system is to transfer load by shear from the surface of the filament to the surface of a metal attachment member. Because of the differences in thermal expansion, cyclic thermal testing will develop cyclic shear stresses in the metal-composite interface.

To test the effect of thermal cycling on the matrix in a composite-to-metal structural joint, a metal-faced tensile specimen with stepped titanium load-transfer members was selected. In the specimen, loads are transferred from the filaments through the matrix into a metal step.

The adhesive systems were tested in a simple, short-beam, three-point-bend, interlaminar shear specimen to measure the effect of thermal cycling on adhesive shear properties. This specimen simulates the role of adhesive in the basic section to transfer loads through shear between a structural laminate and a metal skin or stringer.

Aluminum-boron-epoxy and titanium-boron-epoxy were subjected to subsonic flight temperature extremes of -65° to +160° F (219° to 344° K). Titanium-boron-polyimide was subjected to supersonic flight temperature extremes of -65° to +450° F (219° to 505° K). The specimens were cycled between the temperature extremes and statically tested after a certain number of cycles. The static test results were compared to results from phase I (ref. 1).

Specimens and Testing

The interlaminar shear specimens shown in table 5 were of the same design used in phase I, (ref. 1). The specimens tested the room temperature curing EPON 927 in combination with aluminum, AF 126 (250° F, 394° K cure) in combination with titanium, and FM 34 polyimide (350° F, 450° K cure) in combination with titanium. The load-transfer specimens shown in table 6 were the same design used in the composite load-transfer portion of phase I (ref. 1). Before cycling, each specimen was coated with a film of Dow Corning Silastic 882 silicone to prevent direct contact between the specimen and the heating and cooling fluids.

The thermal cycling apparatus is shown in figure 18. The specimens were placed in racks that were moved by pneumatic cylinders to dip alternately into baths of heating and cooling fluid. Each move was initiated when a thermocouple readout from one of the

specimens reached a preset value. Microswitches stopped the motion into each bath and set up the direction of the next move. A readout from another thermocouple was plotted continuously on a roll chart to provide a record of cycle temperatures. A cold alcohol bath and a hot water bath were used for the -65° to +160° F (219° to 344° K) cycles. A cold alcohol bath and a hot oil bath were used for the -65° to +450° F (219° to 505° K) cycles. The cycling rate depended on specimen heat-up and cool-down rates but averaged between 10 to 20 cycles per hour. After 500, 1000, 2500, and 4000 cycles, interlaminar shear specimens were selected at random and removed from the racks. All load-transfer region specimens were run 4000 cycles.

Results of the load-transfer specimen tensile tests are shown in figure 19. Results of the interlaminar shear specimen tests are shown in figure 20. The stiffness response of the interlaminar shear specimens is shown in figure 21.

Analysis and Discussion

The tension test values of specimens with epoxy (BP 907) shown in figure 19 display a 10% decrease over 4000 temperature cycles, whereas the room temperature strength of the reinforced-titanium specimens with polyimide did not change. These degradation values are smaller than the values from figure 20, which show a 76% degradation of the AF 126 system (250° F, 394° K cure), 60% degradation of the EPON 927 (room temperature), and 33% degradation of the FM 34 system (350° F, 450° K cure). The load-transfer specimens with aluminum-boron-epoxy and titanium-boron-epoxy all used BP 907 (350° F, 450° K, cure) and AF 126 (250° F, 394° K, cure). For these specimens, the rate of degradation, as indicated in figure 19, was quite similar. For the interlaminar shear specimens, however, the titanium-boron-BP 907/AF 126 system showed greater degradation than the aluminum-boron-BP 907/EPON 927 system.

During temperature cycling, all specimens were coated with silicone to prevent contact with the heat-transfer fluids: alcohol, water, and oil. After cycling, the silicone coating was damaged on all polyimide specimens yet little degradation of properties occurred. After cycling, the silicone coating was intact on all epoxy specimens, but one titanium-boron-epoxy specimen completely delaminated in test, and a considerable portion of the bond area showed a yellow discoloration. This indicates that the silicone had been permeated by the heat-transfer fluids, and chemical degradation of the epoxy resulted.

A marked stiffness decrease with number of temperature cycles was observed during testing of the interlaminar shear specimens (fig. 21). The shear strength values obtained by the short-beam test are satisfactory only when the relative stiffness of the specimens remains fairly constant. A stiffness decrease indicates that a growing amount of load is carried by bending of the individual members (composite, metal), and the point of adhesive failure becomes increasingly difficult to establish.

Conclusions and Recommendations

Although the investigation is preliminary in character, some conclusions can be drawn.

- The stepped-joint polyimide specimens showed no decrease in tensile strength after 4000 cycles between temperatures of −65°and 450°F (219°and 505°K).

- The stepped-joint epoxy specimens showed a 10% decrease in tensile strength after 4000 cycles between temperatures of -65°and 160°F (219°and 344°K).

- The AF 126 system showed a 76% degradation in interlaminar shear strength after 4000 cycles between temperatures of -65°and 160°F (219° and 344°K).

- The EPON 927 system showed a 60% degradation in interlaminar shear strength after 4000 cycles between temperatures of -65°and 160°F (219°and 344°K).

  The FM 34 system showed a 33% degradation in interlaminar shear strength after 4000 cycles between temperatures of -65°and 450°F (219°and 505°K).

Additional effort should be devoted to the thermal cycling of metal-composite combinations. A better understanding of the nature of cyclic degradation and its effects on composite properties is desirable.

Also, a full understanding of typical environmental effects such as humidity, salt spray, and hydraulic fluid must be accomplished before structural use.

TABLE 5.– ULTIMATE LOAD P AND APPARENT RELATIVE STIFFNESS OF INTERLAMINAR SHEAR SPECIMENS

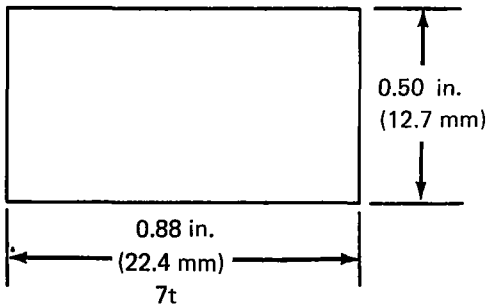

SPECIMEN PLAN VIEW

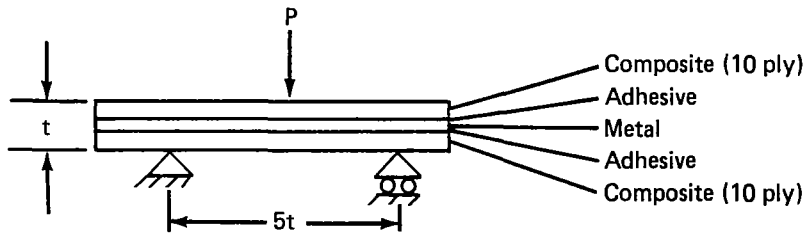

SPECIMEN ELEVATION VIEW
SHOWING TEST LOADING

Specimen	Temperature cycles									
Metal Matrix Adhesive	0		500		1000		2500		4000	
	P_{ult}, lb	Relative stiffness, %	P_{ult}, lb	Relative stiffness, %	P_{ult}, lb	Relative stiffness, %	P_{ult}, lb	Relative stiffness, %	P_{ult}, lb	Relative stiffness, %
0.025-7075-T6			794	67	720	57	624	42	318	24
BP 907	854	100	736	69	710	52	344	27	427	24
Epon 927			816	67	646	52	439	35	272	11
0.007-6Al-4V			784	57	790	53	275	9	271	6
BP 907	1017	100	704	57	766	53	278	8	226	3
AF 126			878	53	768	59	274	9	224	4
0.007-6Al-4V			488	62	402	68	402	66	214	47
35-520	507	100	450	79	406	60	493	76	391	70
FM 34			552	81	437	74	482	68	410	66

[a]Metal code: thickness–alloy

TABLE 6.–STEPPED-JOINT TENSILE TEST VALUES AFTER 4000 TEMPERATURE CYCLES

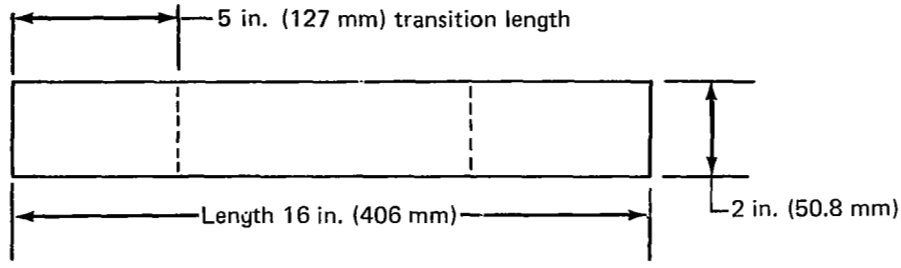

STEPPED-JOINT SPECIMEN PLAN VIEW

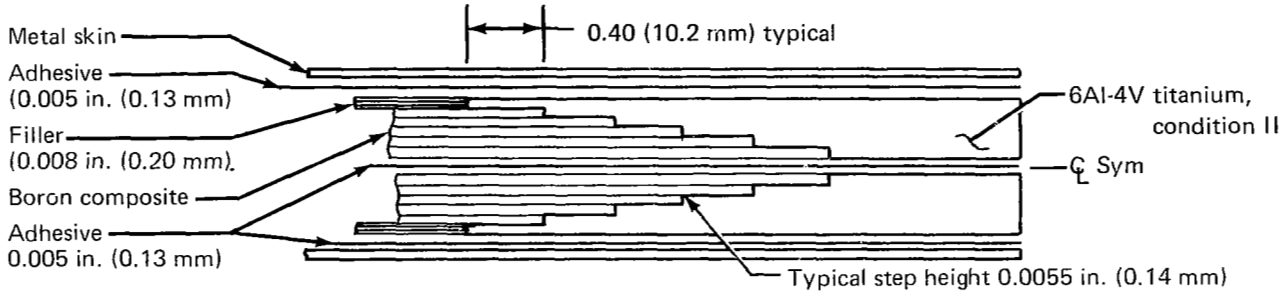

TYPICAL SECTION THROUGH TRANSITION REGION

Specimen Metal[a] Matrix Adhesive	Temperature range °F	 °K	P_{ult}, lb	ϵ_f, μin./in.	σ_f ksi	 kN/mm^2
0.007-6Al-4V BP 907	-65-160	219-344	19 580	5500	322	2.22
AF 126			19 340	5495	318	2.19
0.007-6Al-4V 35-520	-65-450	219-505	19 660	5580	324	2.23
FM-34			18 360	5200	302	2.08
0.025 7075-T6 BP 907	-65-160	219-344	21 740	5280	306	2.10
AF 126			19 400	4730	274	1.89

[a]Metal code: thickness–alloy

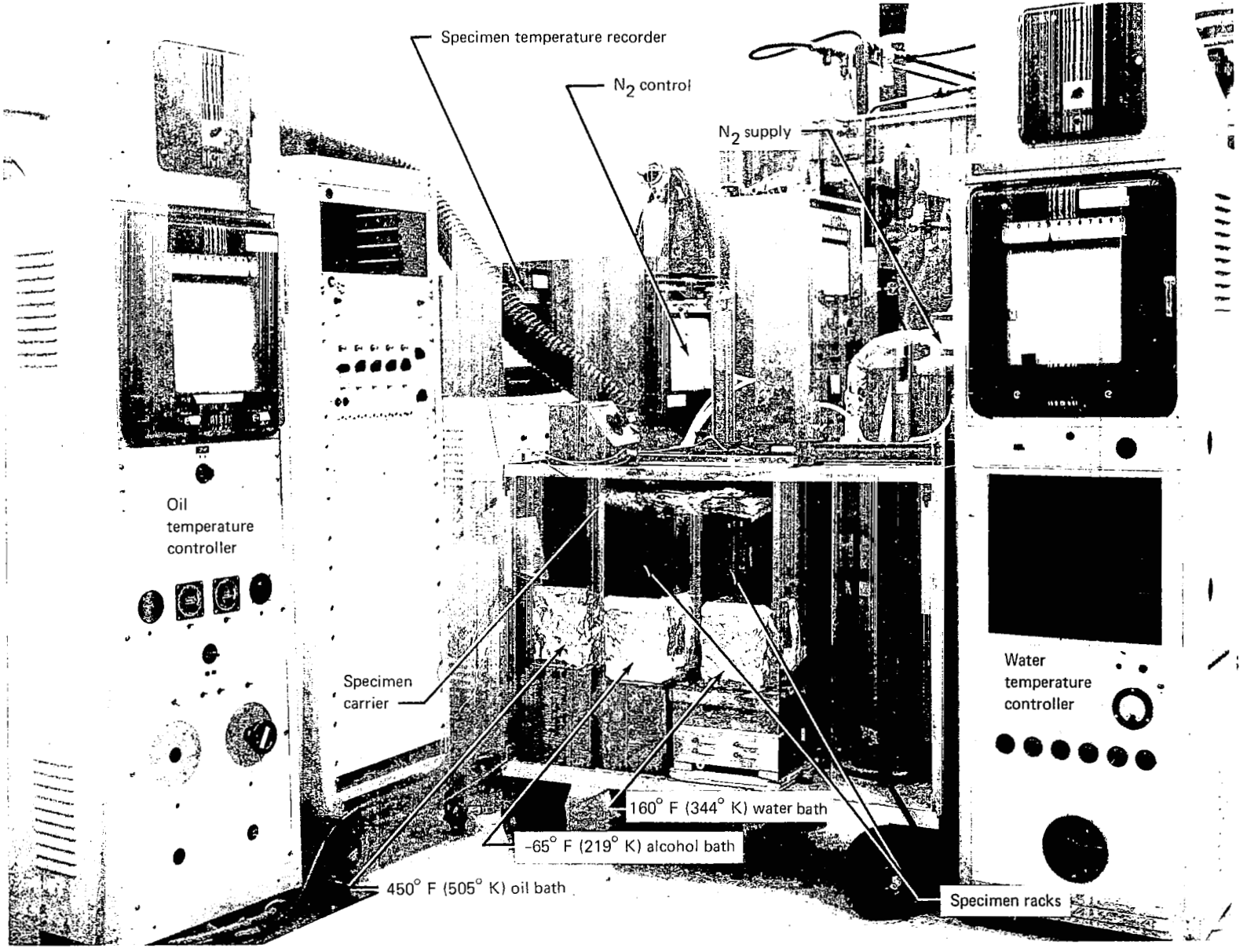

FIGURE 18.–TEMPERATURE CYCLING TEST SETUP

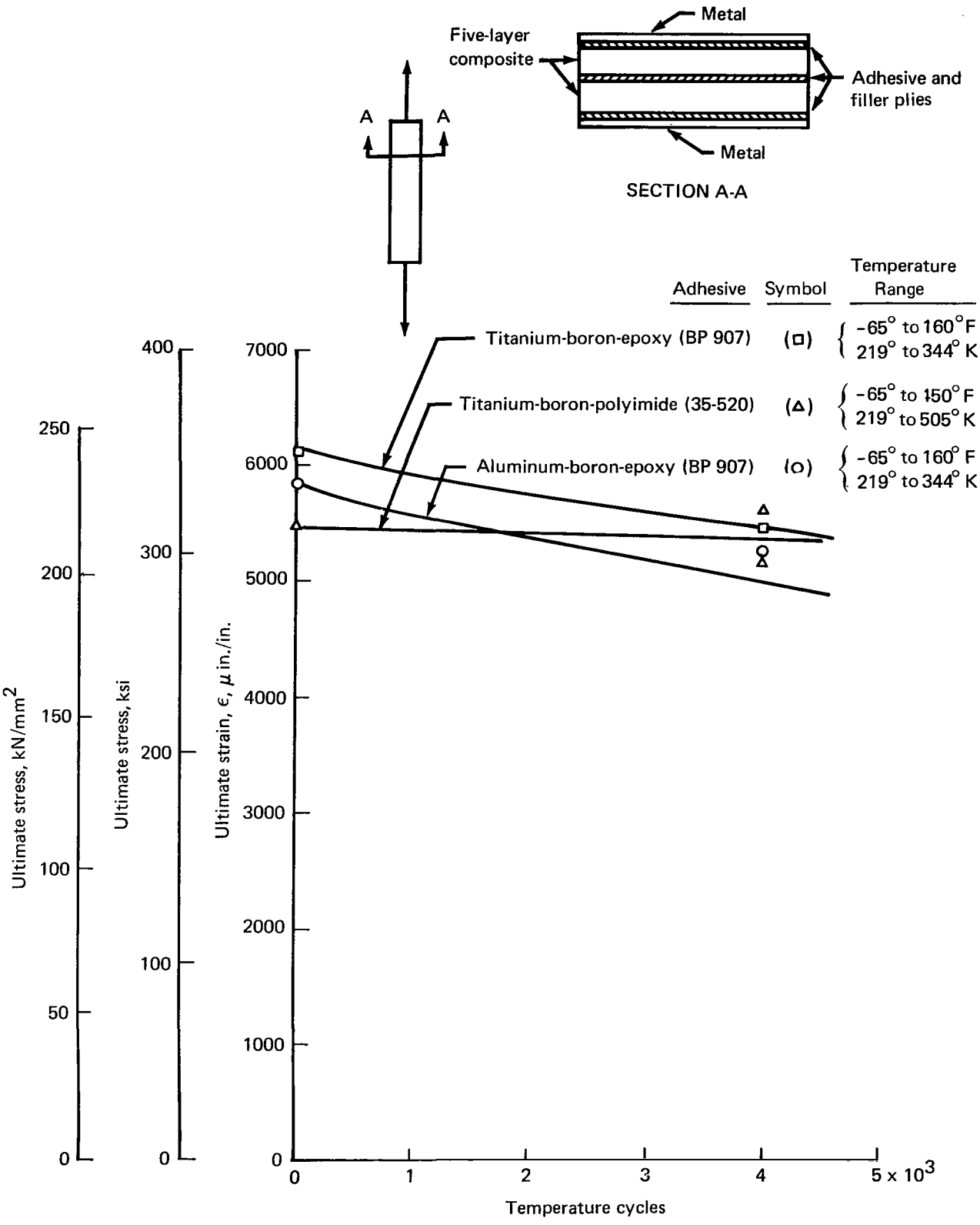

FIGURE 19.—STEPPED-JOINT ULTIMATE FIBER STRENGTH AS A FUNCTION OF TEMPERATURE CYCLES

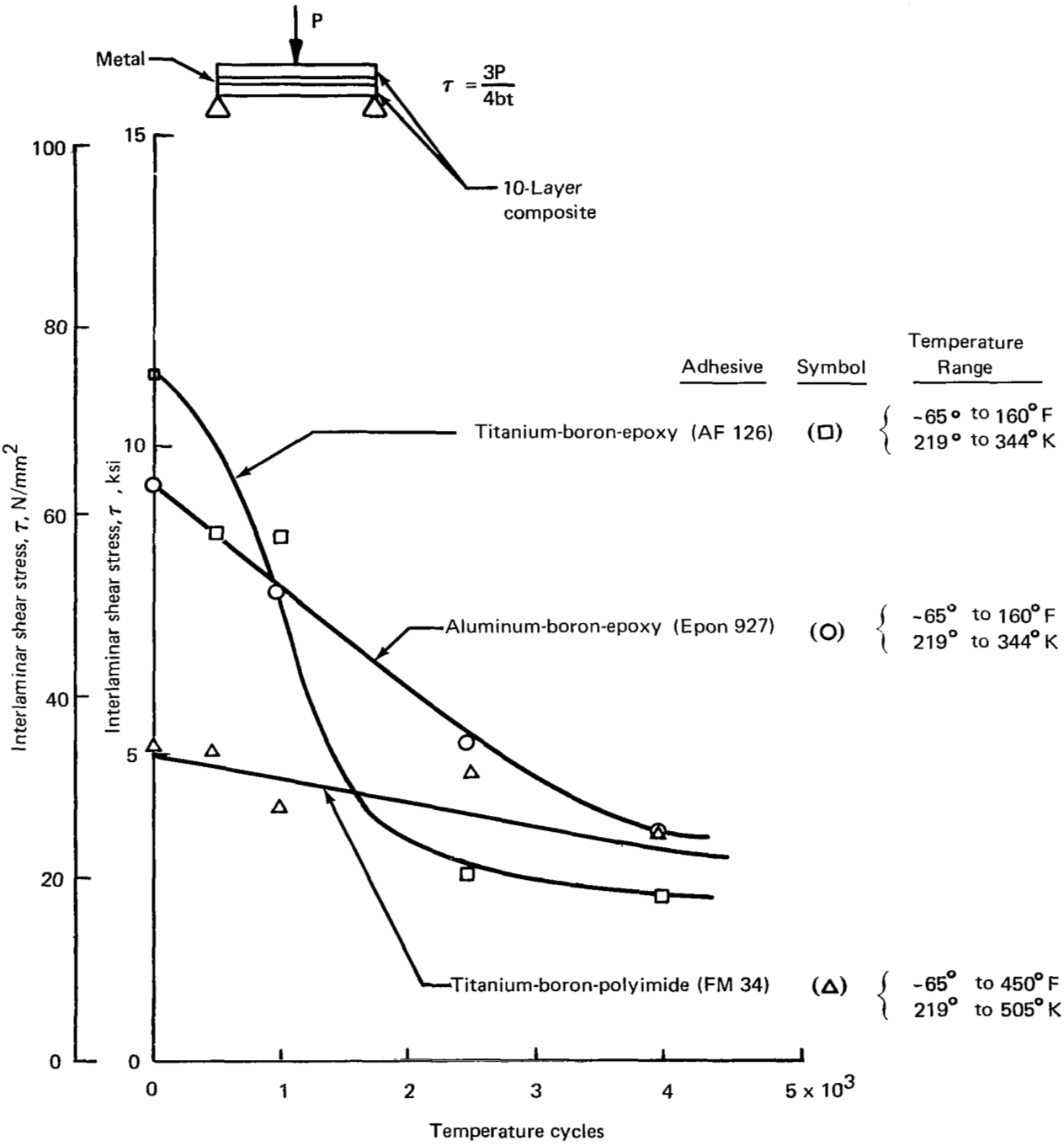

FIGURE 20.–INTERLAMINAR SHEAR STRENGTH AS A FUNCTION OF TEMPERATURE CYCLES

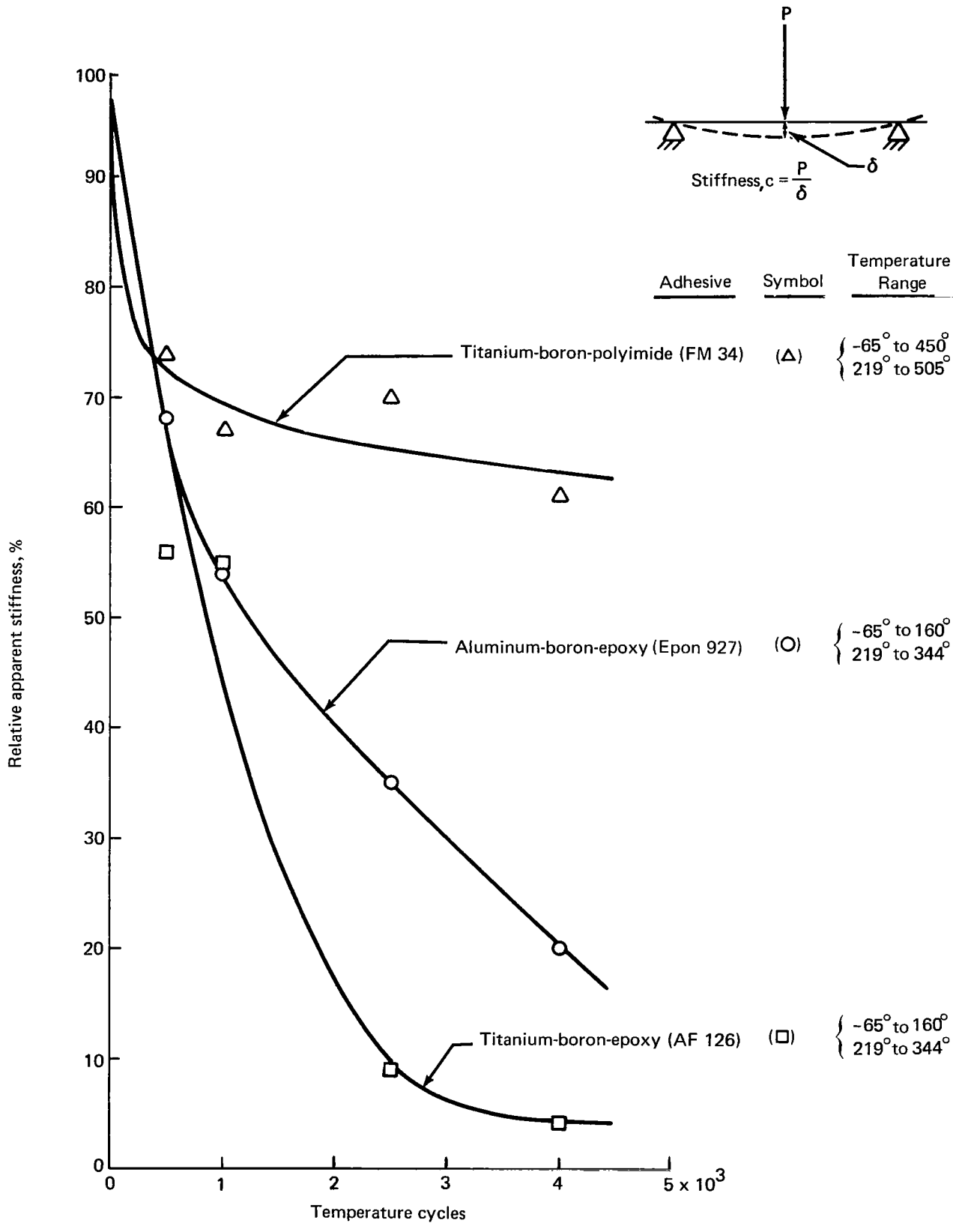

FIGURE 21.—STIFFNESS AS A FUNCTION OF TEMPERATURE CYCLES ON SHORT-BEAM INTERLAMINAR SHEAR SPECIMENS

CREEP TESTING OF A UNIDIRECTIONAL STRUCTURAL LAMINATE

Objective

The creep and delayed rupture investigation was undertaken to determine the creep characteristics of boron composite with a stepped metal load-transfer region.

Background and Approach

Titanium-boron-epoxy specimens were selected for evaluation at a temperature of 160° F (344° K). Titanium-boron-polyimide specimens were selected for evaluation at a temperature of 450° F (505° K). At these temperatures, creep problems were not expected with the boron filaments, but the matrix and adhesive were expected to be vulnerable in the load-transfer region. Test specimens with a load-transfer region on each end were tested under sustained loading at elevated temperatures. Specimens that were unbroken after 1000 hr were tested in static tension at room temperature.

Specimens and Testing

Specimens were fabricated as shown in table 7. Five layers of boron composite were terminated at stepped load-transfer fittings at each end. Step lengths on one end of the specimen were 0.10 in. (2.54 mm) longer than at the other end to reduce the total number of specimens needed to evaluate various step lengths. The matrix resin provided the bond to the titanium step members.

The specimens were tested in the setup shown in figure 22. Load was applied by means of weights on a lever arm. A hydraulic cylinder was used to gradually lower weights to a working position. A cover glass was placed over the open face of the test chamber. No variation in fiber capability is anticipated in the temperature range in question, so the stress level σ_f = 150 ksi (1.032 kN/mm^2) is 44% of estimated ultimate fiber stress σ_f = 340 ksi (2.34 kN/mm^2). It was picked high to reveal problems in the 1000 hr allocated to the test.

Analysis and Discussion

The test specimen data and loads are tabulated in table 7. Figure 23 shows plots of the inelastic deformation δ for each specimen that survived more than 30 hr. The elongation during test is

$$\Delta\lambda = \frac{P\lambda}{\Sigma AE}$$

For ϵ_f = 2590 μin./in. (σ_f = 150 ksi), the elongation over a reference length λ of 3.0 in. (76.2 mm) is

$$\Delta\lambda = (3.0)(2590)(10^{-6}) = 7.80 \times 10^{-3} \text{ in. } (0.198 \text{ mm})$$

The actual deformation along the load-transfer region will vary only slightly from this value (fig. 14). The inelastic deformation (fig. 23) was calculated by

$$\delta = \delta_{measured} - \Delta\lambda$$

The temperature difference necessary to give a $\delta = 0.001$ in. is

$$\Delta T = \frac{\delta}{\lambda \kappa_{co}} = \frac{0.001}{(3.0)(4.05)(10^{-6})} = 82^{\circ}\,F$$

which shows a low sensitivity of δ to small temperature variations. The temperature variation along the test specimens did not exceed 10° F during testing. The deformations shown in figure 23 were obtained by measuring the distance between marks on metal clips attached by friction to the specimens. The original test plan called for a 4.00-in. (102 mm) gage length. The available test equipment permitted only a 3.0-in. (76.2-mm) gage length. This caused the clips nearest to the specimen center to touch the metal part of the load transfer region. On specimens where this happened, the measured deformation is a mixture of the elastic and inelastic deformation taking place along the load-transfer region of the specimens. The negative inelastic deformation measured for specimen 3A is a consequence of the two legs of the clip trying to follow the two different motions of the metal and the composite.

With 0.4- to 0.5-in. (10.2 to 12.7 mm) step lengths, one polyimide specimen (-4) failed during loading, and the other, an epoxy specimen (-1), failed after 18 hr. With 0.5- to 0.6-in. (12.7- to 15.2-mm) step lengths, one polyimide specimen failed during loading, one was tested at room temperature at NASA, and two epoxy specimens ran 21 and 27 hr. With 0.6- to 0.7-in. (15.2- to 17.8-mm) step lengths, the two polyimide specimens ran 622 and 1000 hr; one epoxy specimen ran 1005 hr. The two specimens that ran 1000 hr were static tested to failure at room temperature. The polyimide specimen failed at 2125 lb (9450 N), which is only slightly above creep test load. The epoxy specimen went to 4430 lb (19 600 N) and developed full fiber stress indicating no damage occurred in the creep test.

The tests indicate a great amount of scatter in the performance of the polyimide specimens and a somewhat more predictable behavior of the epoxy specimens. As the step length increases and the shear stresses in the matrix decrease, the time to rupture seems to increase for both epoxy and polyimide specimens. The low value of static strength at room temperature indicated by polyimide specimen -5B and the high degree of scatter experienced with these specimens may have resulted from the sensitivity of polyimide systems to processing variables.

Conclusions and Recommendations

The tests have revealed that creep rupture appears to be a significant problem for the matrix systems investigated—BP 907 at 160° F (344° K) and 35-520 at 450° F (505° K). However, limited testing gives the results a preliminary character.

More work is needed to create an understanding of the basic behavior of matrix and adhesive under long-time shear stress exposure. Also, more effort is needed to develop processes and specifications that ensure that full fiber strength in the concepts is obtained consistently in a flight environment and that there is small scatter in performance values.

TABLE 7. –CREEP AND RUPTURE TEST VALUES

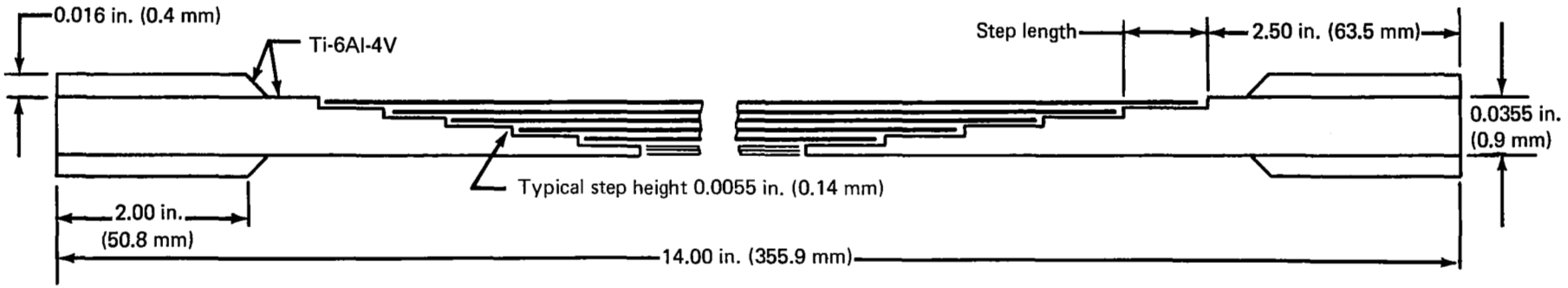

STEPPED-JOINT CREEP SPECIMEN

[1.00 in. (25.4 mm) wide]

Specimen	Temperature		Matrix	Load, lb	Fiber stress, σ_f		Exposure, hr	Step length, in.		Notes
	°F	°K			ksi	kN/mm^2		Short	Long	
-1	160	344	BP 907	1960	150	1.03	18	0.4	0.5[a]	
-2A	160	344	BP 907	2176	166	1.14	27	0.5[a]	0.6	
-2B	160		BP 907	1960	150	1.03	21	0.5[a]	0.6	
-3A	160	344	BP 907	1960	150	1.03	1005	0.6[a]	0.7	Static failure at 70° F, P = 4430 lb
-3B	70	293	BP 907	4065	311	2.14	0	0.6[a]	0.7	Static failure (NASA Langley)
-4	450	505	35-520	1960	150	1.03	0	0.4	0.5[a]	
-5A	450	505	35-520	1960	150	1.03	0	0.5[a]	0.6	
-5B	70	293	35-520	1810	138	0.95	0	0.5[a]	0.6	Static failure (NASA Langley)
-6A	450	505	35-520	1960	150	1.03	1000	0.6	0.7[a]	Static failure at 70° F, P = 2125 lb
-6B	450	505	35-520	1960	150	1.03	622	0.6	0.7[a]	

[a]Failed end.

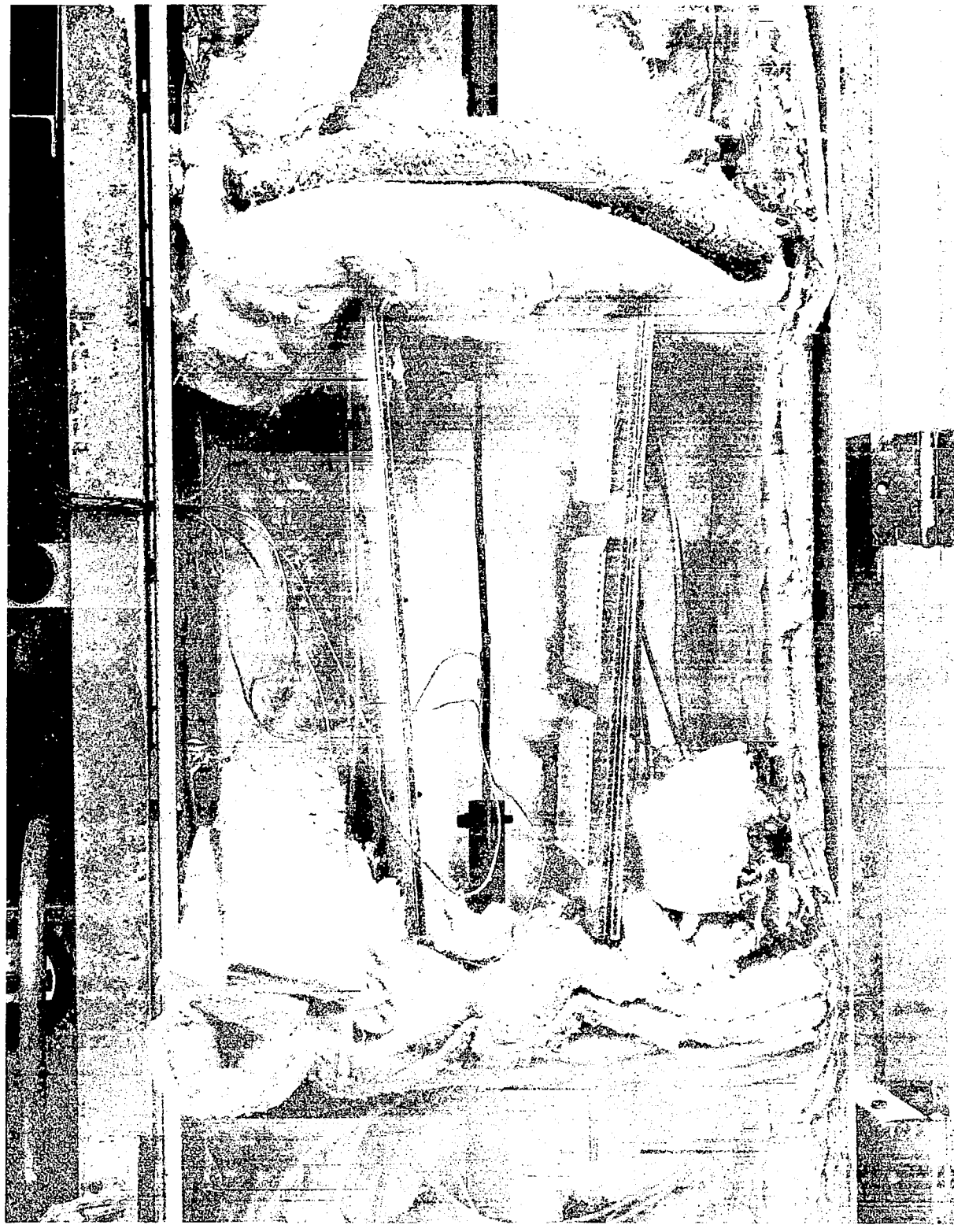

FIGURE 22.–CREEP AND RUPTURE TEST SETUP

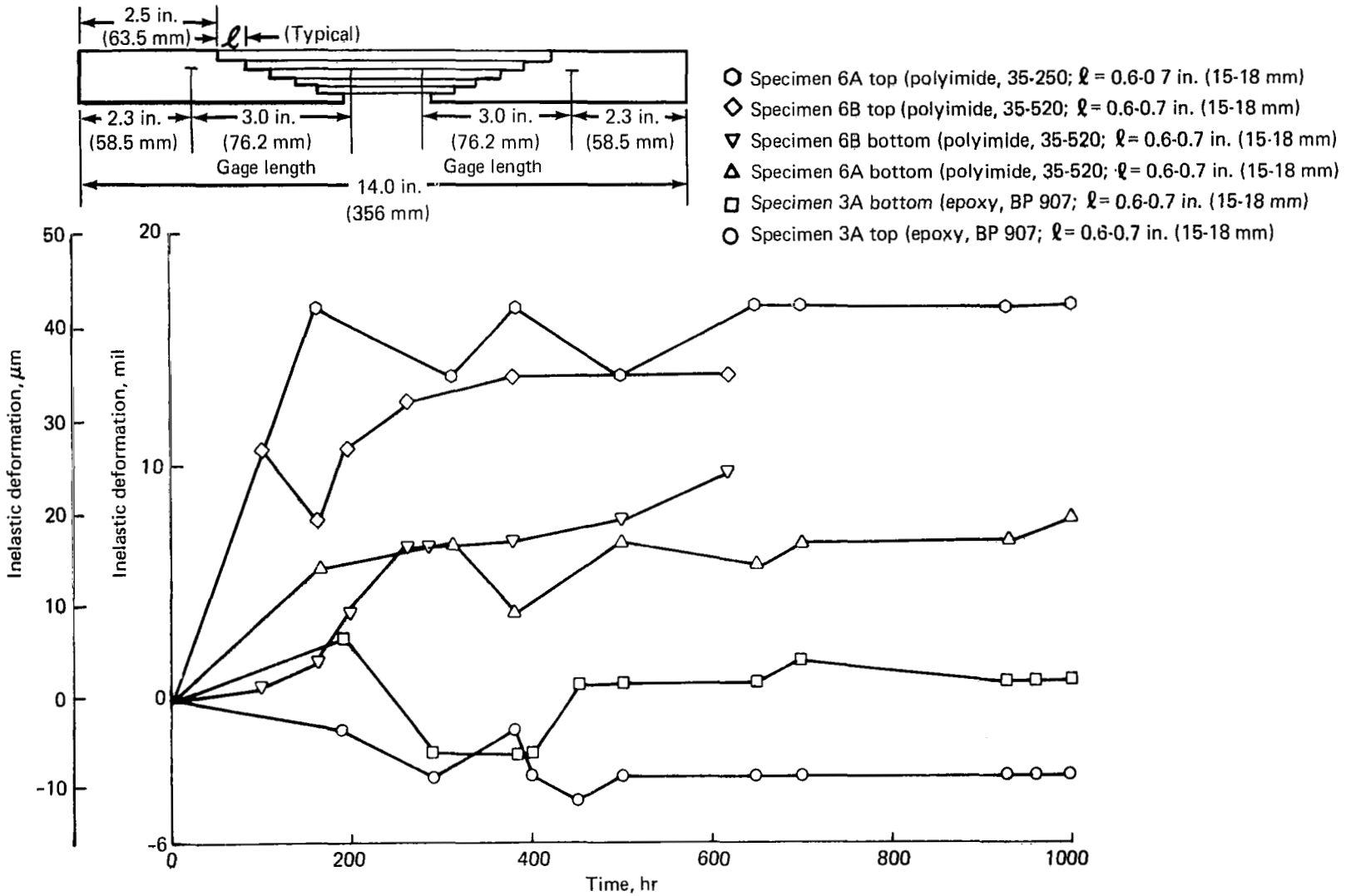

FIGURE 23.–INELASTIC DEFORMATION IN LOAD TRANSFER REGION DURING 1000-HR CREEP TEST

FATIGUE CRACK PROPAGATION AND RESIDUAL STRENGTH

Objective

This portion of the investigation considered the crack propagation and residual strength of several of the metal structural panel concepts reinforced with composites that were introduced in phase I (ref. 1).

Background and Approach

Flat panels of equal size and equal static strength but with different structural concepts were selected. The size selected was 16 by 36 in., (405 by 915 mm). The static design capabilities were:

Axial load = 8.9 kip/in. (1.56 MN/m) compression

Shear = 3.15 kip/in. (0.55 MN/m)

All panels consisted of metal reinforced with unidirectional boron filament composites. Unidirectional composites have little capability to resist shear, so, in each panel design, the minimum amount of metal capable of resisting the in-plane shear was used. Additional metal was used to carry a portion of the axial load in some of the panels. The following categories of panel concepts were studied:

- Minimum metal concepts
  - Honeycomb with distributed reinforcement
  - Honeycomb with concentrated or strap reinforcement
- More-than-minimum metal concepts
  - Hat stringers with simple skin
  - Hat stringers with honeycomb skins

An initiating crack 1 in. (25 mm) long was cut in the center of the skins of each panel. The panels were subjected to cyclic load (R = -1) until the crack had grown to a length of 4 in. (102 mm). After cycling, the panels were tensile tested to destruction to determine the residual strength. The damage containment capability was judged on the basis of cycles required to propagate a crack from 1.0 to 4.0 in. (25 to 100 mm), residual strength, and weight per unit surface area. The results were compared to preliminary design data for aluminum and titanium.

Specimens

Thirteen panels 16 in. (0.406 m) wide by 36 in. (0.915 m) long were fabricated for testing. Figures 24 through 28 show typical section views, detail views, and materials used in the panels. A summary of concepts, and cross-section properties is shown in table 8.

Face skins with distributed reinforcement were made as subassemblies having five plies of composite and the fiber ends terminated into five-step titanium load-transfer regions with the matrix acting as the bond. The concept-1c polyimide panel skins deviated from standard practice. The face skins were chem-milled all over one face so the step transitions were an integral part of the skins.

Straps were fabricated using five plies of boron with five-step titanium load-transfer regions on each end. Four five-ply straps were then laminated using AF-126 epoxy adhesive with epoxy matrix or FM 34 polyimide adhesive with polyimide matrix.

The subassemblies, skins, straps, and stringer caps were bonded to steel or aluminum load blocks on both ends of all panels. Figure 29 shows a steel load block used on a concept-2c honeycomb-strap-titanium-polyimide panel. Figure 30 shows the steel load blocks used on the concept-4b hat stringer-honeycomb skin-titanium-epoxy panel.

Special precautions were taken with the polyimide specimens to ensure unrestricted outgassing of bond lines during cure. All of the honeycomb cells were perforated through the side walls. The end blocks had a number of narrow slots machined in them to provide vent channels as shown in figure 29.

Before testing, crack starters were cut in the center of each face skin of the panels as shown in table 8. A hole was drilled from which a slot was hand sawn and sharpened at the ends with a razor blade.

Testing

Stress excursions for panel testing were selected to be typical of aircraft flight cycles where 1.2-g loads are encountered in taxi and 1-g flight loads plus vertical gusts to 10 fps (3 m/sec) are experienced during cruise. Figure 31 shows tabulated values and plots of the values and defines the excursions.

All panels were cycled in the 150-kip (6700 kN) Electro-Mechanical Research (EMR) test machine shown in figure 32. This machine has the capability of operating at frequencies from 0.53 to 16.7 Hz. The loads are controlled by a controller (at left in fig. 32), which has the capability of accepting inputs in the form of dialed loads or magnetic tape input. The test machine was operated at constant load amplitude. Strain gages were installed on all panels. The loads were based on typical once-per-flight loads (fig. 31) and cross-section properties (table 8), with an estimated fiber strength σ_f = 340 ksi (2.379 kN/mm^2) and ϵ_f = 5860 μin./in. The 29% of ultimate fiber strength (fig. 31) gives ϵ_{test} = +1700 μin./in. Initial cycles were at 32 cpm (0.53 Hz), then the load was adjusted to bring the strain gage readings close to ϵ = +1700 μin./in. The loads were maintained at this level and the panels were cycled at 4 Hz. Dynamic strain gage readings were taken and crack lengths were measured at regular intervals. When a crack length reached 4.0 in. (102 mm) or when the strain readings started to climb, the cycling was stopped. The panel was then loaded to failure, in tension, to determine the residual strength.

Figure 33 shows the concept-3c elevated-temperature test. The clamps, shown close to the grips, were installed in an unsuccessful attempt to prevent skin-stringer debonding during the compression portion of the cycle.

Results

Crack lengths as a function of the number of cycles are shown for all panels in figures 34 through 46. The temperature distributions obtained during elevated-temperature tests are included in figures 37, 41, and 45. Summaries of the cyclic test data and the static failure loads are shown in table 9.

During the testing of concept 1 specimens, debonding was observed during the compression cycle within an oval having the fatigue crack as the major axis. As the debonding grew in size, fatigue cracks developed at 90° to the load axis. Figure 47 shows the distances that the fatigue cracks progressed. Figure 48 is a photograph of the failed panel. The size of the debonded area is indicated by the composite extending beyond the skin fracture.

Figure 49 shows a concept-1c panel tested at 450° F (505° K). This panel broke before the planned cycling was complete. The failure exposed large debonded areas and long boron fibers torn out of the matrix.

Upon examination of the concept-2b panel (fig. 50), it was found that an adhesive layer was missing between the honeycomb and one strap along the full length of the panel. The strap in question is shown under the circle mark closest to the failure. This omission may have contributed to a low failure load.

One titanium honeycomb concept reinforced with boron polyimide straps (-2c) was tested at 70° F (294° K) and another at 450° F (505° K). The panel tested at room temperature debonded near the grips in the first compression cycle, and the subsequent testing was done at R = 0.05. After 35 400 cycles, the crack began to grow rapidly and strain readings increased. This behavior caused suspension of the cycling. During the following static test, the panel failed at a load of 59 kip (262 kN).

Massive debonding was observed in the concept-2c panel tested at 450° F (505° K) (fig. 51). One skin failed in the grip area after debonding (fig. 52). The initial failure occurred after 2170 cycles at R = -1. The cycling continued at R = 0.05 to 43 480 cycles where the crack in one side suddenly grew to 7.05 in. (179 mm). Subsequent static testing failed the panel below the cyclic load.

The concept-3a panel (figs. 53 and 54) failed in the following sequence: The initial failure was a debonding of the skin from all the stringers over an area of half the panel. This failure followed 1326 cycles. The skin crack was grown at R = 0.05 until it reached 4.0 in. (102 mm). The final static failure took place in the remaining adhesive between stringers and skin allowing the stringers to fail near the grips.

The concept-3b panel failed in the same sequence as the concept-3a panel. The initial delamination occurred following 182 cycles at R = -1. Following this failure, the composite

straps were debonded and bent into an S-shape. Cycling was continued at R = 0.05 until one step broke in fatigue after 11 703 cycles. The final static failure occurred in the remaining adhesive between skin and stringers and in the S-curve of the composite load-transfer region.

In an effort to prevent delamination in the two concept-3c panels (fig. 55), rivets were installed to secure the skin to the hat stringers. Delamination occurred between skin and end block during the first compression cycle. Fatigue cracks developed in the skin from the row of rivets closest to the grips. These cracks were seen to progress much faster than the cracks in the center of the panel, and cycling was stopped. The final static failures in the two panels, one tested at 70° F (294° K) and the other at 450° F (505° K), are similar. A closeup of the high-temperature test panel is shown in figure 56. The fatigue failures extending from the end rivets can be seen.

A concept-4b panel is shown in figure 30. The crack was expanded to 4.0 in. (102 mm) in 17 000 cycles at R = -1, and four static loadings were attempted to break the panel. During the first three loadings, the maximum capability of the machine was reached without failure. During the fourth load application, the crack expanded from 4.85 to 8.05 in. (123 to 204 mm). During a fifth loading (184.92 kip, 8225.6 kN), the panel failed slightly under the maximum load (190.16 kip, 8458.7 kN) encountered during the fourth load application. The final failure occurred in the grips (fig. 57).

Analysis and Discussion

The crack retardation and residual strength capabilities of the test panels were evaluated by comparing with a conventional aluminum concept or a titanium honeycomb concept. The desirable parameters are a slow and predictable crack growth rate, a high residual strength after the crack has grown a specified length, and a low structural weight.

The structural weight of the concepts tested are shown together with other currently used or studied concepts in figure 58. The curves are based on:

- A 4.0-in. (102 mm) stringer spacing
- Skin carrying 3.18 kip/in. (0.55 kN/mm) shear
- Fibers and stringers carrying the end load

The mass per unit area W and the ratio α of the strength of the damaged panel to the strength of the undamaged panel is shown as a percentage in figures 34 through 46. These numbers are used to calculate two numbers for each concept: the mass required for a unit of crack growth rate (fig. 59) and the mass required for a unit of residual strength (fig. 60).

Figure 59 is a bar chart comparing the weight of all concepts for unit crack growth rate. The vertical height of each bar represents the weight per square foot divided by the number of cycles to expand a crack 1 in. (25 mm) or panel failure.

The performance comparison in figure 59 shows that most of the reinforced structures were significantly lighter than present-day structure. The concepts most resistant to crack propagation contained distributed fibers, titanium, or both.

Figure 60 is a bar chart comparing the weight per square foot of panel divided by the residual strength in the presence of a crack 4.0 in. (102 mm) long.

The performances of Z-stringer concepts will depend strongly on the area ratio between skin and stringers and will vary according to the application (fuselage, empennage, or wing).

Figure 60 shows that equal or lighter structure is available in several concepts. The best performing concepts have concentrated load paths, titanium, or both.

It is interesting to consider whether the residual stresses due to bonding in the aluminum are responsible for the difference in performance of titanium and aluminum concepts. In concepts 1 and 2, calculated aluminum residual stresses were 11.5 ksi (79 N/mm^2) at room temperature. This stress increment could cause a 10 to 15 times faster crack growth in unreinforced skin. The residual stresses would, however, not affect the residual strength markedly because of the ability of the metal to yield.

Conclusions and Recommendations

To utilize the weight saving potential of composites, concepts are required that have lighter weight per unit residual strength than conventional structures. If present-day standards are to be maintained concerning damage propagation and residual strength, the only composite concepts that can be considered must be better than present Z-stringer concepts. Only the reinforced hat-stringer concepts are clearly in this category. The results shown indicate, however, the possibilities of developing useful structural concepts with combinations of distributed fibers, honeycomb skins, and stringers or straps that may optimize the performance for particular requirements.

Future studies should concentrate on the development of concepts for typical areas in the aircraft (forward fuselage, aft fuselage, lower wing, upper wing, and empennage).

TABLE 8.–CROSS SECTION SUMMARY

Quantity	Concept	Panel type	A_{Al}, in^{2*}	A_{Ti}, in^{2**}	A_B, in^{2***}	A_{matrix} + $A_{adhesive}$, $in^{2\dagger}$	$P/\epsilon = \Sigma AE$,		Mass/unit area	
							lb/μin./in.	MN/m/m	lbm/ft^2	kg/m^2
1	1a	HC (distr fibers)	1.280	–	0.417	0.718 + 0.640	39.4	175	3.13	15.3
1	1b	HC (distr fibers	–	0.640	0.417	0.718 + 0.640	36.3	161	2.90	14.1
2	1c	HC (distr fibers	–	0.640	0.417	0.718 + 0.960	37.9	168	2.73	13.3
1	2a	HC (fiber straps)	1.280		0.417	0.718 + 0.640	39.0	173	3.14	15.3
1	2b	HC (fiber straps)	–	0.640	0.417	0.718 + 0.640	36.3	161	2.91	14.2
2	2c	HC (fiber straps)	–	0.640	0.417	0.718 + 0.960	37.9	168	2.73	13.3
1	3a	Al hats	2.392		0.163	0.233 + 0.039	34.4	153	2.38	11.6
1	3b	Ti hats	–	1.564	0.157	0.270 + 0.050	35.1	156	2.51	12.2
2	3c	Ti hats	–	1.564	0.157	0.270 + 0.140	35.3	157	2.57	12.6
1	4b	Ti hats HC	–	1.564	0.157	0.270 + 0.570	35.7	159	2.86	14.0

*ρ = 0.100 lb/in^3 (2.75 kg/dm^3) **ρ = 0.160 lb/in^3 (4.4 kg/dm^3) ***ρ = 0.100 lb/in^3 (2.75 kg/dm^3) †ρ = 0.044 lb/in^3 (epoxy) (1.21 kg/dm^3) = 0.052 lb/in^3 (polyimide) (1.43 kg/dm^3)

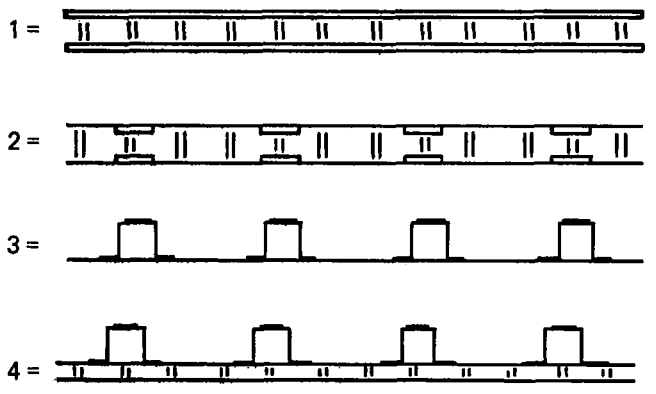

a = Aluminum-boron-epoxy
b = Titanium-boron-epoxy
c = Titanium-boron-polyimide

CONCEPT CODE

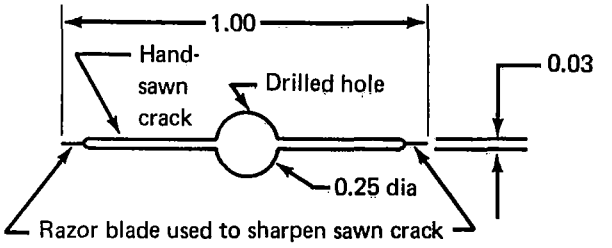

TYPICAL INITIATING CRACK

TABLE 9.–SUMMARY OF PANEL TESTS

Concept	Test temperature °F	Test temperature °K	Stress ratio,R	Load cycles x 10^3	Crack length in.	Crack length cm	Residual load, kip	Theoretical load, kip	% residual strength	Notes
1a	70	293	-1.0	34.0	4.0	10.2	97.8	236	42	90° cracks
1b	70	293	-1.0	87.0	4.0	10.2	128.9	218	59	90° cracks (see fig. 51)
1c	70	293	-1.0	15.5	4.0	10.2	109.6	228	48	
1c	450	505	-1.0	8.0	2.1	5.3	38.9	228	17.1	Failed during cycling
2a	70	293	-1.0	2.3	4.0	10.2	140.1	234	60	
2b	70	293	-1.0, 0.05	60.0	4.0	10.2	109.2	218	50	
2c	70	293	0.05	35.2	3.5	8.9	59.1	228	26	
2c	450	505	-1.0, 0.05	43.0	3.6	9.2	27.6	228	12.3	Failed during cycling
3a	70	293	-1.0, 0.05	6.8	4.0	10.2	125.5	206	61	
3b	70	293	-1.0, 0.05	11.5	2.3	5.8	86.5	210	41	
3c	70	293	0.05	29.6	2.5	6.4	94.2	212	44	
3c	450	505	0.05	36.5	2.2	5.6	90.0	212	42	
4b	70	293	-1.0	17.0	4.0	10.2	190.2	214	89	

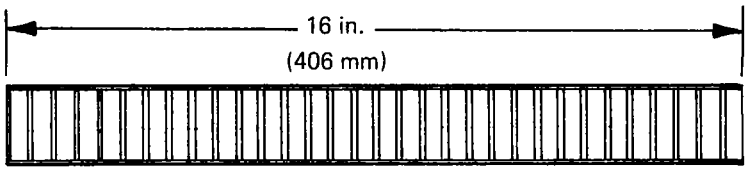

PANEL CROSS SECTION

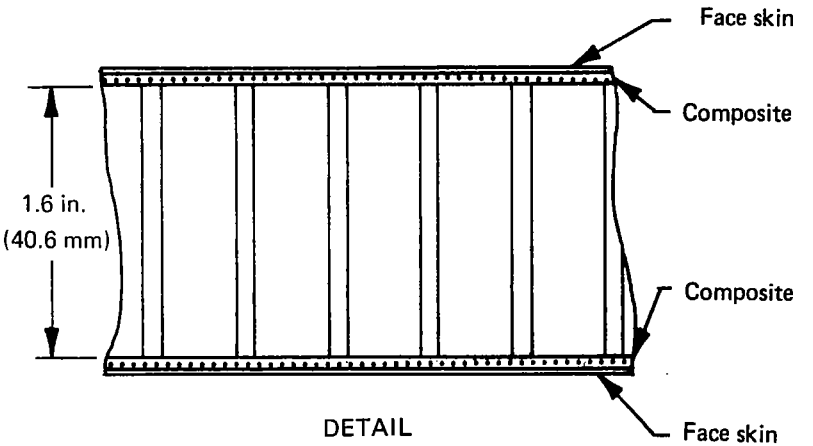

DETAIL

Concept	Face skin			Matrix	Plies/skin	Adhesive	Honeycomb core[a]
	Metal	Gage					
		in.	mm				
1b	Ti-6Al-4V	0.020	0.51	BP 907 epoxy	5	AF 126	8.1-1/8-20 (Al)
1a	Al-7075-T6	0.040	1.01	BP 907 epoxy	5	AF 126	8.1-1/8-20 (Al)
1c	Ti-6Al-4V	0.020	0.51	35-520 polyimide	5	FM 34	5.0-3/16 (HRP)

[a]Numbers indicate weight (lb/cu ft), cell size (in.), and foil thickness (tenths of mil).

FIGURE 24.– HONEYCOMB CONCEPT WITH DISTRIBUTED REINFORCEMENT

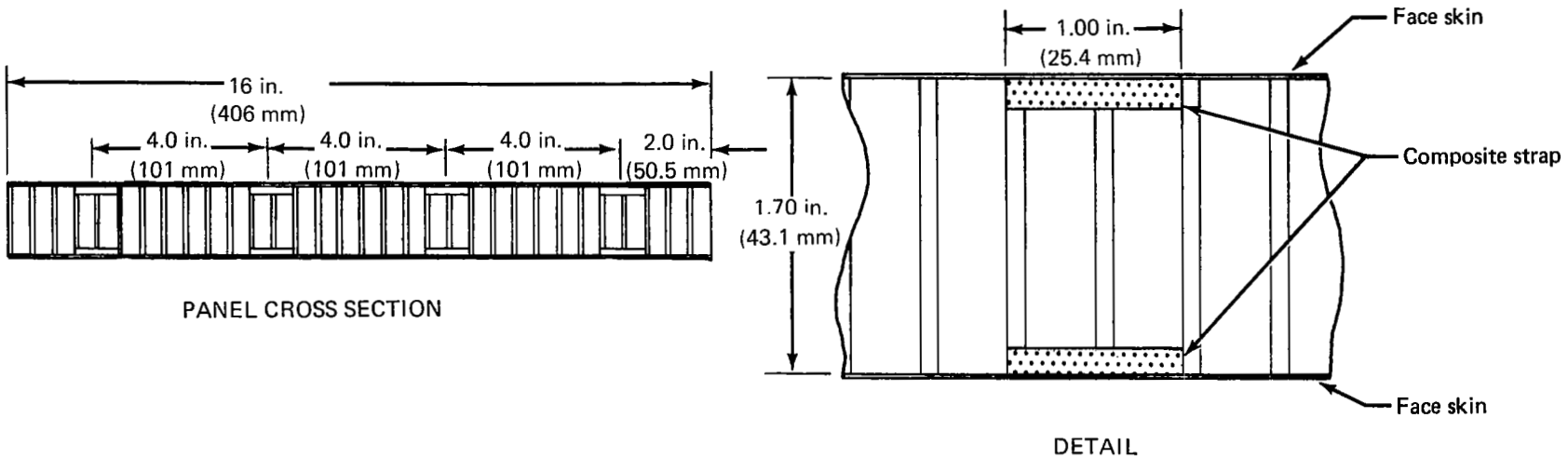

Concept	Face skin			Matrix	Straps	Plies/strap	Adhesive	Honeycomb core[a]
	Metal	Gage						
		in.	mm					
2a	Al-7075-T6	0.040	1.01	BP 907 epoxy	8	20	AF 126	8.1-1/8-20 (Al)
2b	Ti-6Al-4V	0.020	0.50	BP 907 epoxy	8	20	AF 126	8.1-1/8-20 (Al)
2c	Ti-6Al-4V	0.020	0.50	35-520 polyimide	8	20	FM 34	5.0-3/16 (HRP)

[a]Numbers indicate weight (lb/cu ft), cell size (in.), and foil thickness (tenths of mil).

FIGURE 25.–HONEYCOMB CONCEPT WITH STRAP REINFORCEMENT

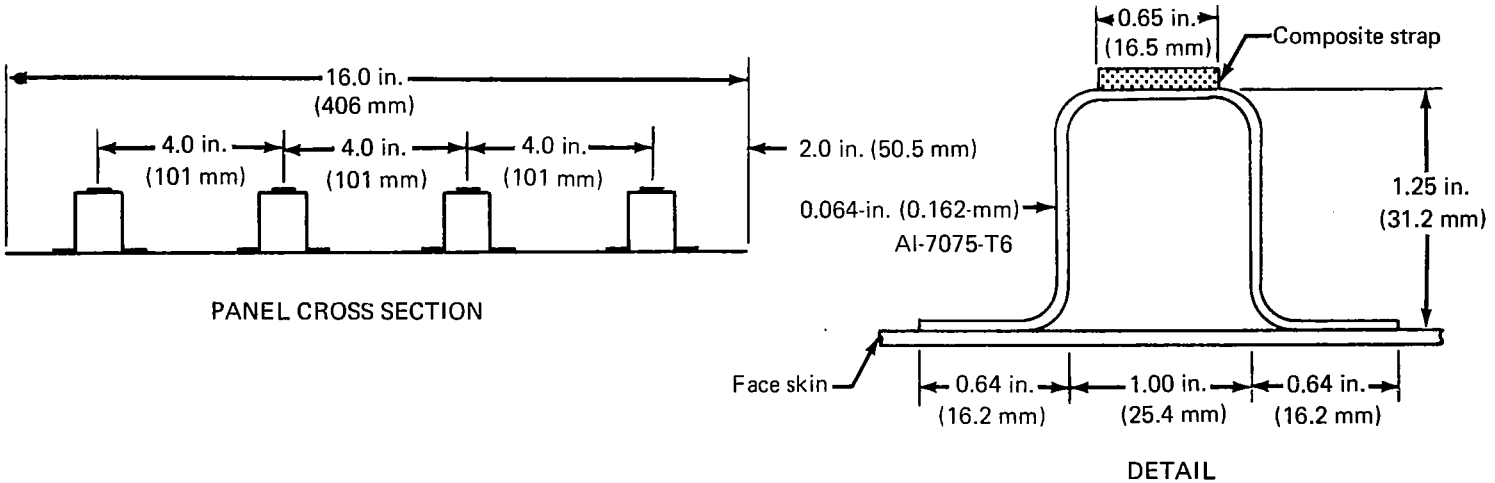

Concept	Face skin			Matrix	Straps	Plies/strap	Adhesive
	Metal	Gage					
		in.	mm				
3a	Al-7075-T6	0.075	0.191	BP 907	4	20	AF 126

FIGURE 26.– ALUMINUM HAT STRINGER CONCEPT

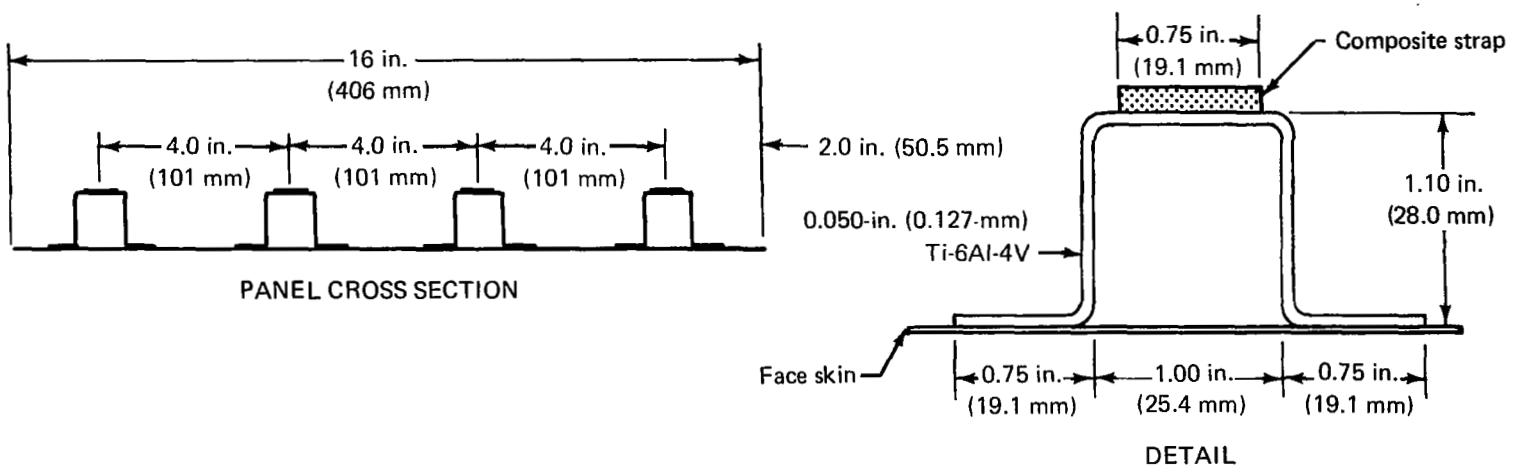

Concept	Face skin			Matrix	Straps	Plies/strap	Adhesive
	Metal	Gage					
		in.	mm				
3b	Ti-6Al-4V	0.040	0.101	BP 907 epoxy	4	20	AF 126
3c	Ti-6Al-4V	0.040	0.101	35-520 polyimide	4	20	FM 34

FIGURE 27.—TITANIUM HAT STRINGER CONCEPT

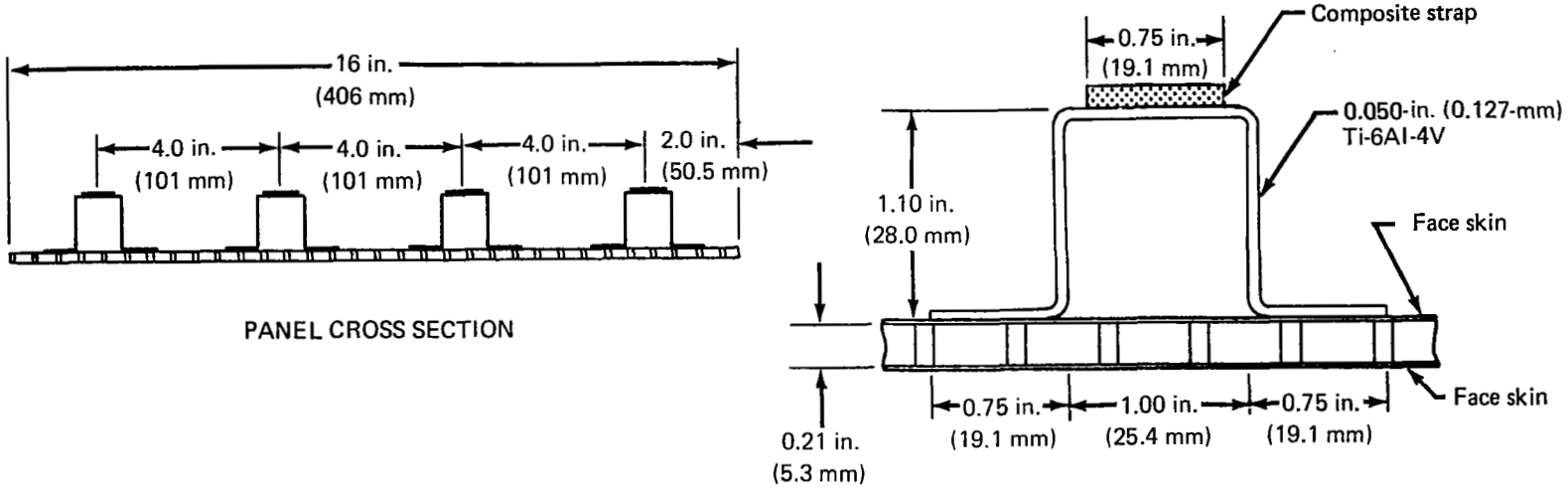

Concept	Face skin			Matrix	Straps	Plies/strap	Adhesive	Honeycomb core[a]
	Metal	Gage						
		in.	mm					
4b	Ti-6Al-4V	0.020	0.51	BP 907	4	20	AF 126	3.1-1/8-20 (5052)

[a]Numbers indicate weight (lb/cu ft), cell size (in.), and foil thickness (tenths of mil).

FIGURE 28.–HAT STRINGER WITH HONEYCOMB STABILIZED SKIN

FIGURE 29.–DETAIL OF GRIP PLATE FOR CONCEPT 2c

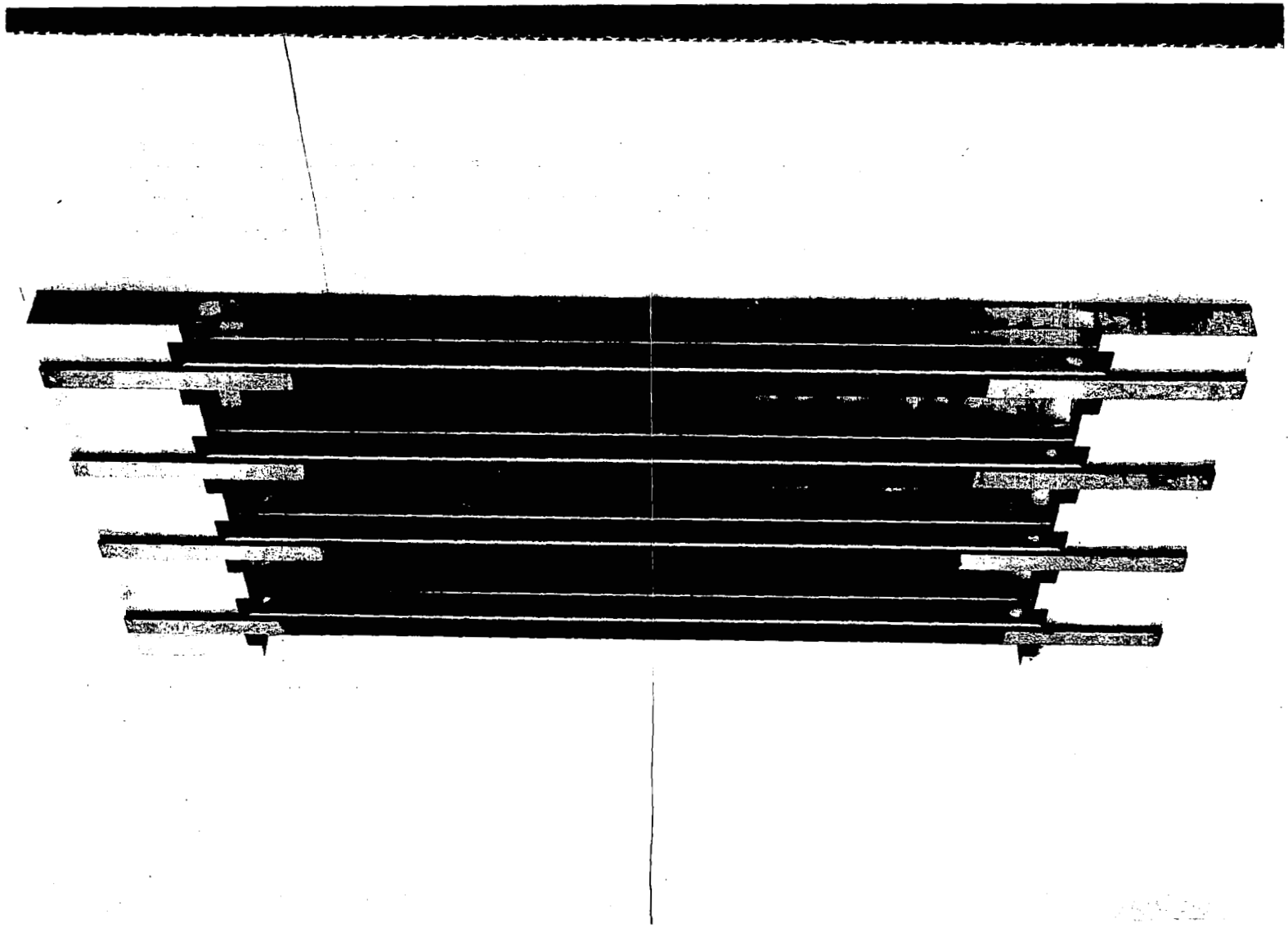

FIGURE 30.– TYPICAL HAT STRINGER PANEL, CONCEPT 4b

$$\text{Stress ratio} = \frac{\sigma_{min}}{\sigma_{max}}$$

$$\text{Amplitude ratio}^{a} = \frac{\text{Flight amplitude}}{\text{Material ultimate amplitude}} (100)$$

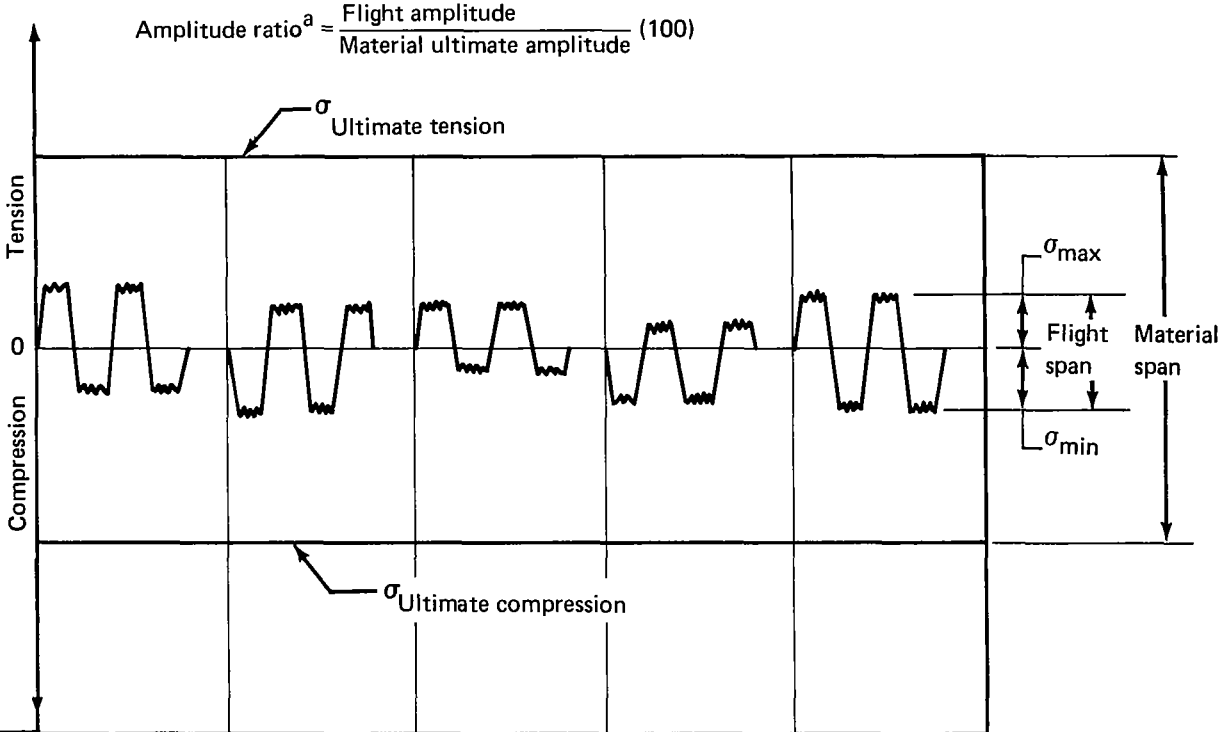

Structure	747 lower wing	747 upper wing	707-320 lower wing	707-320 upper wing	Reinforced test panels
Stress ratio	-0.6	-1.5	-0.4	-2.2	-1.0
Amplitude ratio	27	27	18	20	29

[a]Flight amplitude equals half the flight span; material ultimate amplitude equals half the material span.

FIGURE 31 – STRESS EXCURSIONS

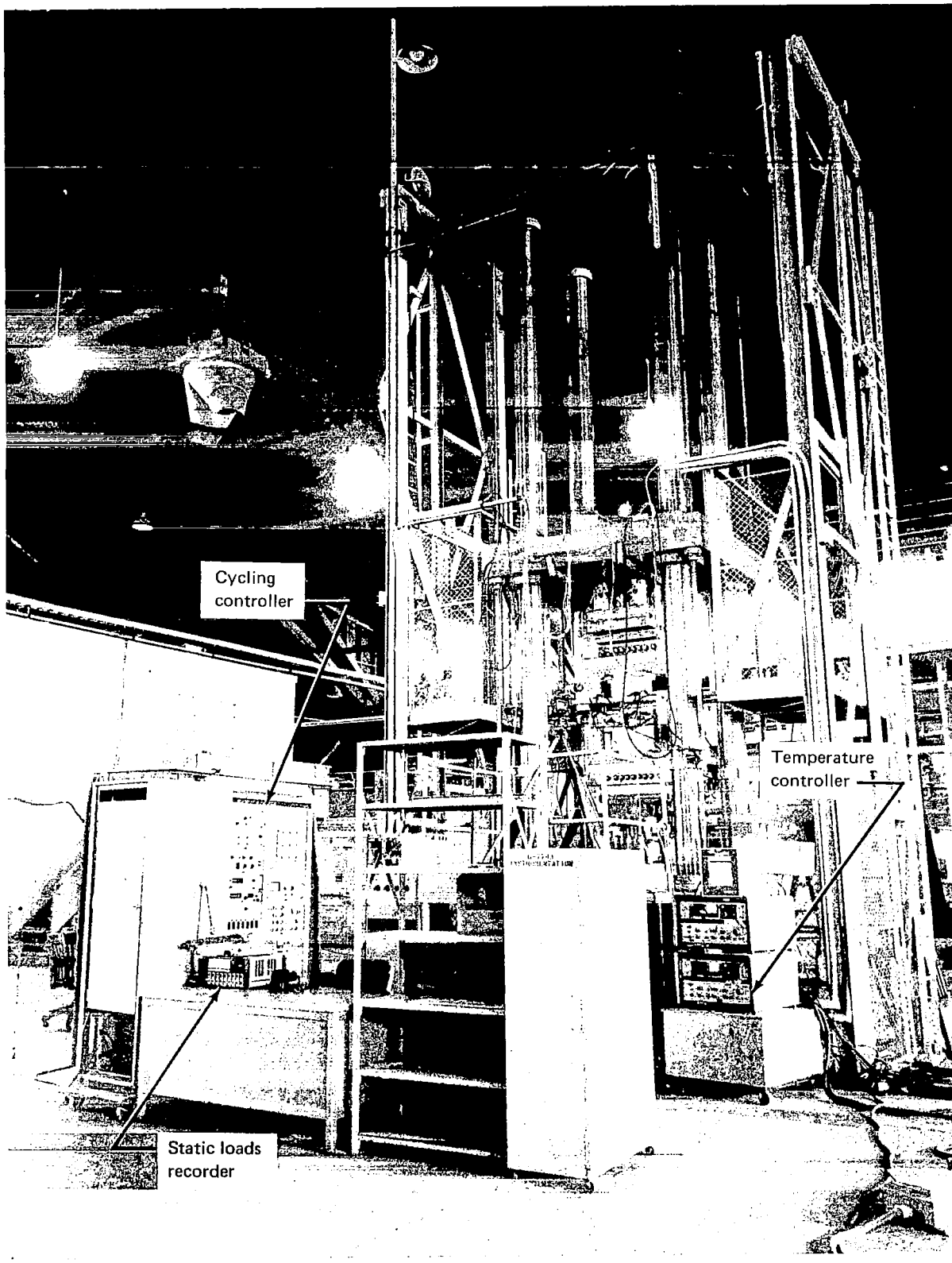

FIGURE 32.– 150-KIP ELECTROMECHANICAL RESEARCH FATIGUE MACHINE

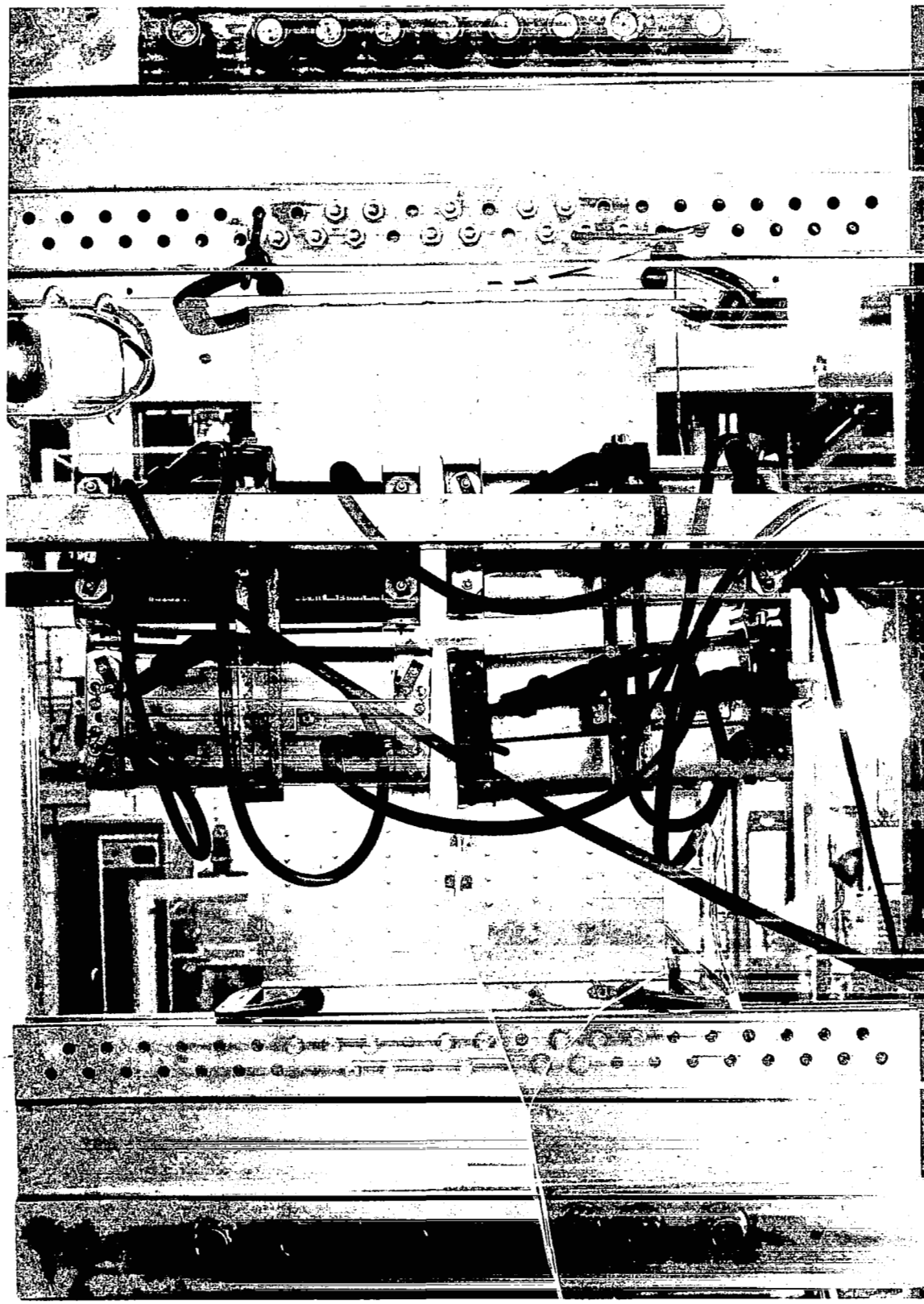

FIGURE 33.—ELEVATED-TEMPERATURE TEST IN 150-KIP ELECTROMECHANICAL RESEARCH MACHINE

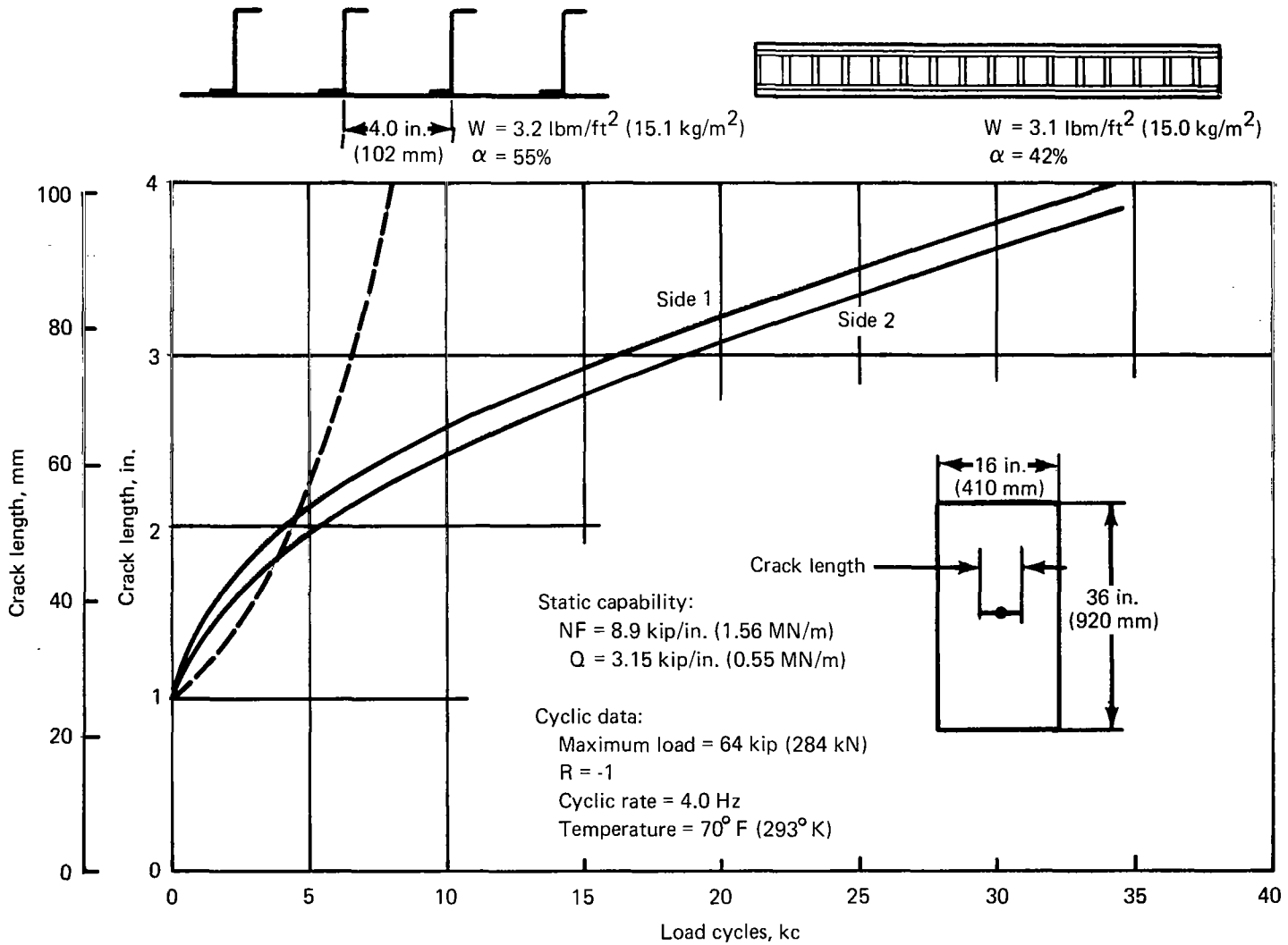

FIGURE 34.—CRACK GROWTH AND RESIDUAL STRENGTH COMPARISON OF FIBER-REINFORCED 7075-T6 AND CONVENTIONAL 7075-T6 ZEE STRINGER CONSTRUCTION

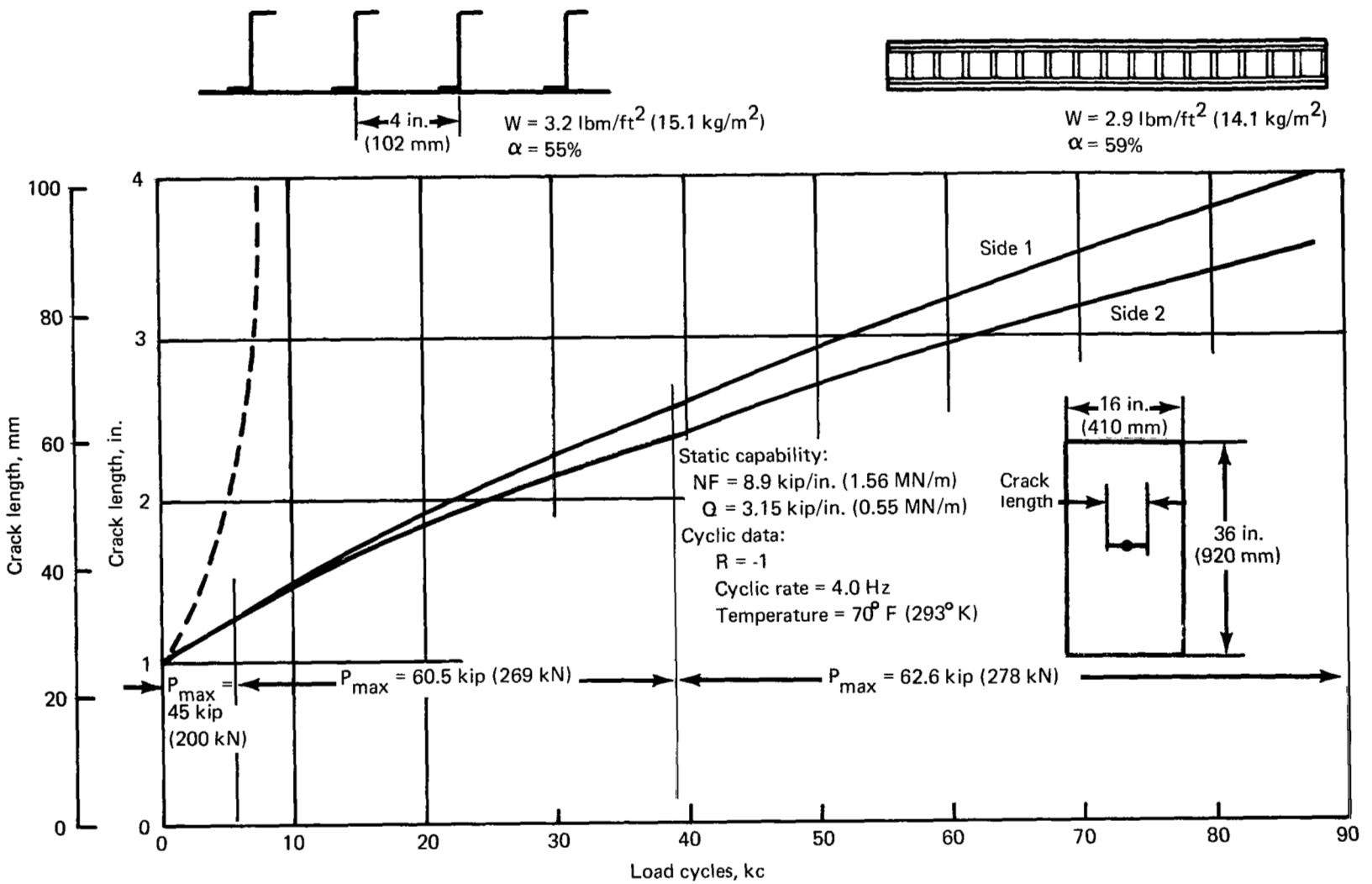

FIGURE 35.—CRACK GROWTH AND RESIDUAL STRENGTH COMPARISON OF FIBER-REINFORCED 6AL-4V TITANIUM AND CONVENTIONAL 7075-T6 ZEE STRINGER CONSTRUCTION

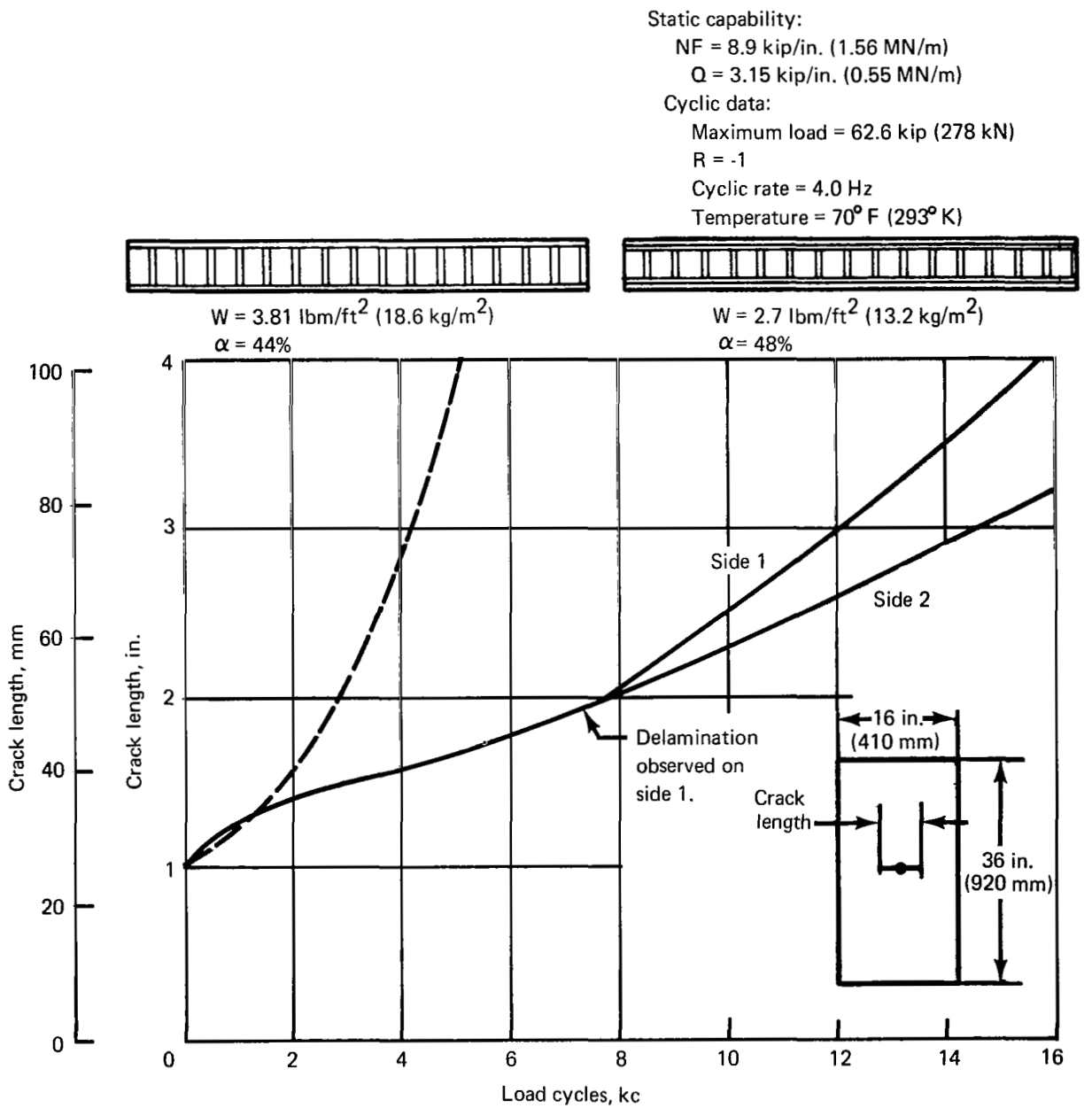

FIGURE 36.–CRACK GROWTH AND RESIDUAL STRENGTH COMPARISON OF FIBER-REINFORCED (BORON-POLYIMIDE) 6AL-4V TITANIUM AND ALL-6AL-4V TITANIUM HONEYCOMB STRUCTURE

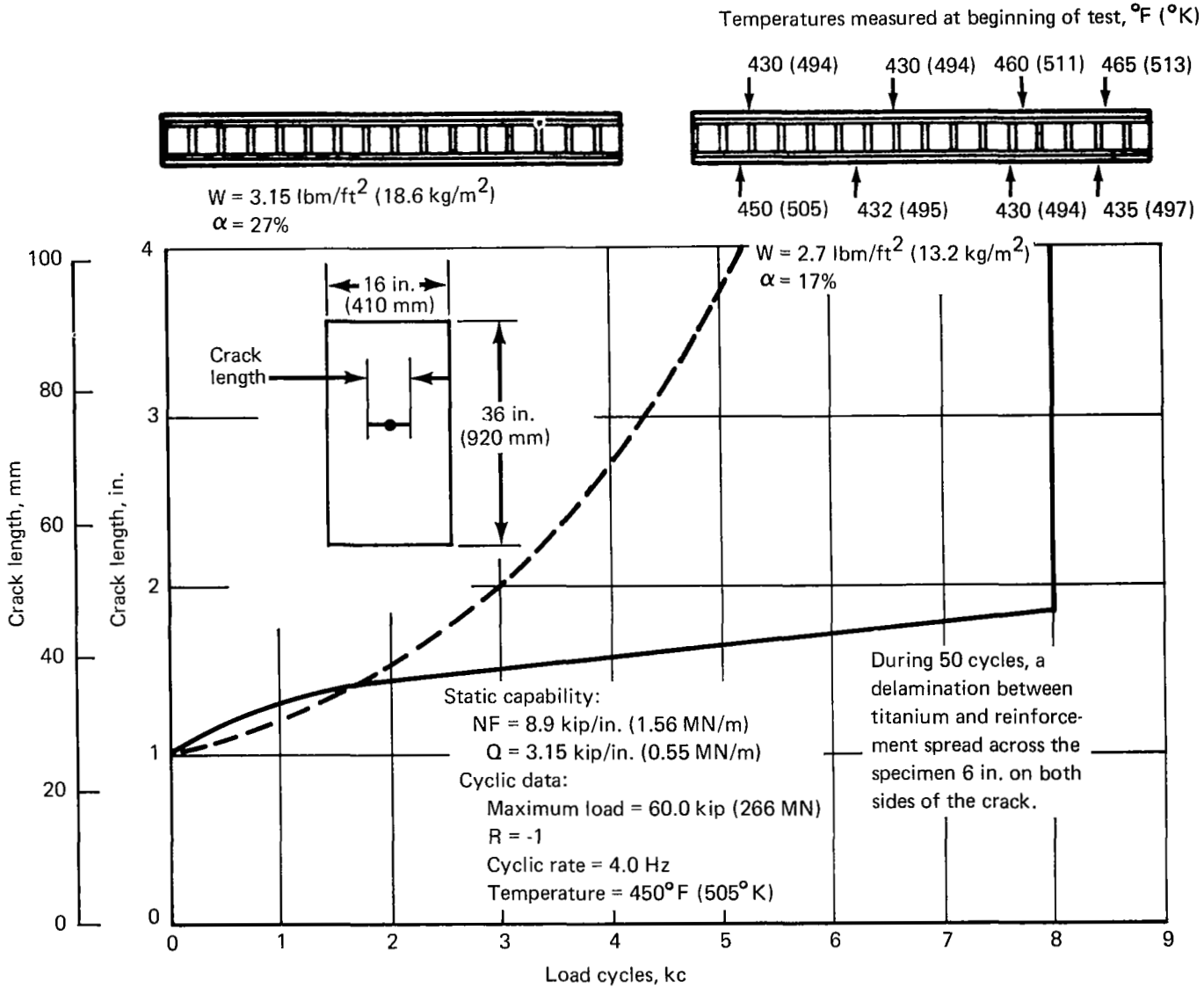

FIGURE 37.—CRACK GROWTH RATE AND RESIDUAL STRENGTH COMPARISON OF FIBER-REINFORCED (BORON POLYIMIDE) 6AL-4V TITANIUM AND ALL-6AL-4V TITANIUM

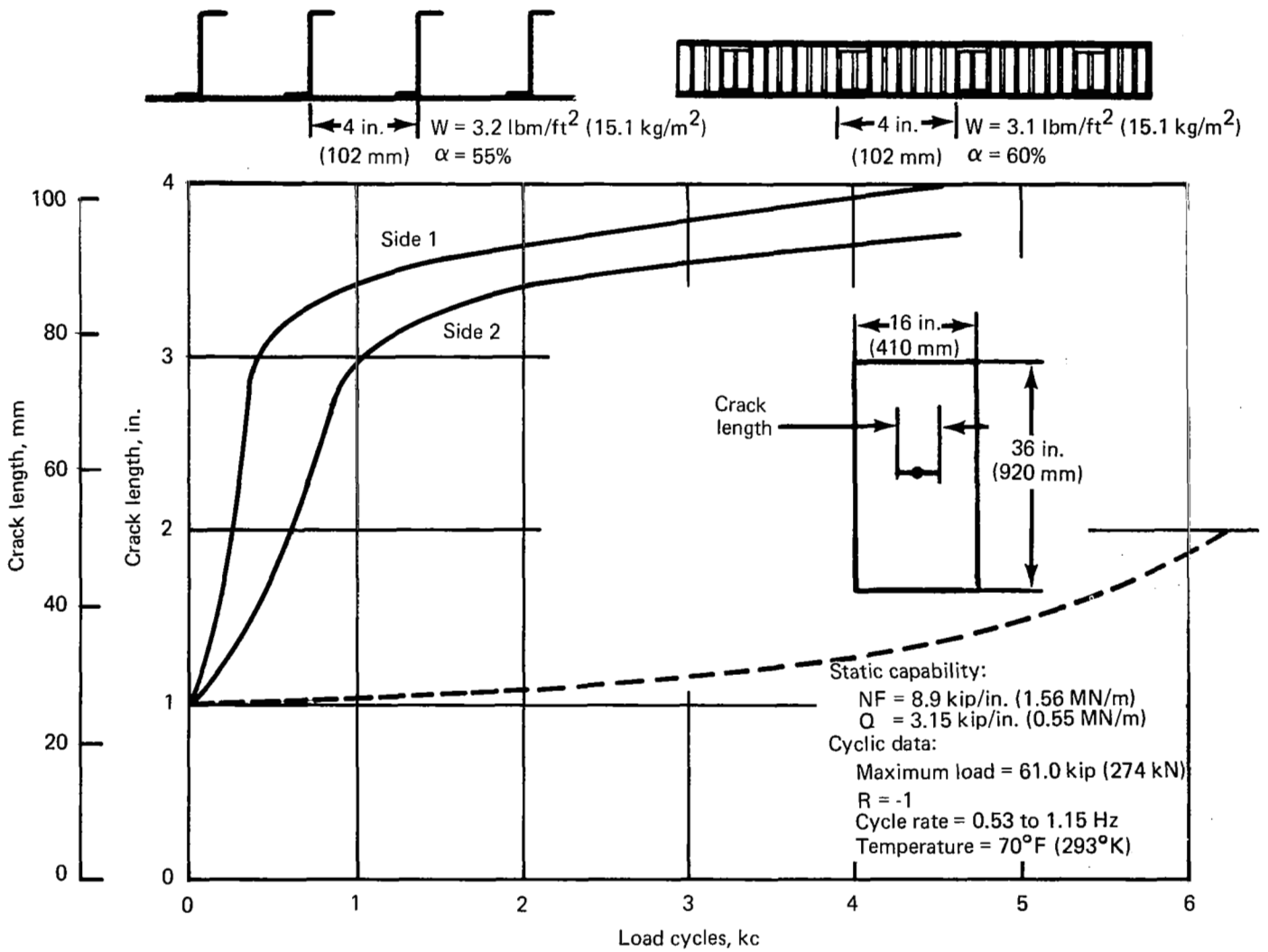

FIGURE 38.–CRACK GROWTH AND RESIDUAL STRENGTH COMPARISON OF FIBER-REINFORCED (BORON EPOXY) 7075-T6 AND CONVENTIONAL 7075-T6 ZEE STRINGER CONSTRUCTION

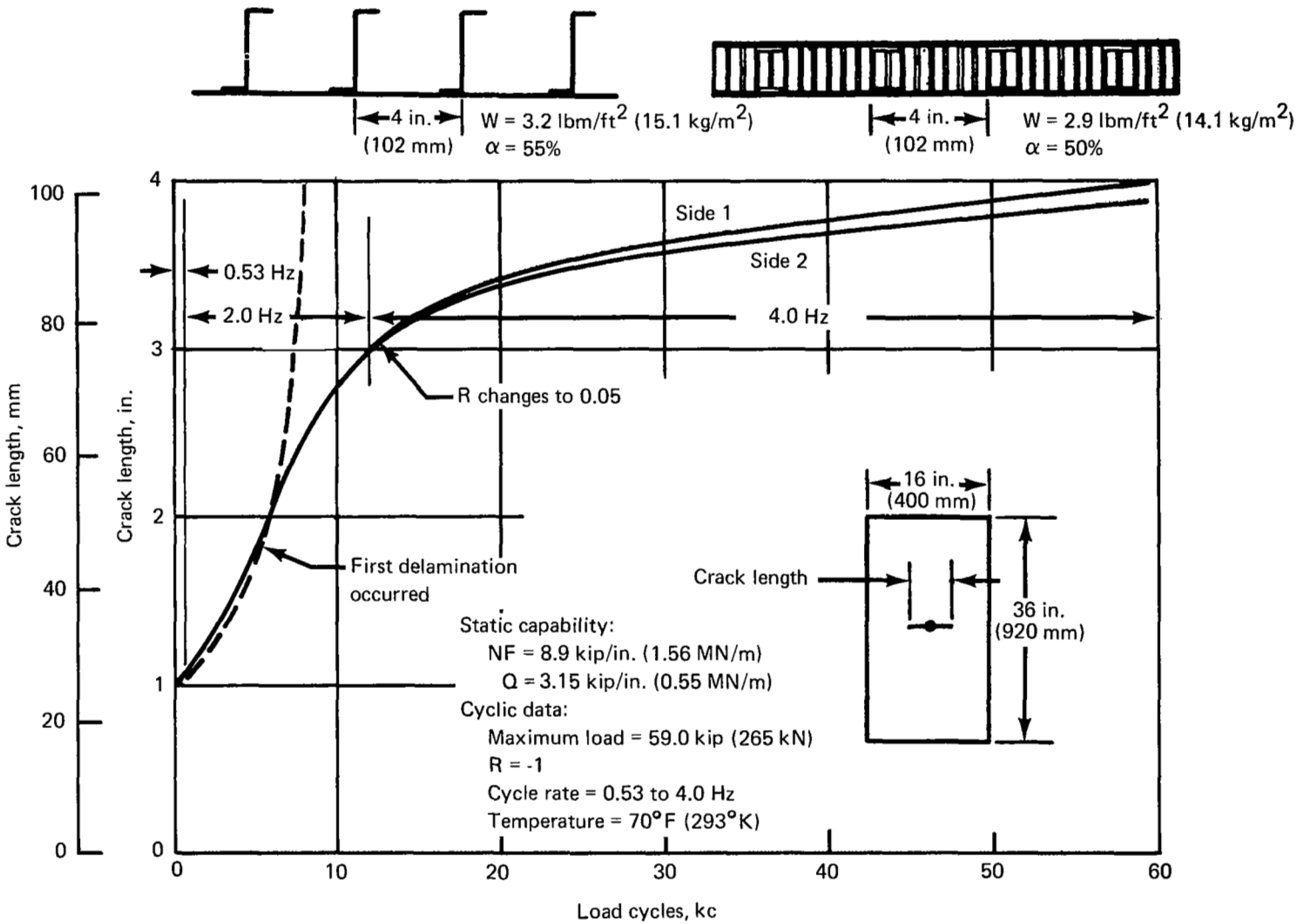

FIGURE 39.–CRACK GROWTH AND RESIDUAL STRENGTH COMPARISON OF FIBER-REINFORCED (BORON-EPOXY) 6AL-4V TITANIUM AND CONVENTIONAL 7075-T6 ZEE STRINGER CONSTRUCTION

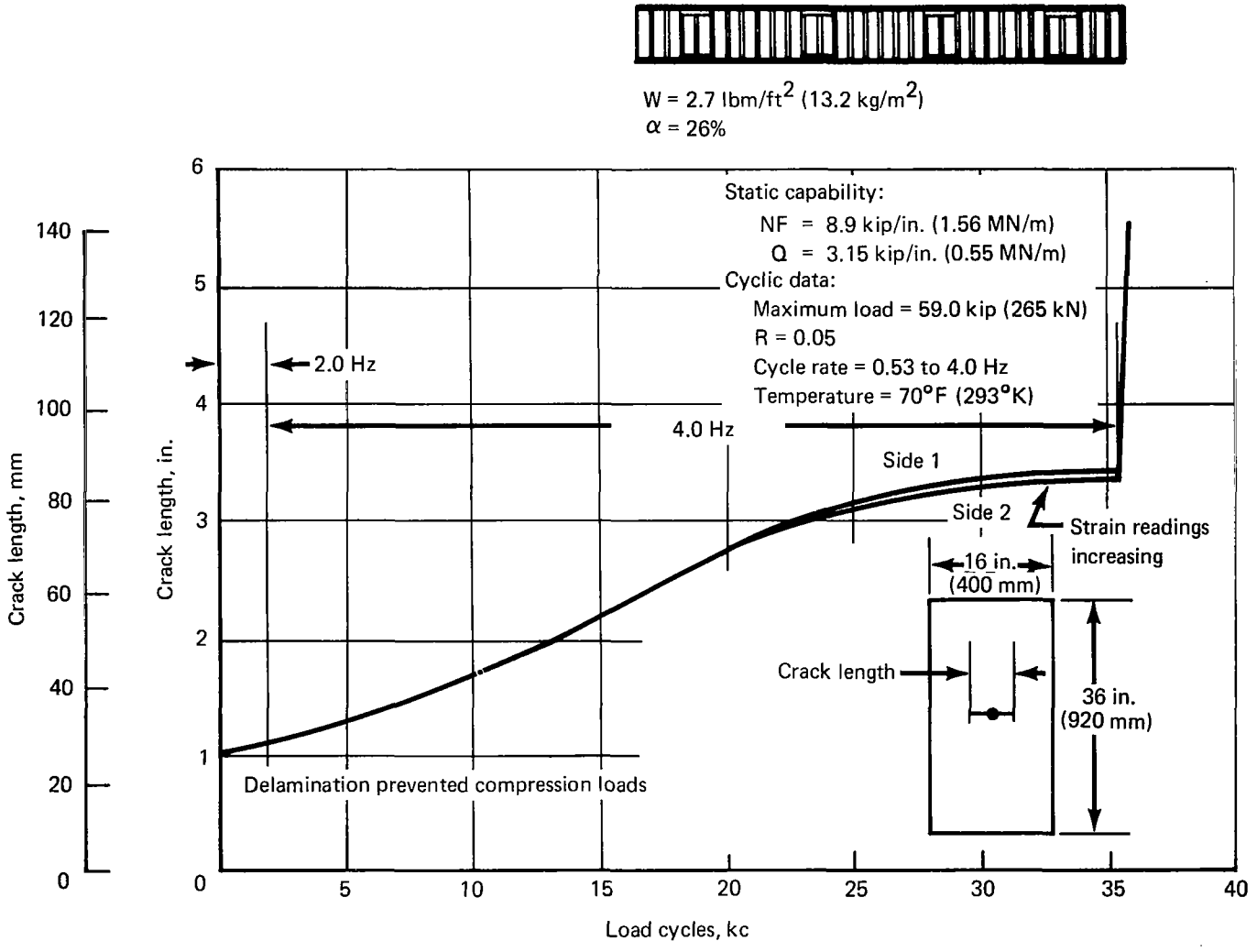

FIGURE 40.–CRACK PROPAGATION AND RESIDUAL STRENGTH RESULTS FOR FIBER-REINFORCED (BORON POLYIMIDE) 6AL-4V TITANIUM

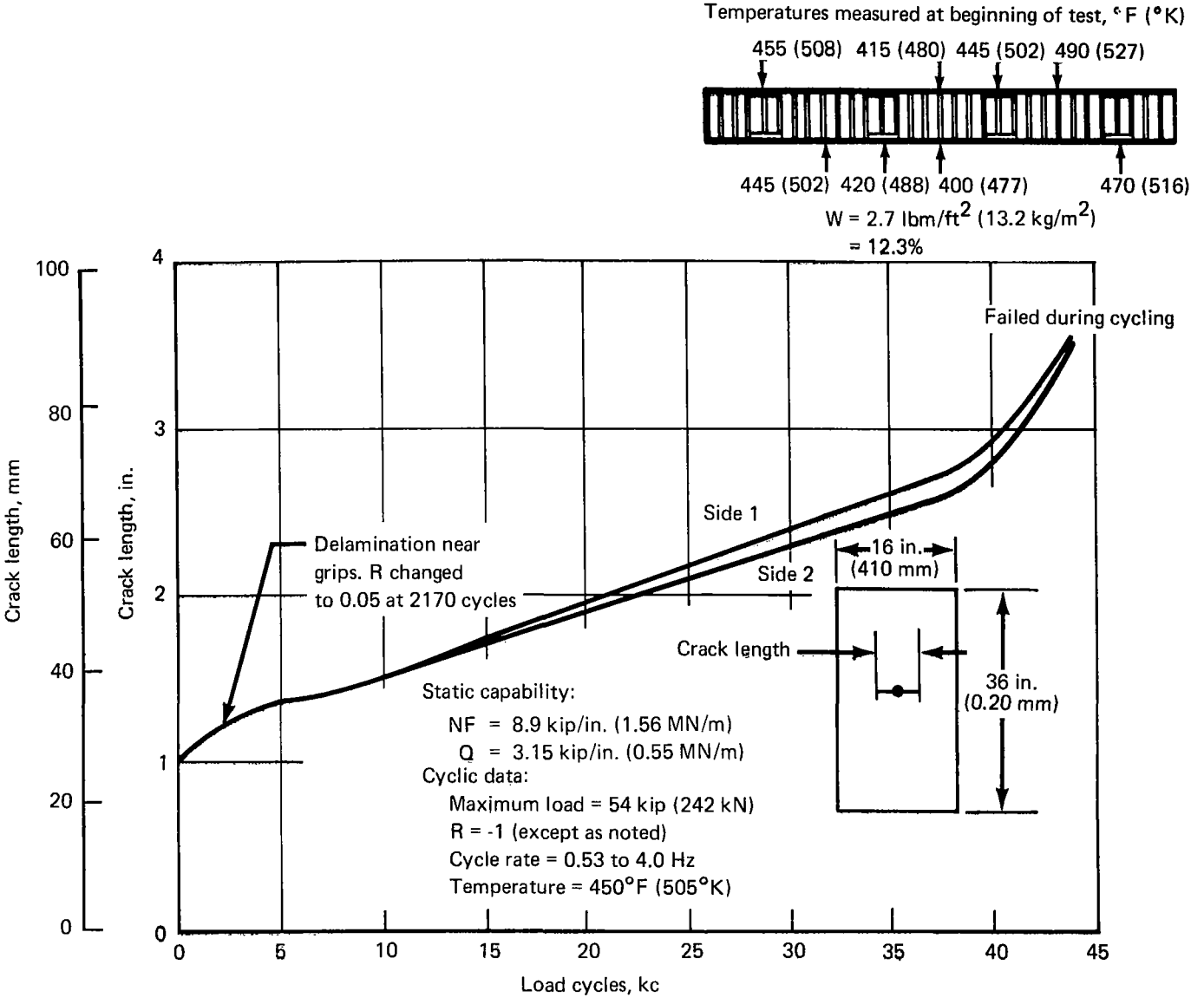

FIGURE 41.—CRACK GROWTH AND RESIDUAL STRENGTH RESULTS FOR FIBER-REINFORCED (BORON POLYIMIDE) 6AL-4V TITANIUM

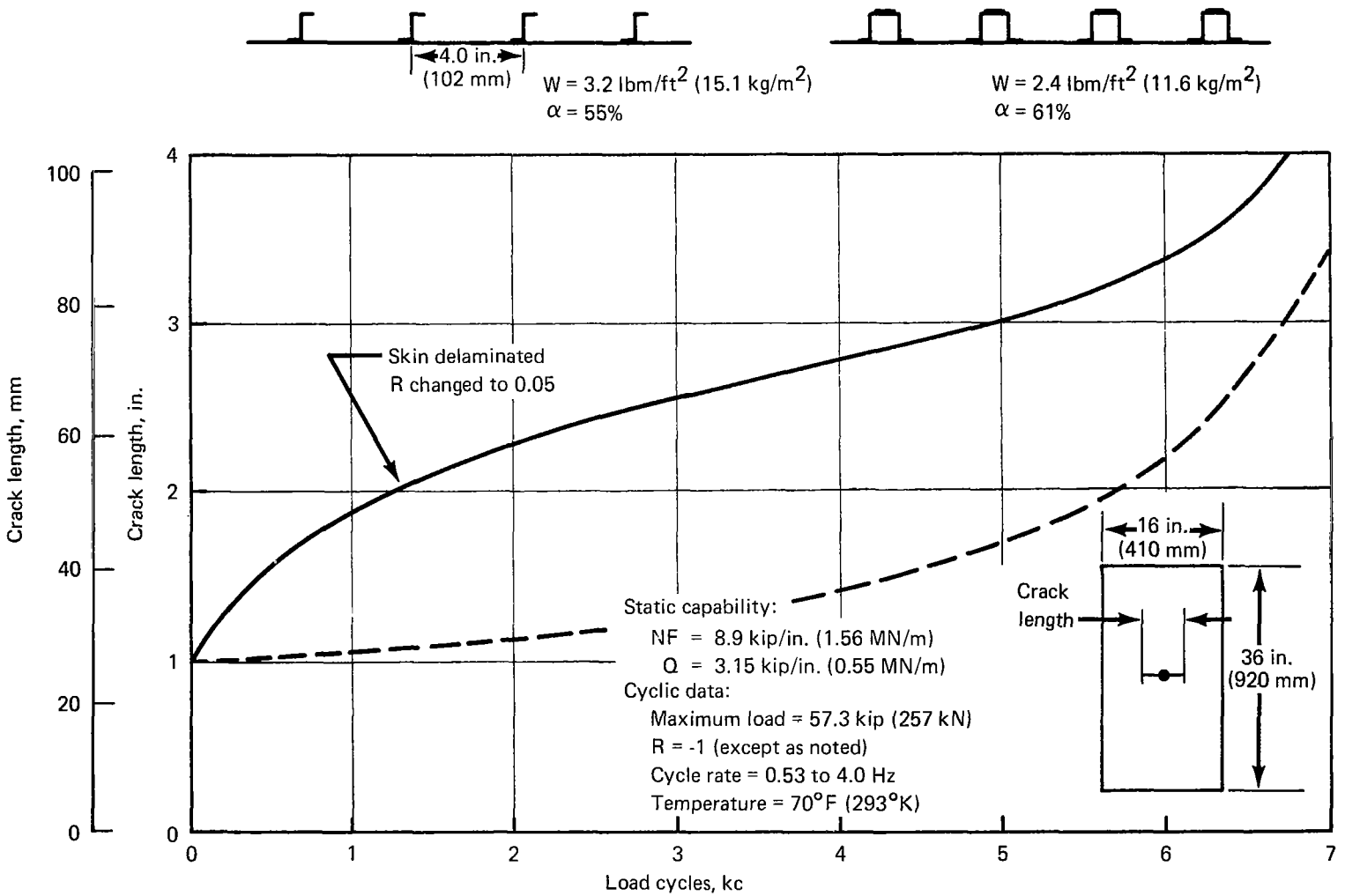

FIGURE 42.–CRACK GROWTH AND RESIDUAL STRENGTH COMPARISON OF FIBER-REINFORCED) (BORON EPOXY) 7075-T6 HAT STRINGER CONSTRUCTION AND CONVENTIONAL 7075-T6 ZEE STRINGER CONSTRUCTION

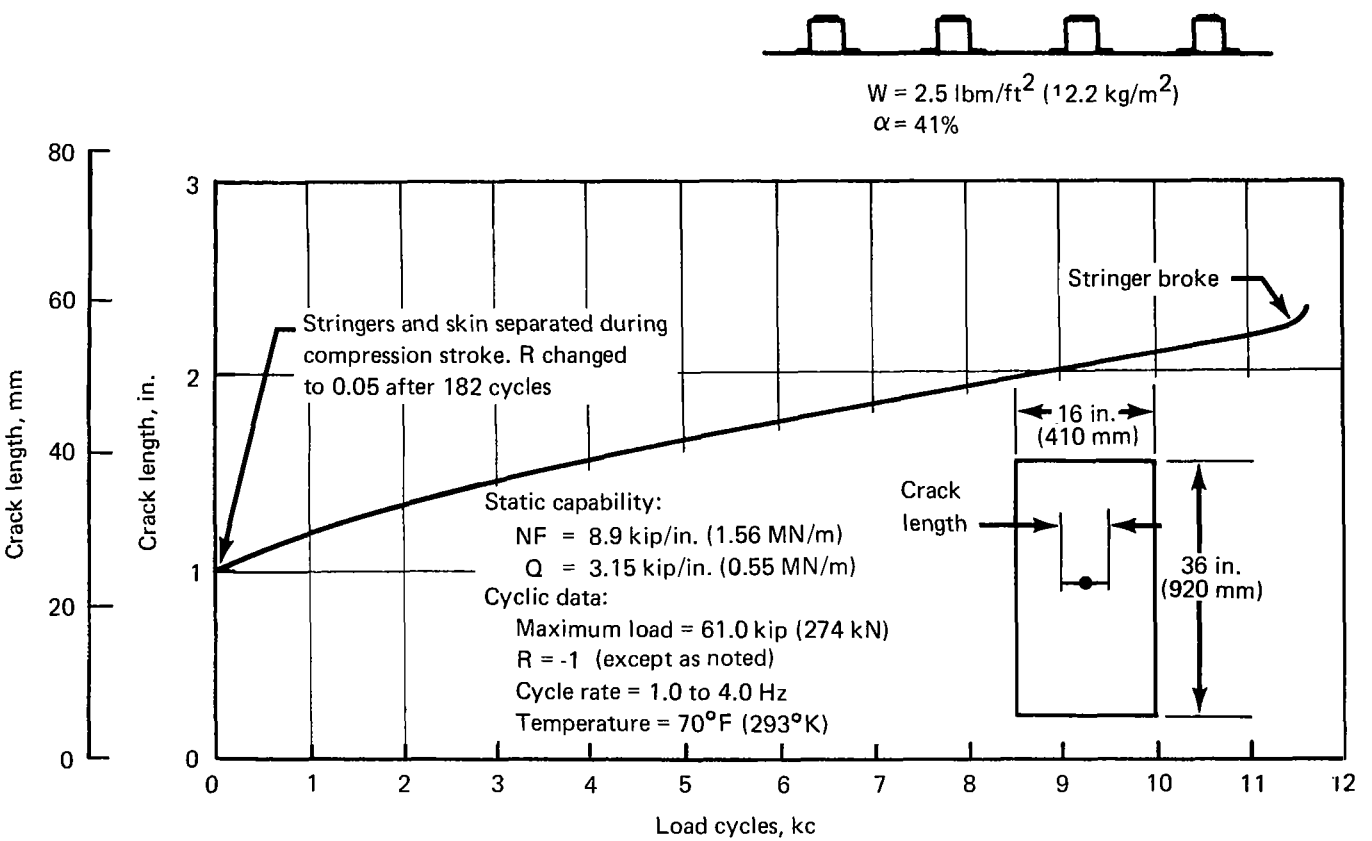

FIGURE 43.–CRACK GROWTH AND RESIDUAL STRENGTH RESULTS FOR FIBER-REINFORCED (BORON EPOXY) TITANIUM HAT STRINGER CONSTRUCTION

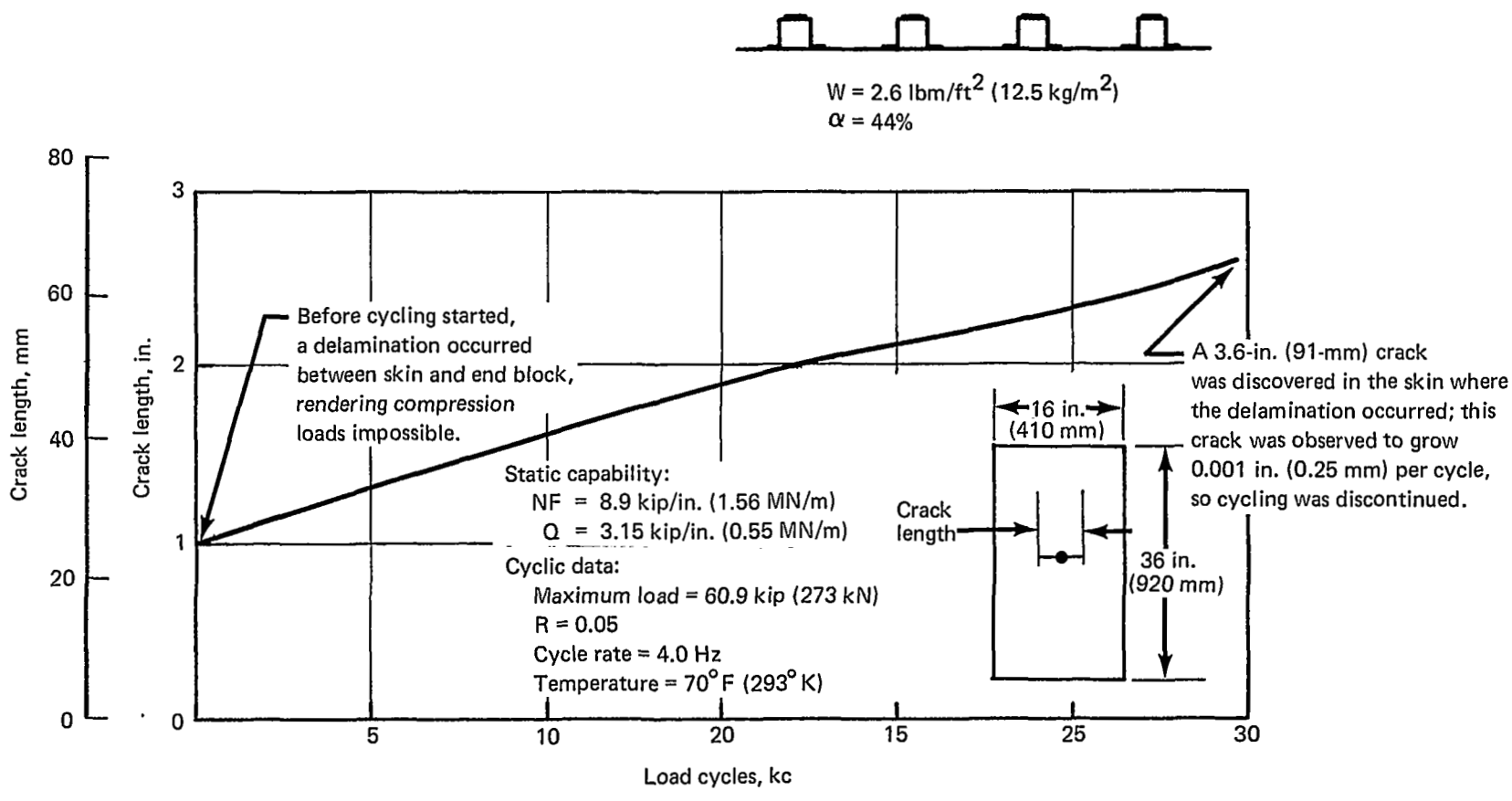

FIGURE 44.—CRACK GROWTH AND RESIDUAL STRENGTH RESULTS FOR FIBER-REINFORCED (BORON POLYIMIDE) TITANIUM HAT STRINGER CONCEPT

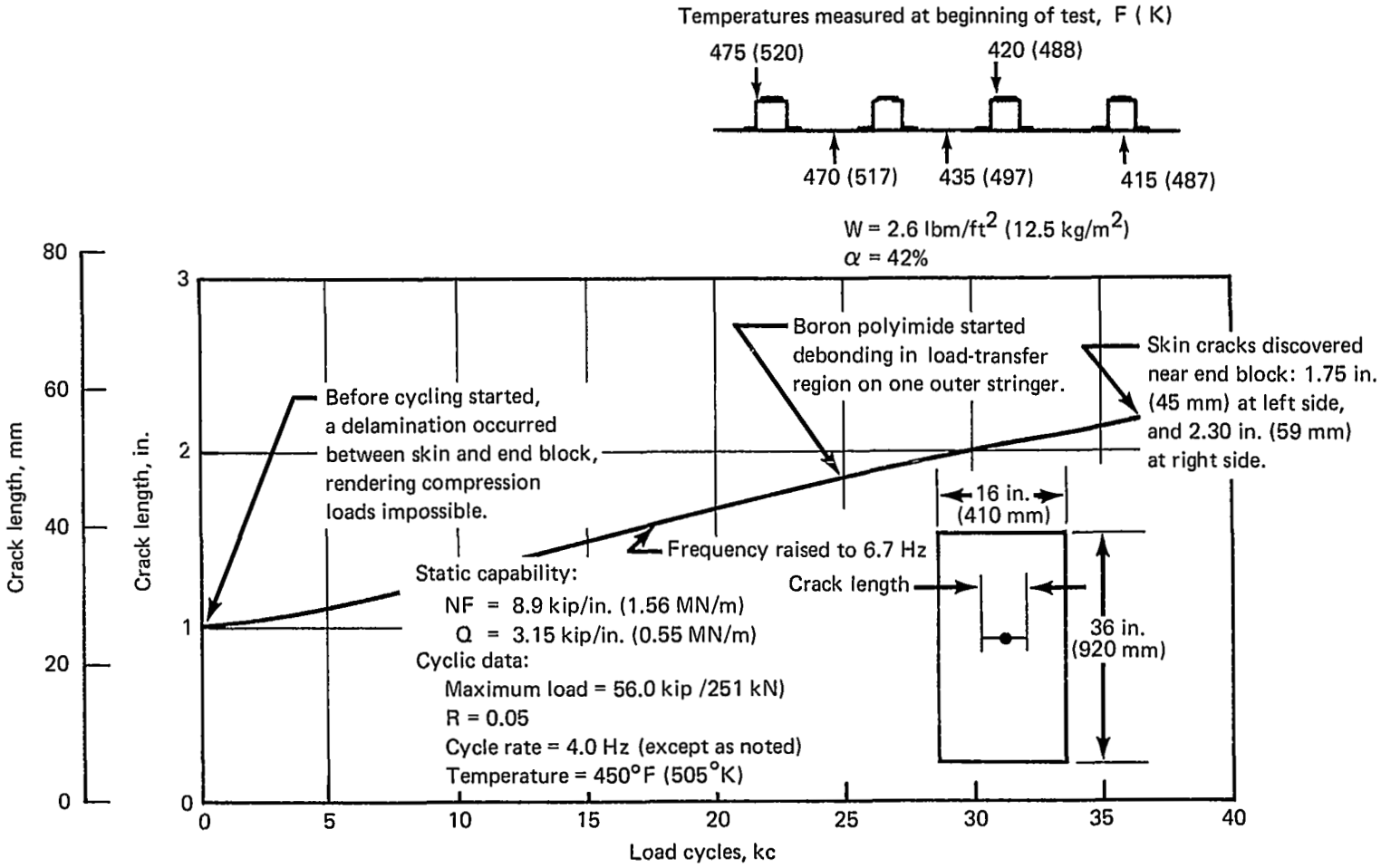

FIGURE 45.—CRACK GROWTH AND RESIDUAL STRENGTH RESULTS FOR FIBER-REINFORCED (BORON POLYIMIDE) TITANIUM HAT STRINGER PANEL

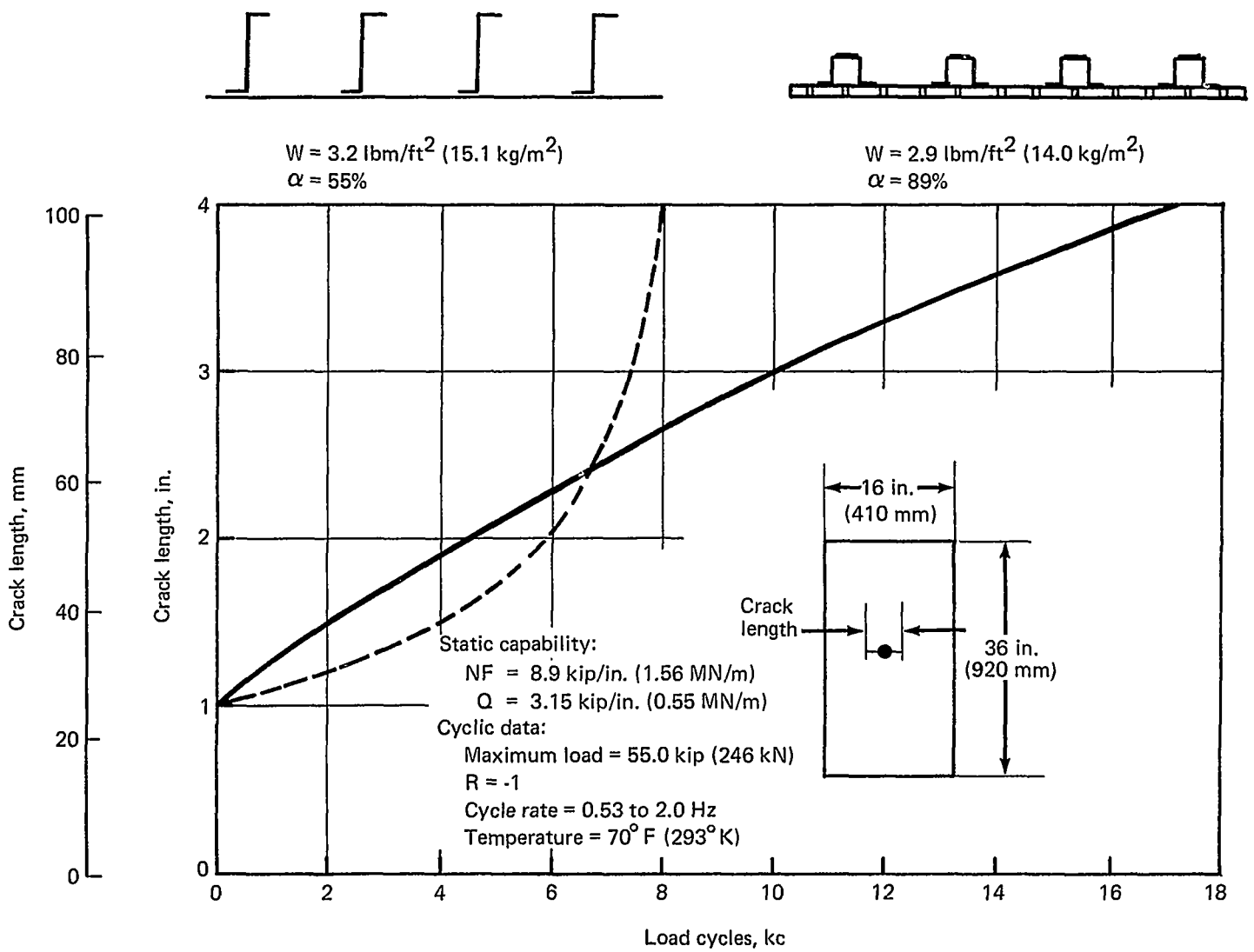

FIGURE 46.—CRACK GROWTH AND RESIDUAL STRENGTH COMPARISON OF FIBER-REINFORCED (BORON EPOXY) TITANIUM HAT STRINGER CONCEPT AND CONVENTIONAL 7075-T6 ZEE STRINGER CONCEPT

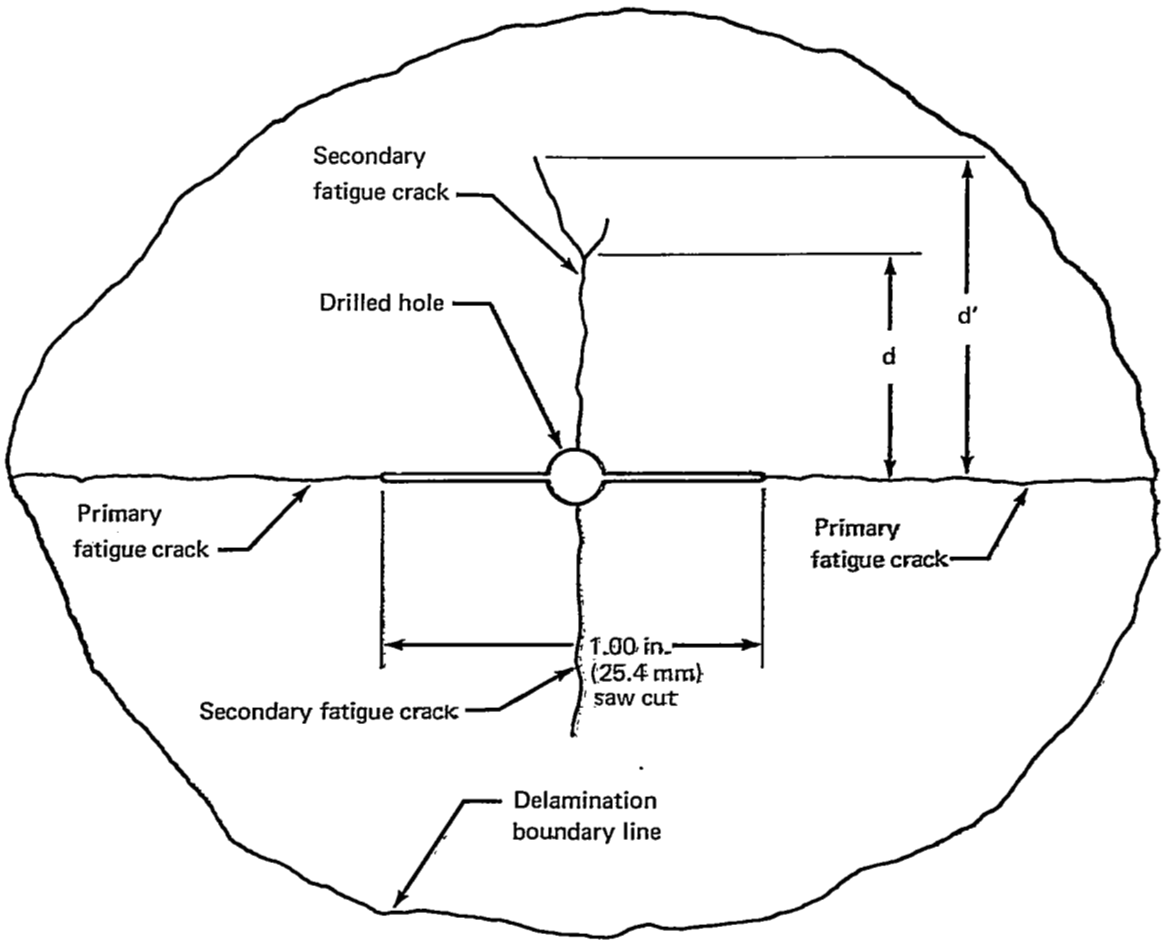

Specimen	Metal	Secondary cracks							
		Side 1				Side 2			
		d		d'		d		d'	
		in.	mm	in.	mm	in.	mm	in.	mm
Concept 1b	Ti-6Al-4V	0.350	8.9	0.460	11.7	0.400	10.2	0.460	11.7
		0.310	7.9	0.400	10.2	0.340	8.6	0.530	13.5
Concept 1a	Al-7075-T6	0.260	6.6	0.310	7.9	0.390	9.9	0.390	9.9
		0.220	5.6	0.260	6.6	0.410	10.4	0.410	10.4

FIGURE 47.– SECONDARY CRACKS IN CONCEPTS 1a AND 1b

FIGURE 48.– FRACTURE IN CONCEPT 1b WITH 90° SECONDARY CRACKS

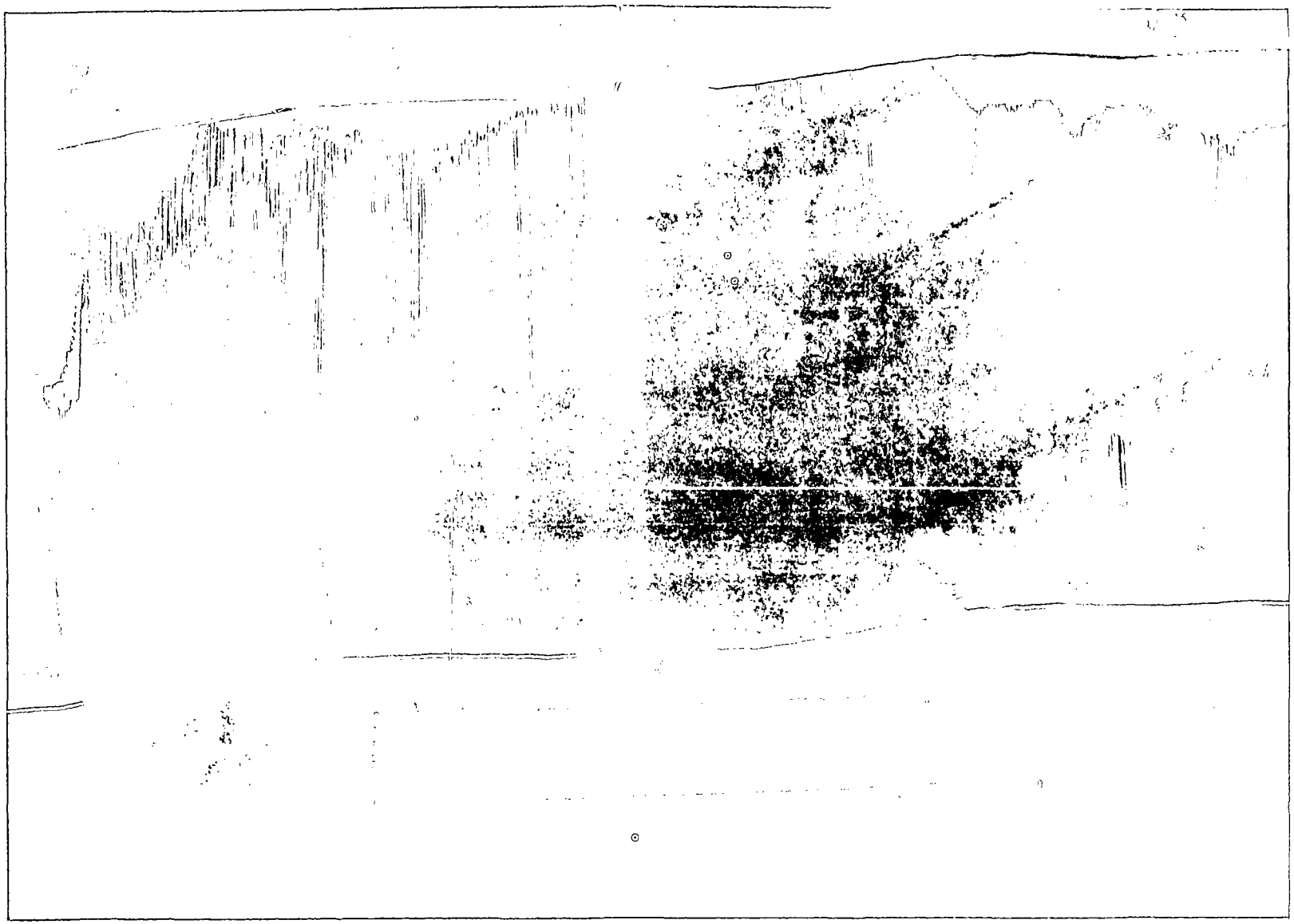

FIGURE 49.—FRACTURE IN CONCEPT 1c AFTER ELEVATED-TEMPERATURE TEST

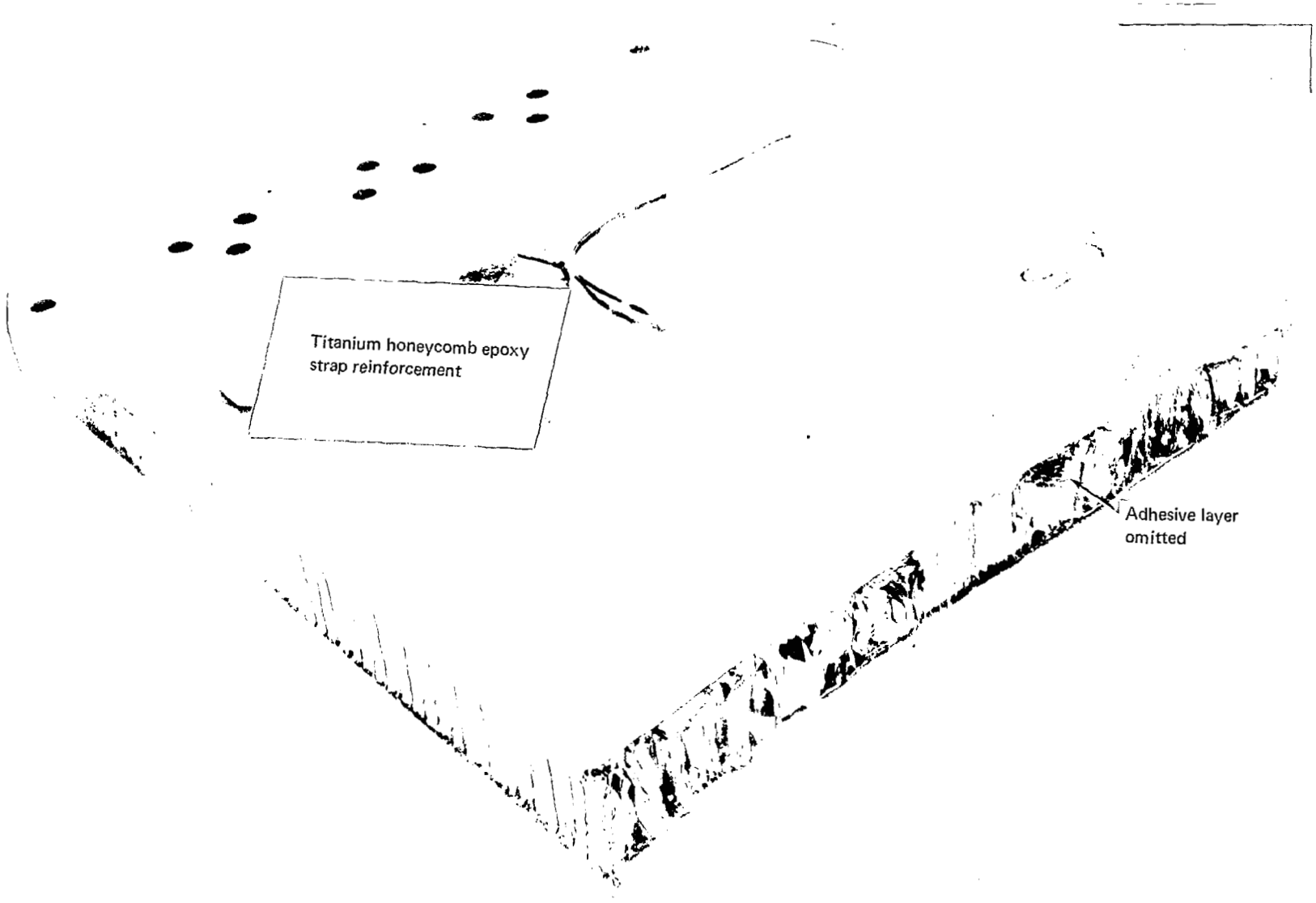

FIGURE 50.—FRACTURE IN CONCEPT 2b

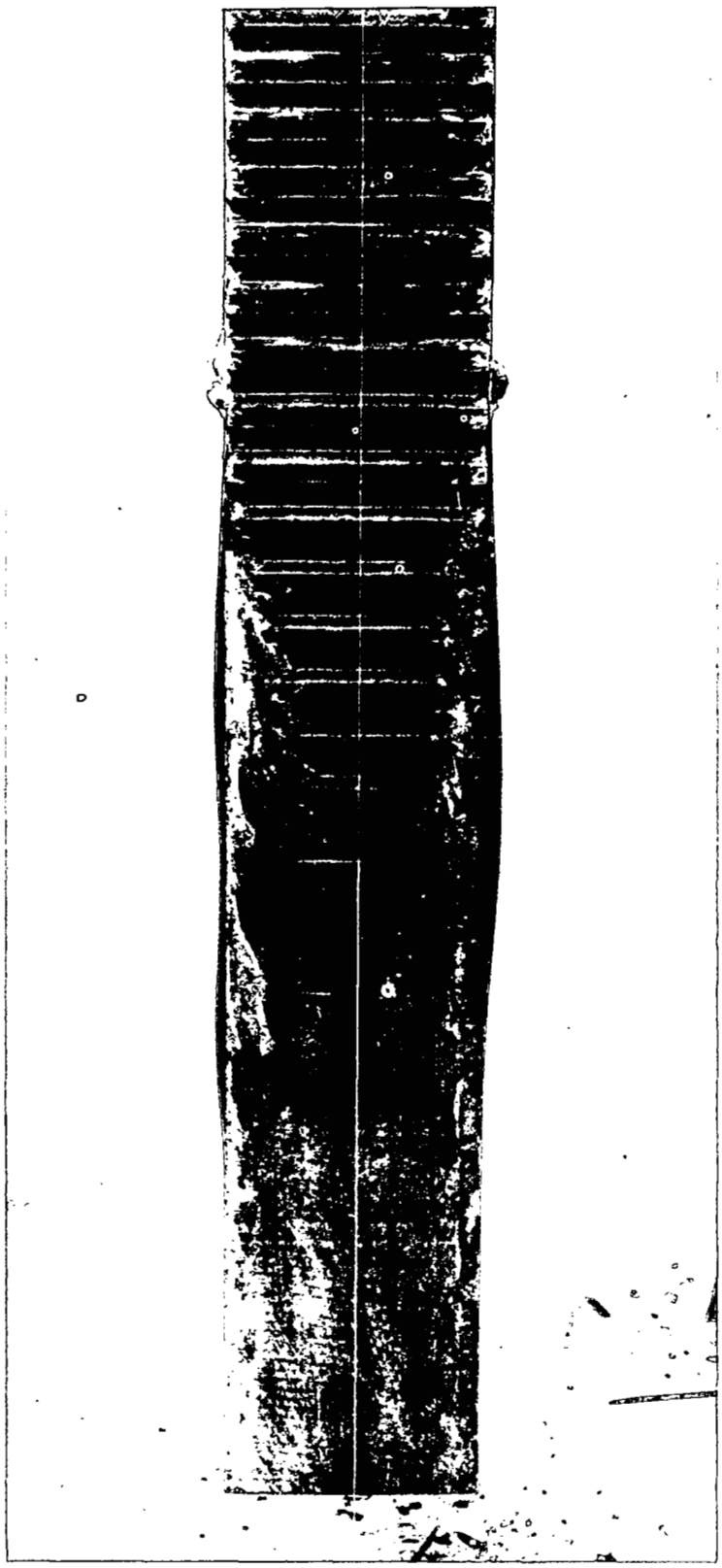

FIGURE 51.—COMPRESSION DEBONDING IN CONCEPT 2c

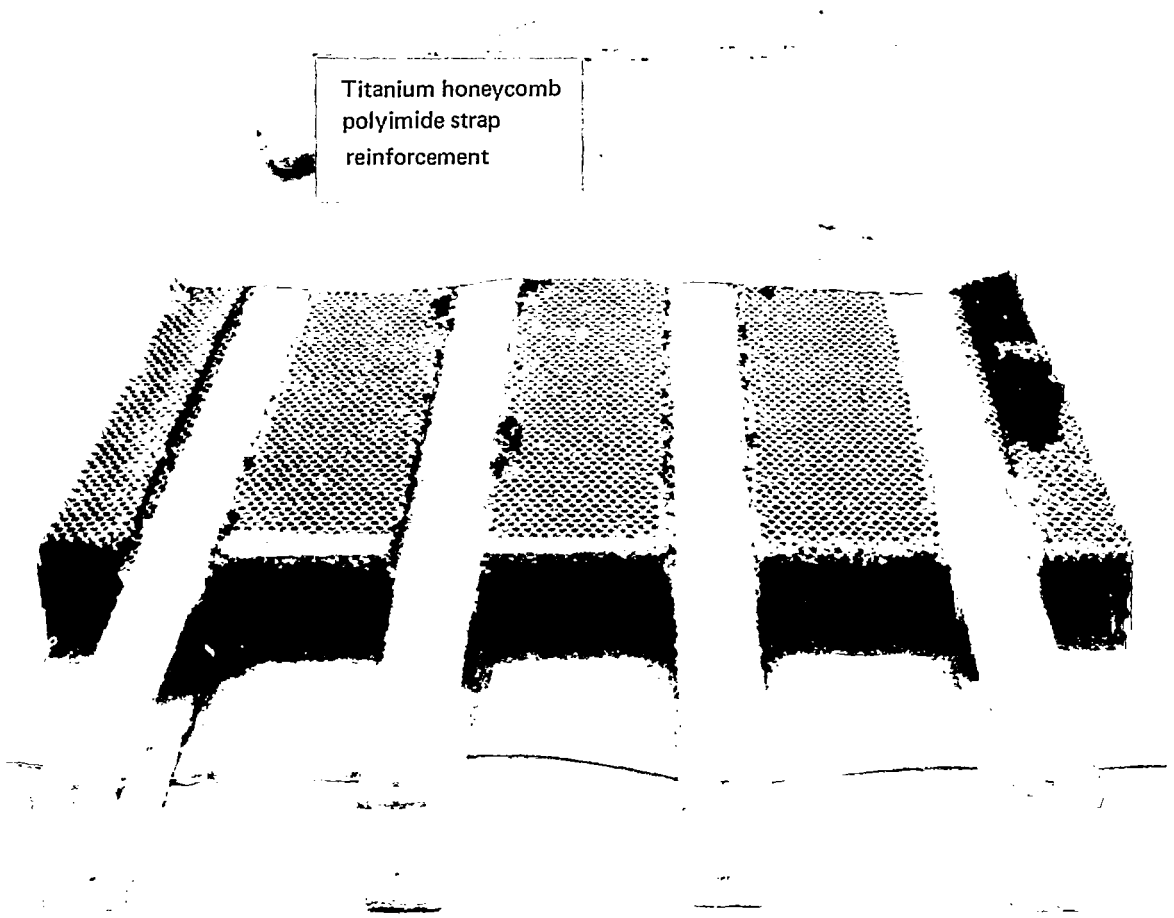

FIGURE 52.—FRACTURE IN CONCEPT 2c AFTER ELEVATED-TEMPERATURE TEST

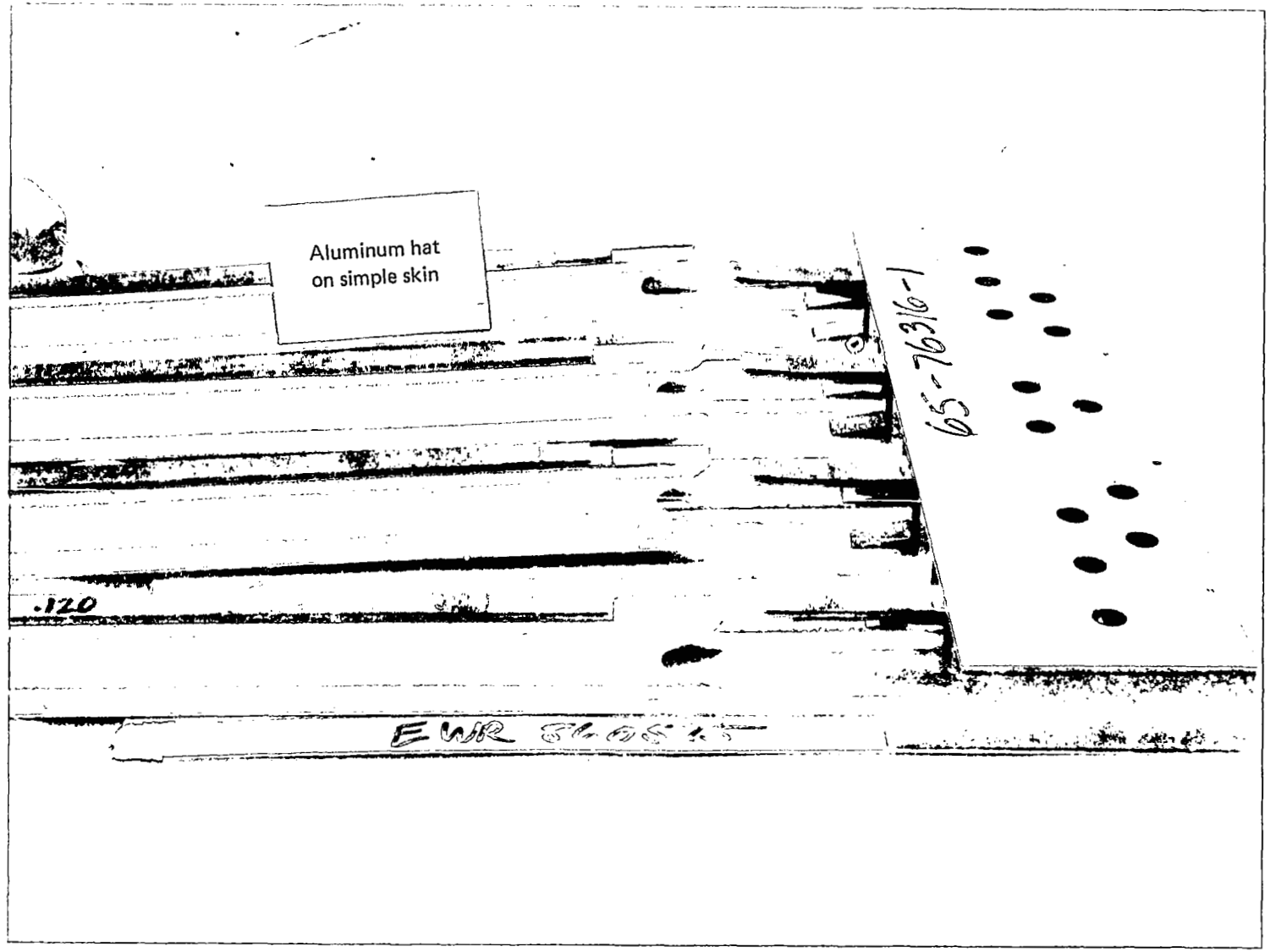

FIGURE 53.—FRACTURE IN CONCEPT 3a

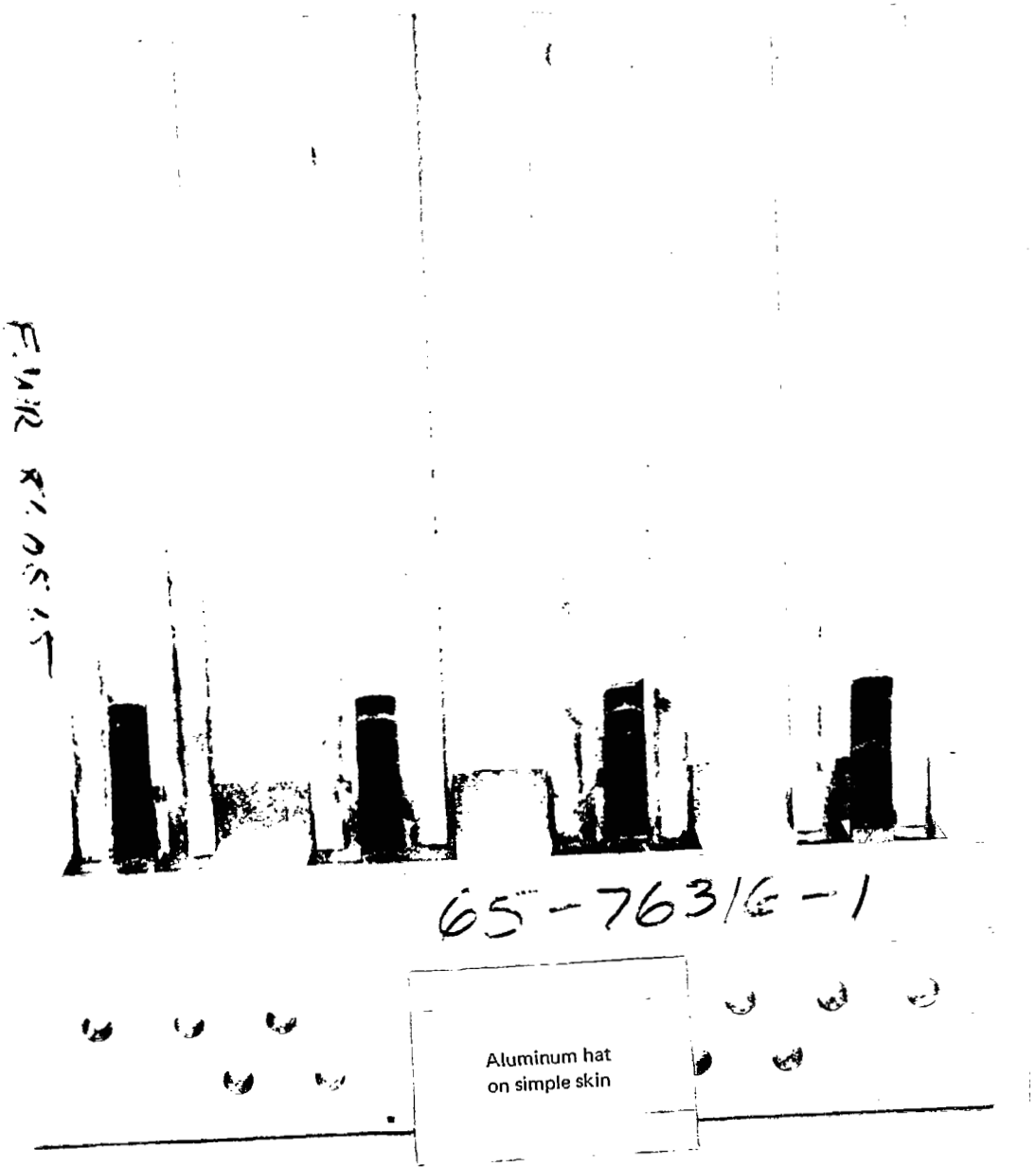

FIGURE 54.—ADHESIVE FAILURE SURFACES ON CONCEPT 3a AFTER COMPRESSION DEBONDING

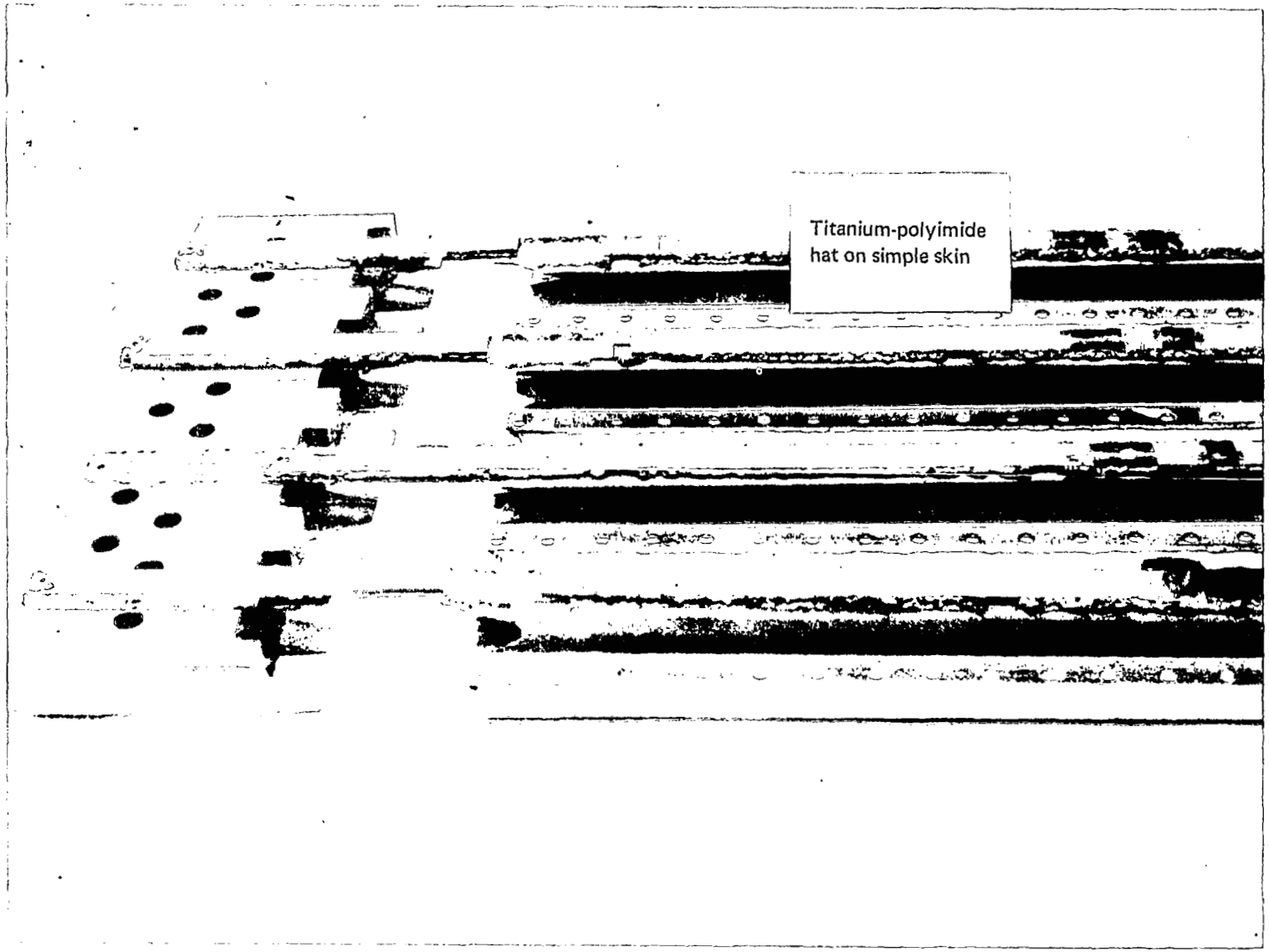

FIGURE 55.—FRACTURE IN CONCEPT 3c AFTER ELEVATED-TEMPERATURE TEST

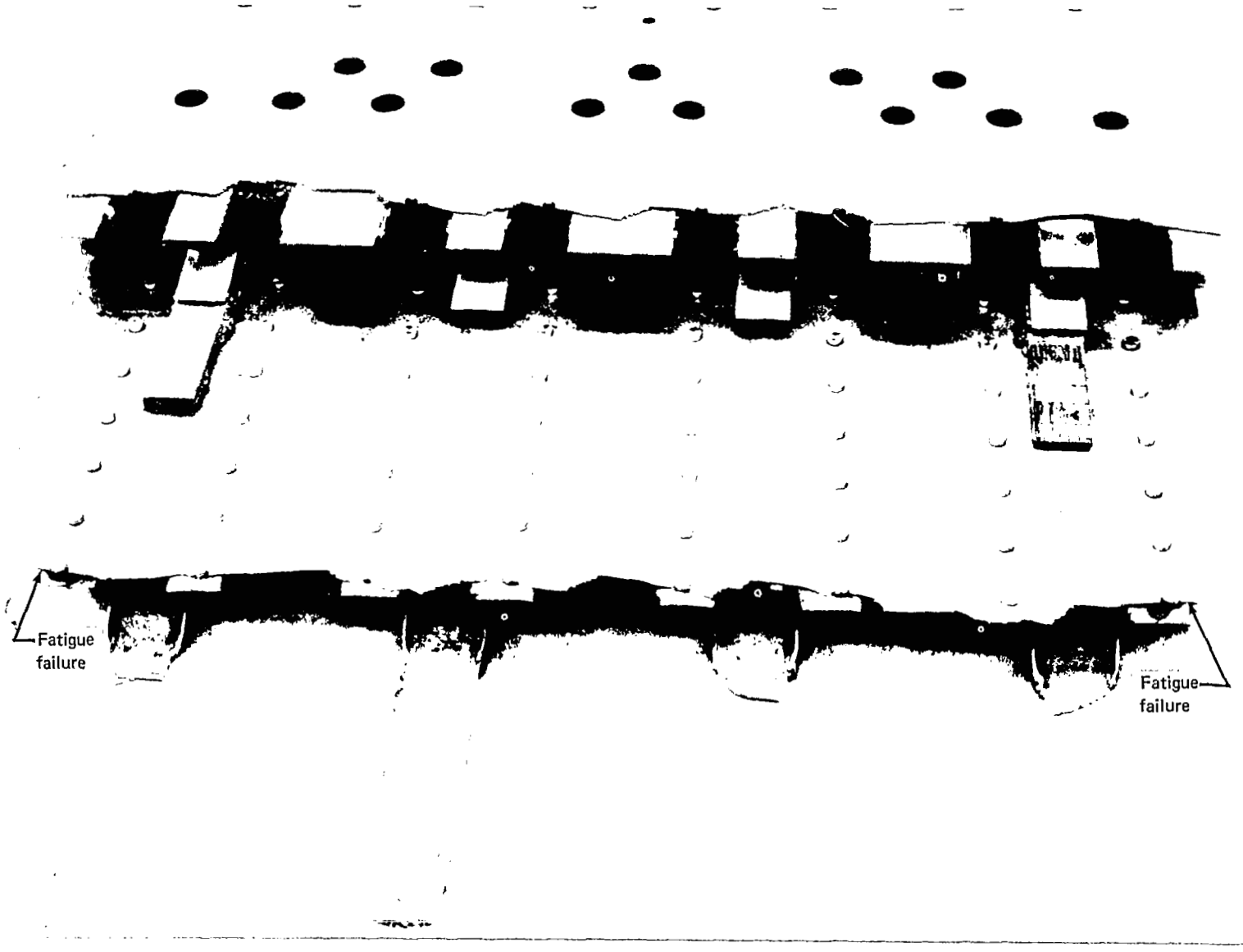

FIGURE 56.–FRACTURE SURFACE IN CONCEPT 3c

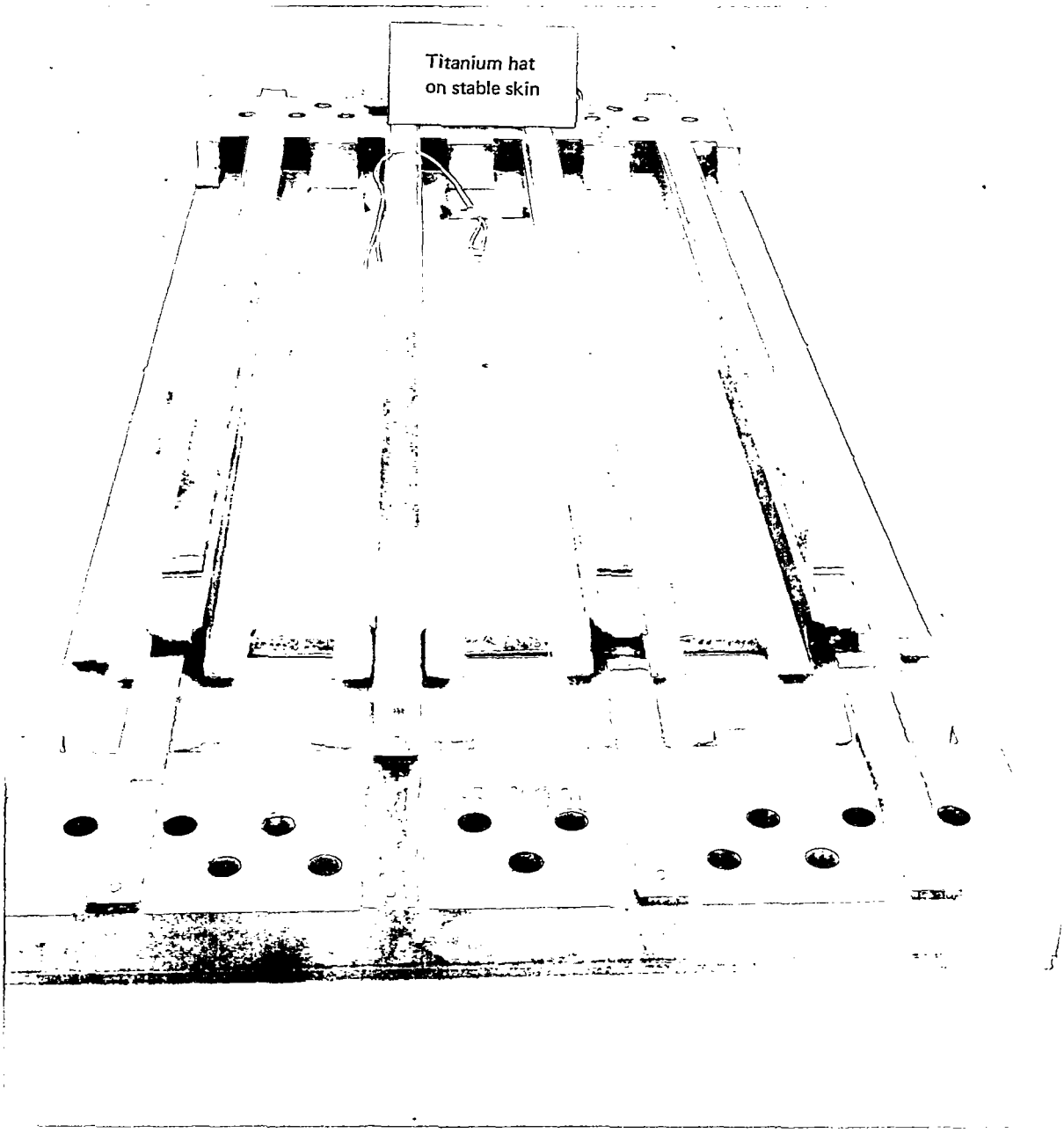

FIGURE 57.—FRACTURE IN CONCEPT 4b

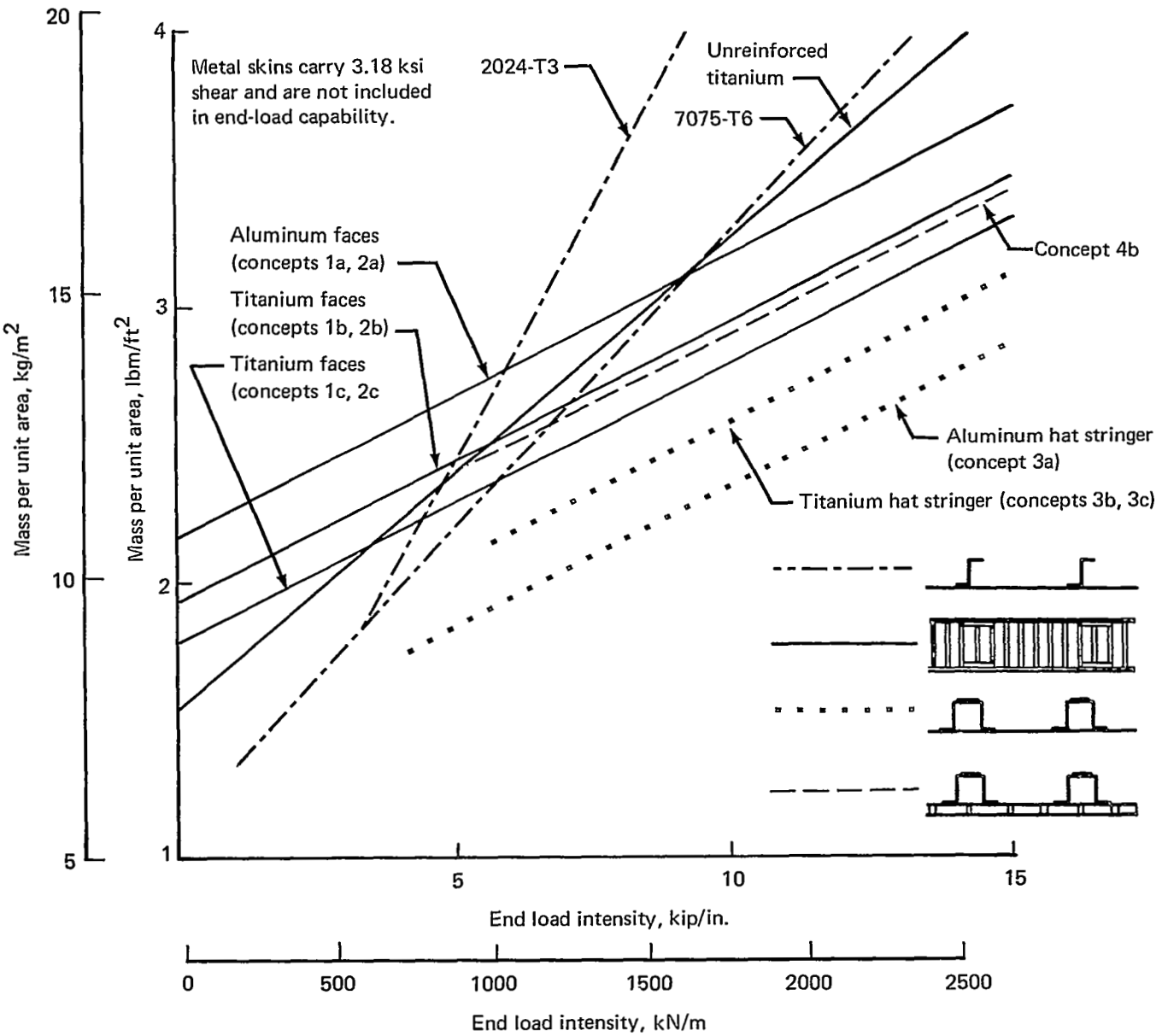

FIGURE 58.–PANEL WEIGHT AS A FUNCTION OF ULTIMATE LOAD

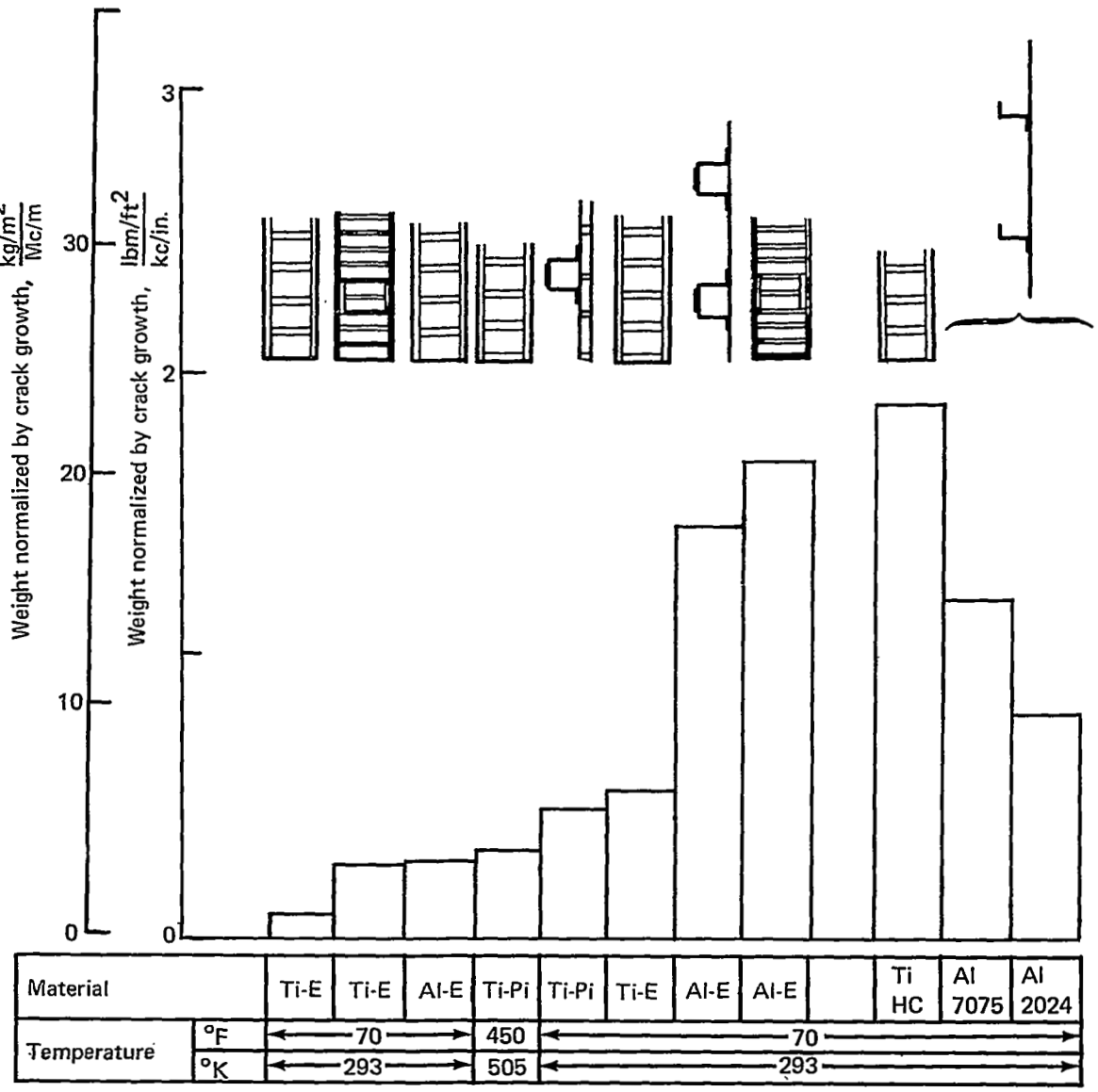

FIGURE 59.—WEIGHT COMPARISON BASED ON CRACK GROWTH RATE

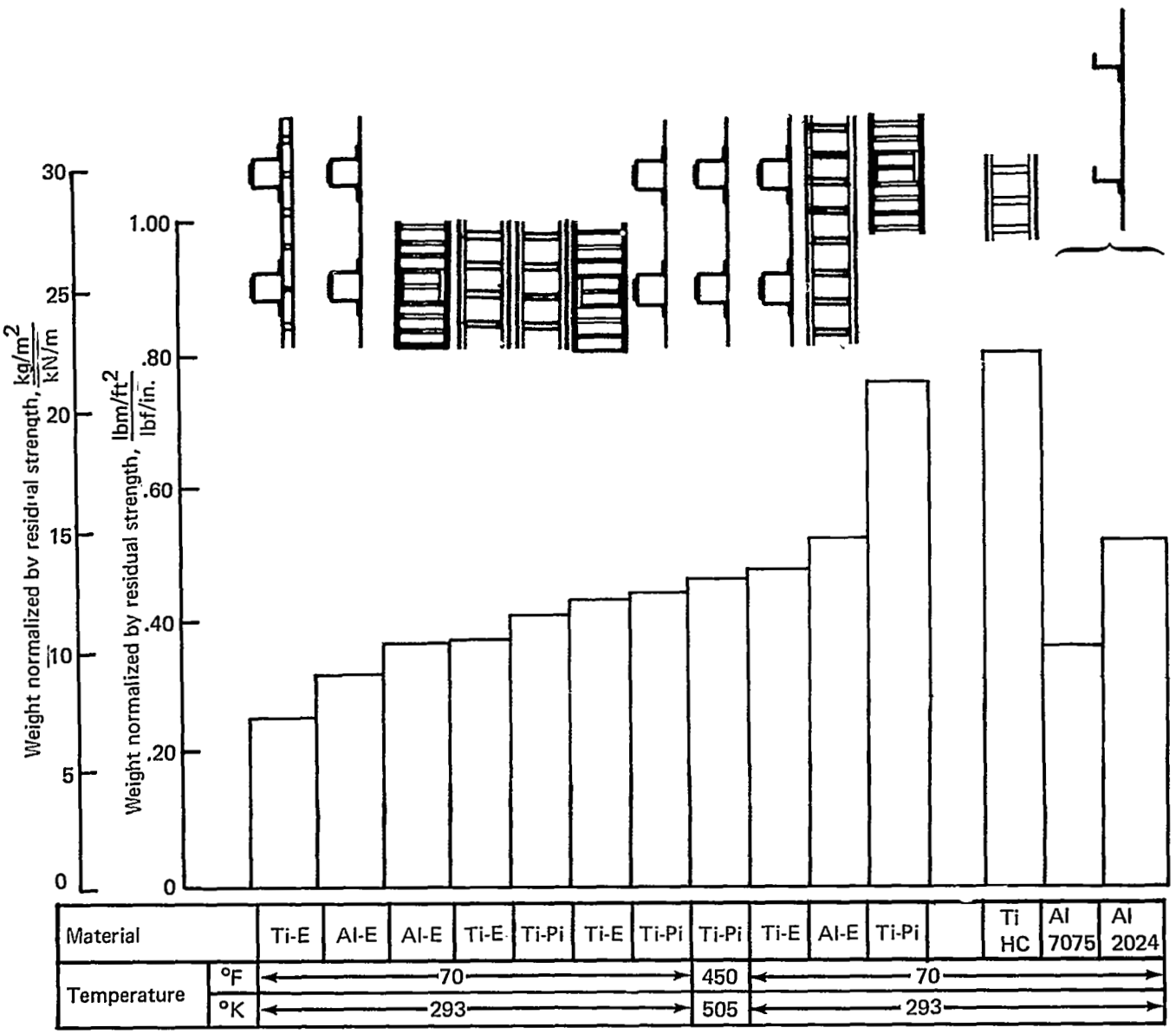

FIGURE 60.—WEIGHT COMPARISON BASED ON RESIDUAL STRENGTH

APPENDIX
TEST SPECIMEN MATERIALS

The following materials were used to fabricate test specimens:

Aluminum sheet and formed sections were alloy 7075-T6 per QQ-A-250/13.

Titanium sheet was alloy 6Al-4V per MIL-T-9046F, type III, composition C (annealed) or type III, composition C (solution treated and aged).

Steel spacer bars were annealed CRES 321.

Aluminum honeycomb was per MIL-C-7438, type 8.1-1/8-20 (5052).

Polyimide-fiberglass honeycomb was HRH-324 3/16-GF26-5.0 purchased from Hexcel Products, Incorporated.

Boron filaments were obtained from the Hamilton Standard Division of United Aircraft. These were 0.004-in. (0.10-mm) diameter filaments of boron vapor deposited onto a tungsten wire substrate.

BP 907 adhesive was obtained from the Bloomingdale Department of American Cyanamid Company. This is a film adhesive of epoxy resin impregnated into a scrim of type 104 glass fabric. The material thickness is 0.003 in. (0.076 mm). This material has a shelf life of 6 months at room temperature. It is used primarily for drum winding with boron filament to form sheets of uncured boron-epoxy material. When used in adhesive bonding, liquid primer EC 2320 is used on all faying surfaces. The cure cycle is shown in figure 61.

AF 126 adhesive was obtained from the Minnesota Mining and Manufacturing Company. This is a film adhesive of epoxy resin impregnated into a dacron fiber mat or veil. The material thickness is 0.005 in. (0.13 mm) for bonding plane surfaces or 0.015 in. (0.38 mm) for bonding honeycomb surfaces. Liquid primer EC 2320 is used on all faying surfaces. The cure cycle used is shown in figure 61.

EPON 933 adhesive was obtained from the Shell Chemical Company. This is the same epoxy resin used to manufacture EPON 927, but it is filled with a mixture of chopped fiberglass and asbestos to form a viscous material suitable for knife application to fill irregular bond surfaces. The cure cycle is shown in figure 62.

The adhesive 35-520 Pyralin was obtained from E. I. DuPont De Nemours. This is a film adhesive of 2507 polyimide resin impregnated into a scrim of type 104 glass fabric. The material thickness is 0.003 in. (0.076 mm). It is used primarily for drum winding with boron filament to form sheets of uncured boron-polyimide material. The cure and postcure cycles are shown in figure 63.

FM 34 adhesive was obtained from Bloomingdale Department of American Cyanamid Company. This is a film adhesive of filled polyimide resin impregnated into glass fabric. The

material thickness is 0.015 in. (0.38 mm) for plane surfaces and honeycomb core. BR 34 liquid primer is used on all faying surfaces. The cure cycle is shown in figure 62.

The test specimen material properties used in the analysis are listed in tables 10, 11, and 12. Unless otherwise noted, values were obtained from MIL-HDBK-5A, from the AFML *Structural Design Guide for Advanced Composite Applications,* or from Boeing test data.

The prepreg used to make the structural laminates consisted of drum-wound boron fibers on the matrix film materials BP 907 or 35-520 Pyralin. The fiber spacing corresponded to 208 fibers per inch (8.19 per mm), and this material provided a thickness per ply of 0.0055 in. (0.140 mm) in the cured condition.

TABLE 10.– ROOM TEMPERATURE PROPERTIES OF TITANIUM, ALUMINUM, AND BORON

Property	Ti-6Al-4V (annealed)	Ti-6Al-4V (treated and aged)	Al-7075-T6	Boron filament
Tensile ultimate strength, $lb/in^2 \times 10^3$ ($N/m^2 \times 10^6$)	134 (923)	157 (1081)	76 (523)	450 (3,100)
Tensile yield strength, $lb/in^2 \times 10^3$ ($N/m^2 \times 10^6$)	126 (868)	143 (985)	65 (447)	–
Compressive yield strength, $lb/in^2 \times 10^3$ ($N/m^2 \times 10^6$)	132 (909)	152 (1047)	67 (461)	–
Shear ultimate strength, $lb/in^2 \times 10^3$ ($N/m^2 \times 10^6$)	79 (544)	98 (675)	46 (317)	–
Elongation, %	8	3	7	–
Modulus of elasticity, $lb/in^2 \times 10^6$ ($N/m^2 \times 10^9$)	16.0 (110.2)	16.0 (110.2)	10.3 (70.9)	58 (400)
Compressive modulus, $lb/in^2 \times 10^6$ ($N/m^2 \times 10^9$)	16.4 (113.0)	16.4 (113.0)	10.5 (72.3)	58 (400)
Shear modulus, $lb/in^2 \times 10^6$ ($N/m^2 \times 10^9$)	6.2 (42.7)	6.2 (42.7)	3.9 (26.8)	25 (172)
Poisson's ratio	0.30	0.30	0.33	0.20
Coefficient of thermal expansion, μin./in./°F (μm/m/°K)	5.3 (9.5)	5.3 (9.5)	12.9 (23.2)	2.7 (4.9)

TABLE 11.–ROOM TEMPERATURE PROPERTIES OF MATRICES

Property	BP 907	35-520
Tensile modulus, longitudinal, $lb/in^2 \times 10^6$ ($N/m^2 \times 10^9$)	1.175 (8.096)	1.94 (13.36)
Compressive modulus, longitudinal, $lb/in^2 \times 10^6$ ($N/m^2 \times 10^9$)	1.175 (8.096)	1.94 (13.36)
Shear modulus, $lb/in^2 \times 10^6$ ($N/m^2 \times 10^9$)	0.452 (3.114)	–
Poisson's ratio	0.30	–
Coefficient at thermal expansion, μin./in./°F (μm/m/°K)	15.0 (27.0)	4.6 (8.6)

TABLE 12.–COMPRESSIVE MODULUS OF TEST MATERIALS AT TEST TEMPERATURES
[$lb/in.^2 \times 10^6$ (kN/mm^2)]

Temperature						
°F	°K	BP 907	35-520	Al-7075-T6	Ti-6Al-4V	Boron filament
-65	218	[a]1.175 (8.10)	2.24 (15.43)	10.0 (68.9)	18.3 (126.09)	58.0 (400)
70	294	1.175 (8.10)	1.94 (13.36)	9.7 (66.8)	16.4 (113.0)	58.0 (400)
165	346	[a]0.800 (5.51)	–	9.4 (64.7)	–	58.0 (400)
450	504	–	1.94 (13.36)	–	14.1 (97.1)	58.0 (400)

[a]Assumed values.

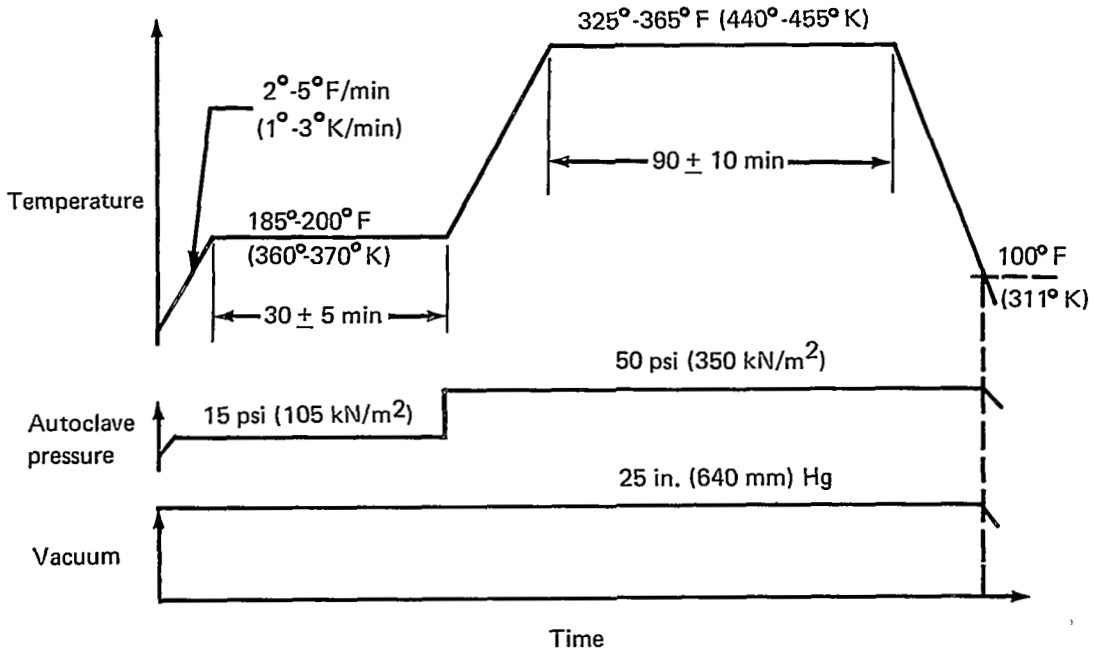

BP 907 CURE CYCLE

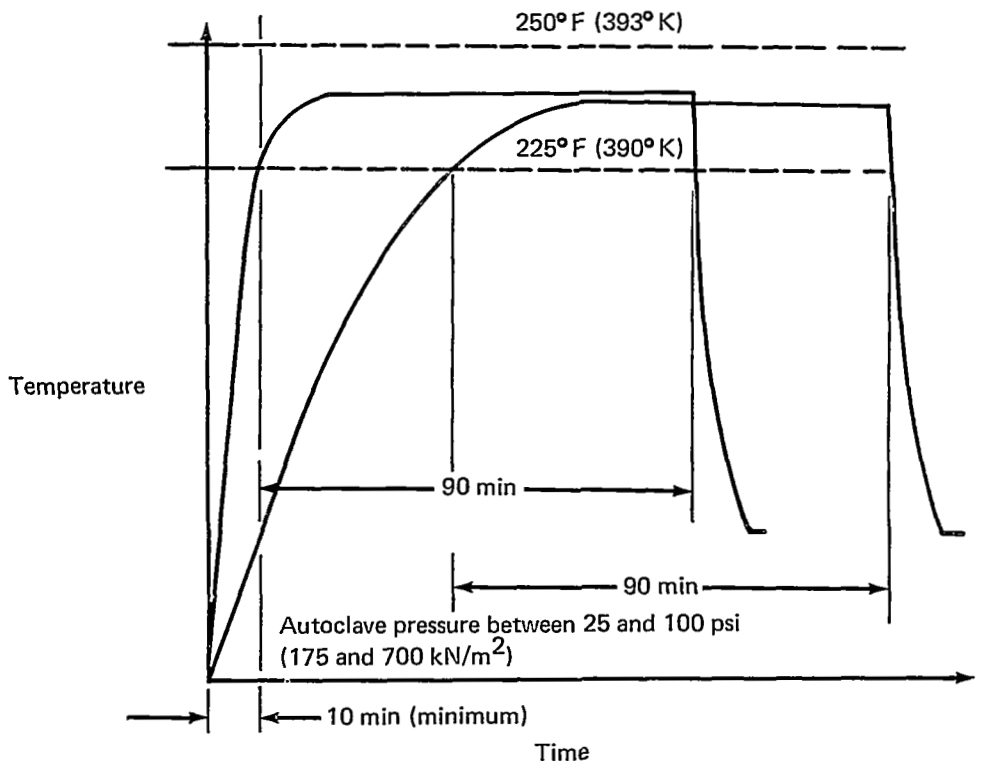

AF 126 CURE CYCLE

FIGURE 61.– CURE CYCLES FOR BP 907 AND AF 126 EPOXY ADHESIVES

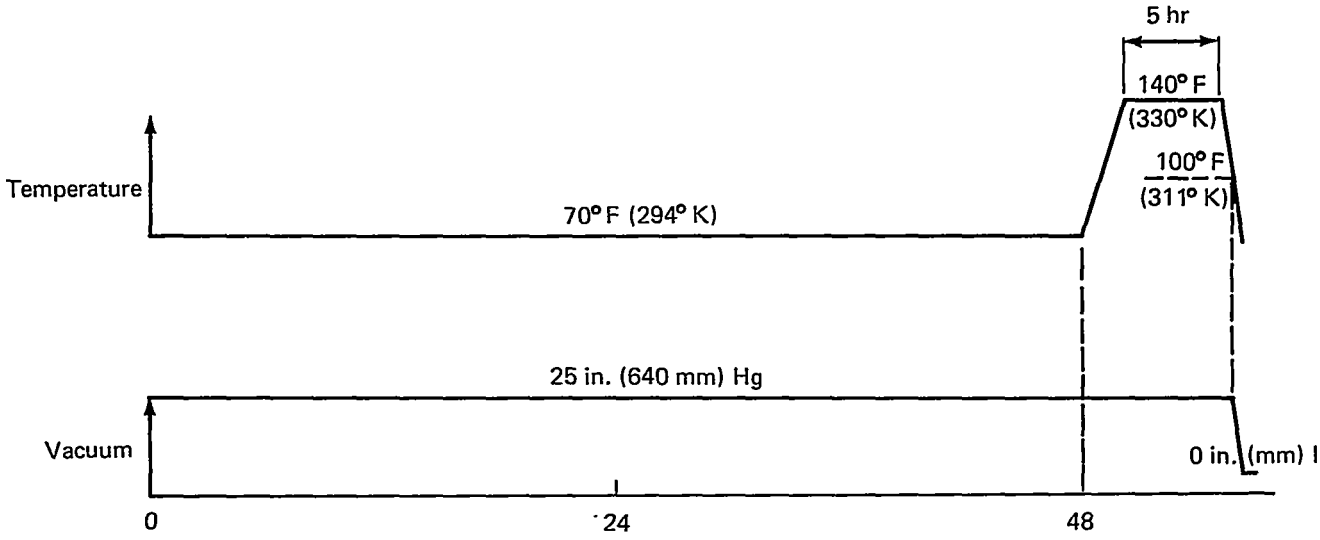

EPON 927 AND 933 CURE CYCLES

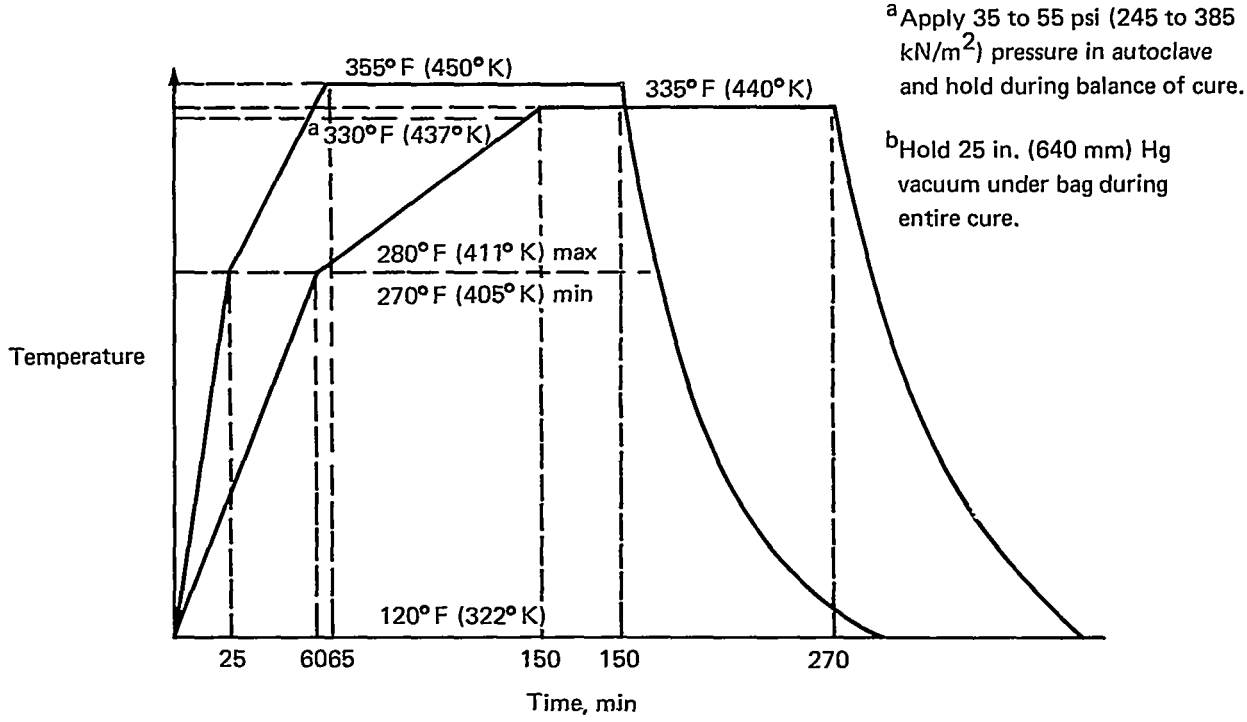

FM 34 CURE CYCLE [b]

FIGURE 62.—CURE CYCLES FOR EPON 927 AND 933 EPOXY AND FM 34 POLYIMIDE ADHESIVES

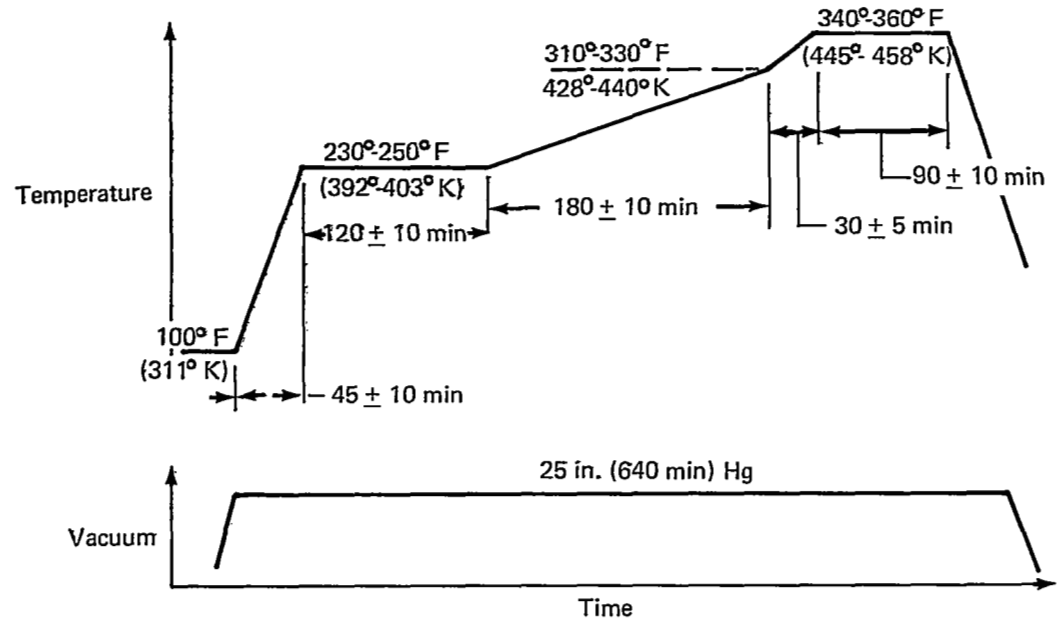

35-520 CURE CYCLE

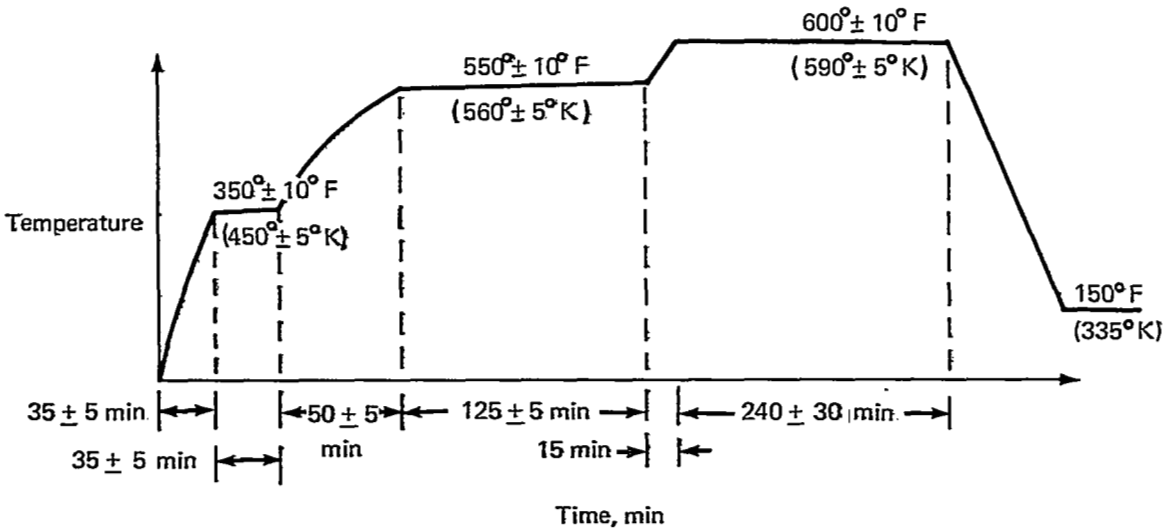

35-520 AND FM 34 POSTCURE CYCLE

FIGURE 63.– CURE CYCLE FOR 35-520 AND POSTCURE CYCLE FOR 35-520 AND FM 34 POLYIMIDE ADHESIVES

REFERENCES

1. Oken, S. and June, R. R.: Analytical and Experimental Investigation of Aircraft Metal Structures Reinforced With Filamentary Composites; Phase I: Concept Development and Feasibility. NASA CR-1859, 1971.

2. Hardrath, H. F. and Illg, W.: Fatigue Tests at Stresses Producing Failure in 2 to 10 000 Cycles. NACA TN3132, 1954.

3. Grover, H. J. Hyler, W. S., and Jackson, L. R.: Fatigue Strength of Aircraft Materials. NACA TN 2639, 1952.

4. White, D. L. and Watson, H. T.: Determination of Design Data for Heat Treated Titanium Alloy Sheet. ASD-TDR-62-335, vol. 2b, U.S. Air Force, May 1962.

5. Frocht, M.: Factors of Stress Concentration Photoelastically Determined. Am. Soc. Mech. Eng., J. Appl. Mech., vol. 2, no. 2, 1935, p. A-67.